ABSTRACT

PROPERTIES OF GAMMA-RAY TRANSITIONS IN ^{56}Co FROM ^{56}Ni DECAY AND $^{56}Fe(p,n\gamma)^{56}Co$

By

Lawrence Edward Samuelson

The ^{56}Ni beta decay and the $^{56}Fe(p,n\gamma)^{56}Co$ reaction with beam energies between 5.5 and 8.4 MeV have been used with Ge(Li) spectrometers to study properties of γ rays from states of ^{56}Co below 2.85 MeV of excitation. The ^{56}Ni decay γ-ray spectrum and γ-γ coincidences were studied. γ-γ coincidences, γ-ray excitation functions, γ-ray angular distributions, and absolute cross sections were measured for the $^{56}Fe(p,n\gamma)^{56}Co$ reaction. A beta-decay scheme for ^{56}Ni, which includes six γ rays, and an energy-level diagram for ^{56}Co, which includes 35 γ rays (14 of which are reported for the first time) from 20 excited states, are presented. Comparisons of the data from $^{56}Fe(p,n\gamma)^{56}Co$ with predictions of the statistical compound nuclear model have resulted in spin assignments (in parentheses) for the following states (energies in keV) of ^{56}Co: 158.4 (3), 576.6 (5), 829.7 (4), 970.3 (2), 1009.2 (5), 1114.6 (3), 1450.8 (0), and 1720.3 (1). Branching ratios are presented for 14 γ rays from these eight states and multipole mixing ratios are given for 12 of these γ rays (10 are predominantly M1). The data are consistent with a

spin 4 assignment to the ground state. Contrary to previous suggestions, evidence from all experiments indicates that only one state exists in ^{56}Co in the neighborhood of 1451 keV of excitation. The level energies, γ-ray multipole mixing ratios and γ-ray branching ratios agree, in general, with shell-model predictions of McGrory.

PROPERTIES OF GAMMA-RAY TRANSITIONS IN ^{56}Co FROM ^{56}Ni DECAY AND $^{56}Fe(p,n\gamma)^{56}Co$

By

Lawrence Edward Samuelson

A THESIS

Submitted to
Michigan State University
in partial fulfillment of the requirements
for the degree of

DOCTOR OF PHILOSOPHY

Department of Physics

1972

ACKNOWLEDGMENTS

I wish to thank Dr. W. H. Kelly for suggesting this area of study. His encouragement and constant interest during the experimental work and his guidance and patience during the preparation of this thesis are deeply appreciated.

I also wish to thank most sincerely Dr. R. A. Warner for his invaluable assistance and encouragement in all phases of this work. Many fruitful discussions led to solutions of apparently insurmountable problems.

Drs. Wm. C. McHarris, F. M. Bernthal and B. H. Wildenthal have contributed to various phases of this investigation through informal discussion. Dr. J. B. McGrory was very kind to send shell-model calculations on ^{56}Co. Their generous cooperation is gratefully acknowledged.

Dr. H. G. Blosser and Mr. H. Hilbert have assisted with the operation of the Michigan State University sector-focused cyclotron.

Dr. E. M. Bernstein, Dr. R. Shamu and Mr. Eric Warren assisted considerably with the operation of the Western Michigan University tandem Van de Graaff. Their unselfish generosity is gratefully appreciated.

Dr. R. E. Doebler, Dr. R. R. Todd, Dr. R. W. Goles, Mr. C. B. Morgan and Mr. W. B. Chaffee aided in data collection and interpretation.

Mrs. Carol VanderMeer and Mrs. Peri-Anne Warstler aided greatly by typing the various versions of this manuscript.

Much of the financial assistance for this research has been provided by the National Science Foundation, the U.S. Atomic Energy Commission, and Michigan State University.

TABLE OF CONTENTS

LIST OF TABLES

LIST OF FIGURES

I. INTRODUCTION

The earliest investigations[1-6] of the low-lying excited states of ^{56}Co began with the beta decay of ^{56}Ni. These studies, which included measurements of the ^{56}Ni half life,[1] the γ-ray spectrum,[1,3,4] γ-γ angular-correlations,[1,3] the internal-conversion electron spectrum,[2] and lifetimes of some ^{56}Co states,[1] produced valuable information. However, only selected states below 1.8 MeV could be populated and unambiguous spin assignments for these states could not be made.

More recently, experiments involving the two-particle transfer reactions ^{54}Fe(^{3}He,p)^{56}Co,[7-10] ^{54}Fe(α,d)^{56}Co,[11] ^{58}Ni(p,^{3}He)^{56}Co,[12] and ^{58}Ni(d,α)^{56}Co[8,9,13-15] and the charge-exchange reactions ^{56}Fe(p,n)-^{56}Co[16,17] and ^{56}Fe(^{3}He,t)^{56}Co[18-21] have increased the knowledge of the properties of these and additional states. However, the interpretations of these experiments depend strongly upon assumed ^{56}Co wave functions and reaction mechanisms. Neither is well-known.

In particular, the J^{π} of a state in ^{56}Co at 1451 keV has been somewhat controversial. In the early ^{56}Ni decay work, 1^{-} or $2^{\pm}$ seemed most consistent with the data, with $1^{-}(2^{-})$ being favored by Ohnuma *et al.*,[3] and 2^{+} by Jenkins *et al.*[2] and Wells.[22] Later, Belote *et al.*,[8] observing $\ell = 0$ transfers in (^{3}He,p) and (d,α) and a weak (d,α) cross section, chose 0^{+}. Belote *et al.*[8] then conjectured that this state was an anti-analog of the ^{56}Fe ground state ($J^{\pi} = 0^{+}$). Subsequent particle transfer work has confirmed $J^{\pi} = 0^{+}$ (e.g. see Ref. 12 and 15). However, Roos and Goodman[19] reported an $\ell = 1$ transfer in the (^{3}He,t) reaction, implying $J^{\pi} = 1^{-}$; they then suggested that possibly a 0^{+} *and* a 1^{-} state occur within a few keV of each

other at this energy.

The $^{56}Fe(p,n\gamma)^{56}Co$ reaction[23,24] near threshold was chosen for the present study because the reaction should be well described by the statistical compound nuclear (CN) theories of Wolfenstein,[25] Hauser and Feshbach,[26] Biedenharn and Rose,[27] Satchler,[28] and Sheldon and Van Patter.[29] Since all states for which there are sufficient energy and angular momentum are excited in this type of reaction, both members of the doublet (if they exist) at 1451 keV should be populated quite strongly because of their expected low spins. Comparisons of the results of the present work with the predictions of the statistical CN theory and with previously measured ^{56}Co γ-ray characteristics have lead to unambiguous spin assignments for all ^{56}Co states below 1.8 MeV. In addition, γ-ray multipole mixing ratios, precise level energies and γ-ray branching ratios are obtained. This experimental information is compared with shell-model level energies and B(M1) and B(E2) values for ^{56}Co calculated recently by McGrory.[30]

As a supplement to the $(p,n\gamma)$ work, the γ-ray spectrum accompanying the ^{56}Ni beta decay was reinvestigated. These experiments corroborated the previous ^{56}Ni decay work and the energies of some ^{56}Co γ-rays. In particular, the 1451 keV state was examined very carefully in the decay study for any evidence of it being a doublet.

II. THE BETA DECAY OF ^{56}Ni

Ge(Li) detectors were used to measure the γ-ray spectrum and γ-γ coincidences accompanying the ^{56}Ni beta decay. These experiments yielded γ-ray energies and intensities and confirmed the placement of γ-rays in the ^{56}Ni decay scheme.

A. Source Preparation

The 6.1-day ^{56}Ni activities were produced via the ^{56}Fe(^{3}He,3n)^{56}Ni reaction (Q = -16.3 MeV) by bombarding 0.02 gm/cm^2 iron foils with 45-MeV ^{3}He particles from the Michigan State University sector-focused cyclotron. After allowing about 10 days for the undesired 1.5-day ^{57}Ni activity to decay, chemical separations were performed.

The iron foils were first dissolved in hot 15N HCl, evaporated to dryness, and redissolved in 10N HCl. The samples were then passed through a column of Dowex 1-X8 anion exchange resin previously brought into equilibrium with 10N HCl. This procedure[31] removed all detectable contaminant cobalt activities such as ^{56}Co and ^{58}Co. The desired ^{56}Ni activities were then separated from the remaining contaminant radioisotopes such as ^{51}Cr, ^{52}Mn, and ^{54}Mn by the standard procedure of precipitation of nickel dimethylglyoxime (Ni-DMG).[32] The Ni-DMG was finally dissolved in 15N HCl and placed in thin-walled plastic vials for counting.

B. The γ-Ray Spectrum

Three different Ge(Li) detectors were used to take γ-ray singles spectra: (1) a 2.5%-efficient (compared to a 7.6 cm × 7.6 cm NaI(Tl) detector at 25 cm and at a γ-ray energy of 1332 keV) Ge(Li) detector with a 15:1 peak-to-Compton ratio and a FWHM resolution of 2.34 keV at a γ-ray energy of 1332 keV; (2) a 4.5%-efficient Ge(Li) detector with a 22:1 peak-to-Compton ratio and a FWHM resolution of 2.10 keV; and (3) a 10.4%-efficient Ge(Li) detector with a 30:1 peak-to-Compton ratio and a FWHM resolution of 2.28 keV. A typical ^{56}Ni decay γ-ray singles spectrum is shown in Fig. 1. Optimum resolution and the most symmetric peaks were obtained using an ORTEC model #450 Research Amplifier direct-coupled into a Northern Scientific 50-MHz analog-to-digital converter. The data were accumulated in either the MSU Cyclotron Laboratory's Xerox Data System Σ-7 time-sharing computer using a pulse-height analysis routine,[33] or in a Digital Equipment Corporation PDP-9 computer loaded with another pulse-height analysis routine. Peak centroids and areas were determined off-line by the peak-fitting code SAMPO,[34] which was especially useful in stripping unresolved multiplets.

Since it offered the best over-all resolution, the 4.5%-efficient Ge(Li) detector was used to take the spectra for the γ-ray energy measurements. For these measurements, spectra from a ^{56}Ni source were taken in the presence of various combinations of such well-known γ-ray energy standards as ^{57}Co, ^{139}Ce, ^{203}Hg, ^{51}Cr, ^{207}Bi, ^{137}Cs, ^{54}Mn, ^{56}Co, ^{88}Y, ^{65}Zn, ^{60}Co, ^{22}Na, ^{40}K, and ^{192}Ir. The calibration energies assumed can be found elsewhere.[5,35,36] Care was taken so that standard

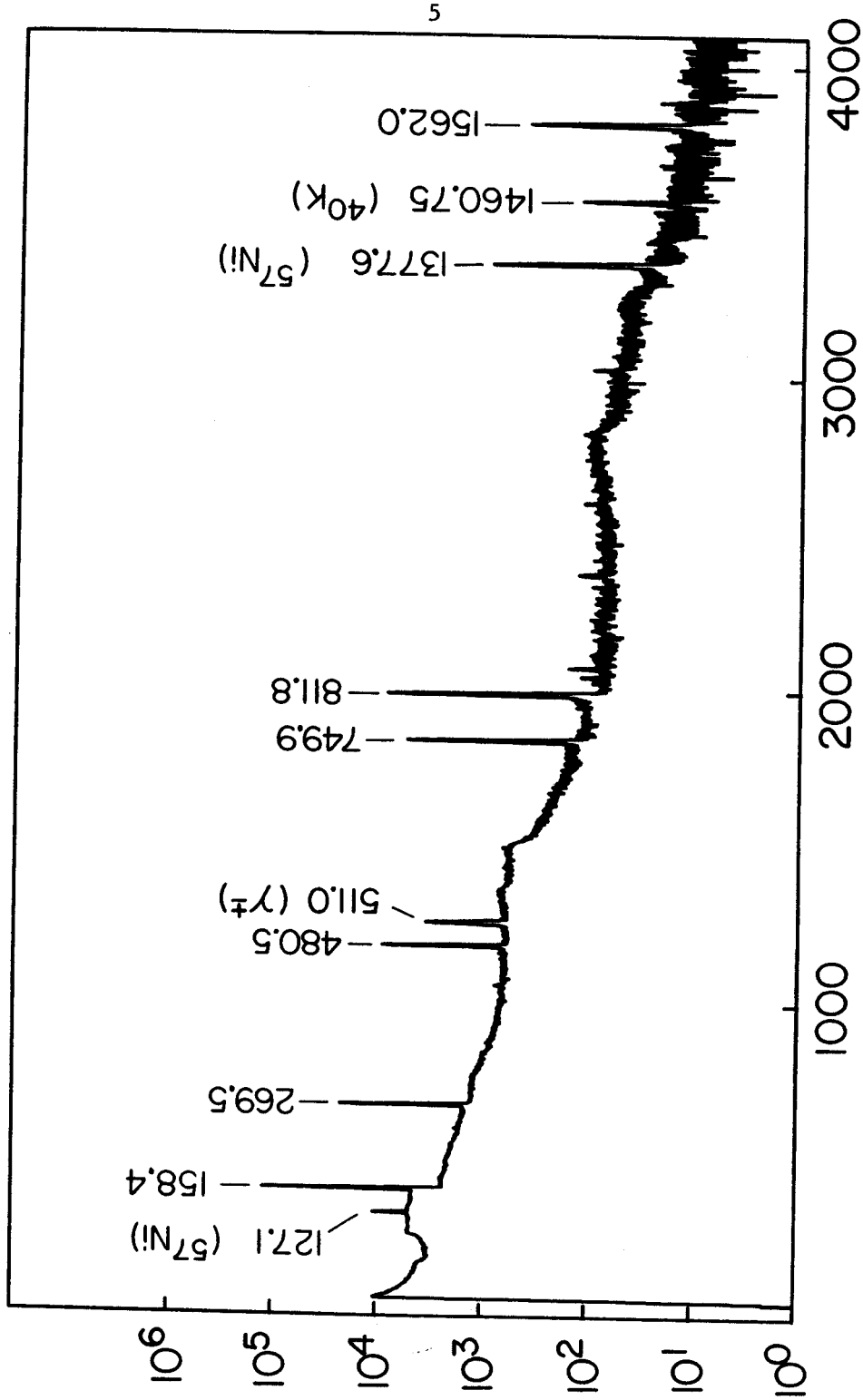

Figure 1. Typical ^{56}Ni singles spectrum taken with the 2.5% efficient Ge(Li) spectrometer.

peaks and the ^{56}Ni decay peaks grew into the spectra at roughly equal rates. A quadratic fit was then made to the calibration energies versus measured centroids in two energy regions (100-800 keV and 700-2000 keV). The ^{56}Co γ-ray energies were then calculated by computer using this calibration and are listed in Table I.

The 2.5%- and 10.4%-efficient Ge(Li) detectors were both used for γ-ray intensity determinations. Separate singles spectra were taken using each detector with the ^{56}Ni source placed both at 5 cm and at 25 cm from the face of the detector. The use of two detectors with highly different efficiencies and of two source-to-detector distances allowed for sum-peak identification. Background spectra (with the source removed) were also taken with each detector. The relative efficiency curves were determined using the γ-ray intensity standards ^{160}Tb, ^{203}Hg, ^{180m}Hf, ^{110m}Ag, ^{177m}Lu, ^{56}Co, ^{88}Y, ^{60}Co, and ^{24}Na. The relative intensities of the γ-rays from these standards can be found elsewhere.[5,37-39] The intensities presented in Table I were obtained by averaging the four sets of data.

Table I. Energies and relative intensities of the γ rays in ^{56}Co from the beta decay of ^{56}Ni.

E_γ (keV)		I_γ	
Present work	Piluso *et al.*[a]	Present work	Piluso *et al.*[b]
158.4±0.1	158.3±0.2	≡ 100.	≡ 100.
269.5±0.1	269.6±0.1	36.0±1.4	40.0±0.7
480.5±0.1	480.7±0.1	36.0±1.5	41.4±1.4
749.9±0.1	750.6±0.1	50.5±2.5	54.3±3.5
811.8±0.1	812.2±0.2	88.5±4.4	91.3±3.5
1562.0±0.2	1562.5±0.2	14.3±1.4	12.8±1.4

[a] See Ref. 4.

[b] The relative γ-ray intensities presented by Piluso *et al.* (Ref. 4) have been renormalized here to 100 for the intensity of the 158.4-keV transition.

C. γ-γ Coincidences

Prompt γ-ray coincidences in the ^{56}Ni beta decay were determined with a Ge(Li)-Ge(Li) spectrometer using the 4.5%- and 10.4%-efficient detectors arranged in 150° geometry with a graded (Pb-Sn-Cu) absorber placed between them to minimize Compton scattering from one detector into the other. A typical two-parameter, fast-slow coincidence arrangement (resolving time $2\tau \cong 100$ nsec) was used. Addresses corresponding to the energies of coincident γ-rays were listed in pairs on magnetic tape.[40] This listing yielded a 4096×4096-channel array of prompt coincidence events which were later sorted off-line in gated slices.[41] The gated slices included careful subtraction of background coincidences which were determined from the adjacent continuum.

The integral coincidence spectrum from each detector is shown at the top of Fig. 2. Each spectrum represents 330,000 coincidences. Beneath each integral spectrum in Fig. 2 are shown spectra in coincidence with the various ^{56}Co peaks. The results are summarized in Table II.

Figure 2. Integral coincidence and gated spectra from the ^{56}Ni γ-γ coincidence experiment. Peaks labeled with a Σ were identified as triple coincidences where two of the three coincident γ rays have been summed in one detector. Peaks labeled in parentheses are believed to be from chance coincidences or insufficient background subtraction.

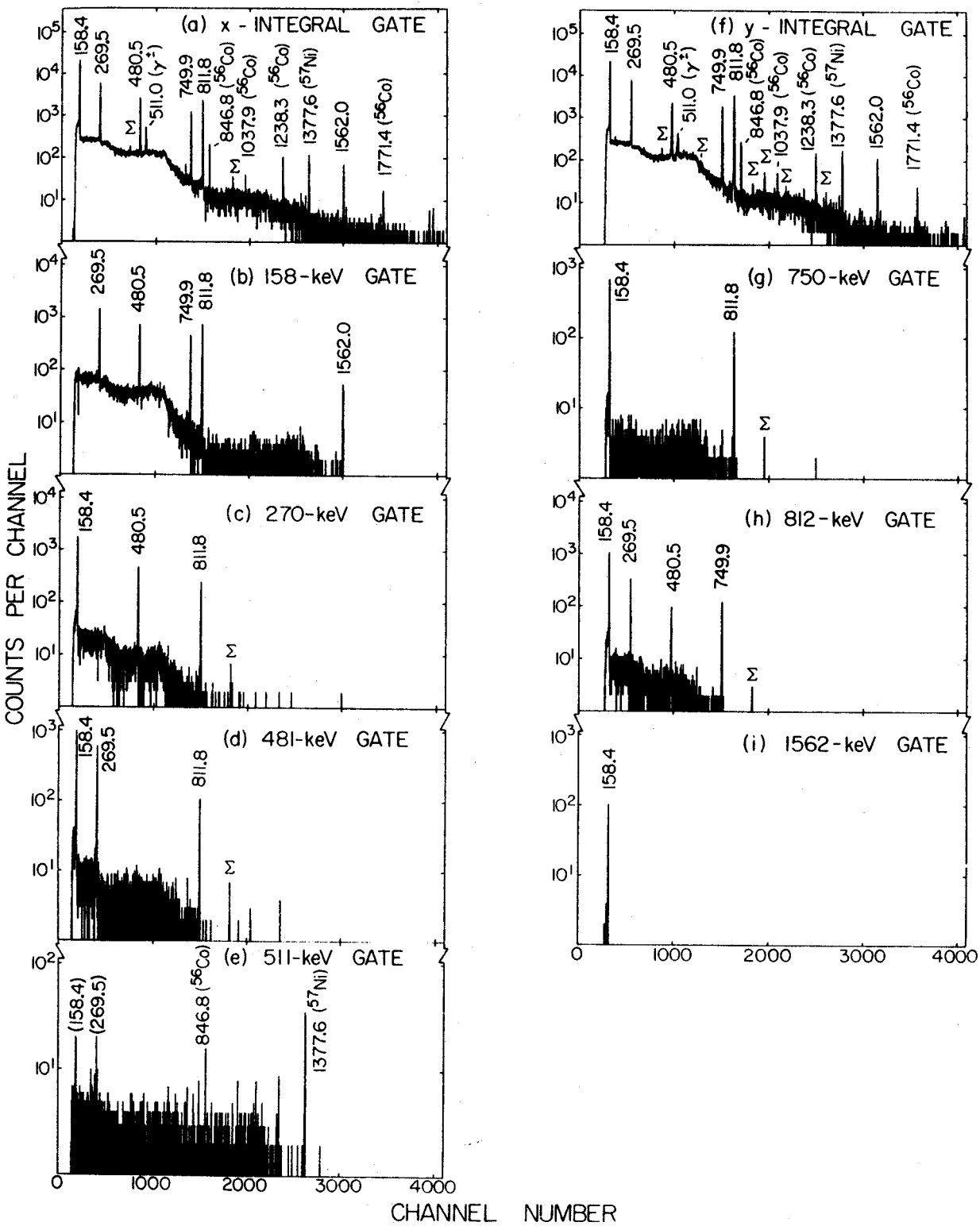
(a) x - INTEGRAL GATE
158.4
269.5
480.5
511.0 (γ±)
749.9
811.8
846.8 (56Co)
1037.9 (56Co)
1238.3 (56Co)
1377.6 (57Ni)
1562.0
1771.4 (56Co)
Σ
(b) 158-keV GATE
(c) 270-keV GATE
(d) 481-keV GATE
(e) 511-keV GATE
(158.4)
(269.5)
(f) y - INTEGRAL GATE
(g) 750-keV GATE
(h) 812-keV GATE
(i) 1562-keV GATE
COUNTS PER CHANNEL
CHANNEL NUMBER
0
1000
2000
3000
4000

Figure 2

Table II. Summary of two-parameter γ-γ coincidence results for the $^{56}Ni \xrightarrow{\epsilon} {}^{56}Co$ decay.

E_γ / E_γ (keV)	158	270	481	511($\gamma^{\pm}$)	750	812	1562
158	---	yes	yes	no	yes	yes	yes
270	yes	---	yes	no	no	yes	no
481	yes	yes	---	no	no	yes	no
511($\gamma^{\pm}$)	no	no	no	---	no	no	no
750	yes	no	no	no	---	yes	no
812	yes	yes	yes	no	yes	---	no
1562	yes	no	no	no	no	no	---

D. The ^{56}Ni Beta-Decay Scheme

The ^{56}Ni beta-decay scheme is shown in Fig. 3. Corrections for internal conversion are included using coefficients measured by Jenkins and Meyerhof.[2] The intensities are normalized to 100 for the 158.4-keV transition strength. The values shown for the half life of ^{56}Ni and the half lives of the 158.4-, 970.2- and 1450.7-keV states of ^{56}Co are those measured by Wells *et al.*[1] The Q_ε value of 2.134±0.011 MeV is from mass differences recently calculated by Ewbank and Raman.[42] The spin and parity assignments shown are based on ^{56}Fe$(p,n\gamma)^{56}$Co experiments and will be discussed in detail later.

The limits on the beta-feeding intensities and associated log ft values shown in Fig. 3 were computed using the experimental uncertainties in the imbalances of the electromagnetic decay intensities. A minimum of 92% and a maximum of 100% for beta feeding to the 1720.2-keV state, results in a log ft between 4.38 and 4.42. A recent shell-model calculation by Goode and Zamick[43] predicts log ft = 5.8 for this 0^+ to 1^+ allowed transition. A maximum of 4% beta feeding to the 1450.7-keV state yields log ft > 6.3. The 0^+ to 0^+ transition to this state is an isospin forbidden ($\Delta T = 1$) Fermi transition[44] for which one might expect[45] log $ft \approx 7.8$. The lower limits of 6.5 and 7.1 on the log ft values for the 0^+ to 2^+ transition to the 970.2-keV state and the 0^+ to 3^+ transition to the 158.3-keV state, respectively, are very small compared to log $ft \approx 12$ expected[45] for these second-forbidden transitions. These discrepancies indicate the difficulty of measuring log ft values to high precision.

The Q_ε value of 2.134 MeV allows the possibility of positron

Figure 3. Decay scheme of ^{56}Ni. The γ-ray energies were measured using the ^{56}Ni decay. The intensities have been rounded off and are normalized to 100 for the 158.4-keV transition strength. The ^{56}Ni decay half life and the half lives of the 158.4-, 970.2-, and 1450.7-keV states are from Ref. 1. The ^{56}Co ground-state half life is from Ref. 5. The Q_{ε} value is from Ref. 42. The spin and parity assignments are from ^{56}Fe$(p,n\gamma)^{56}$Co and are discussed in the text. Log ft values are also discussed in the text.

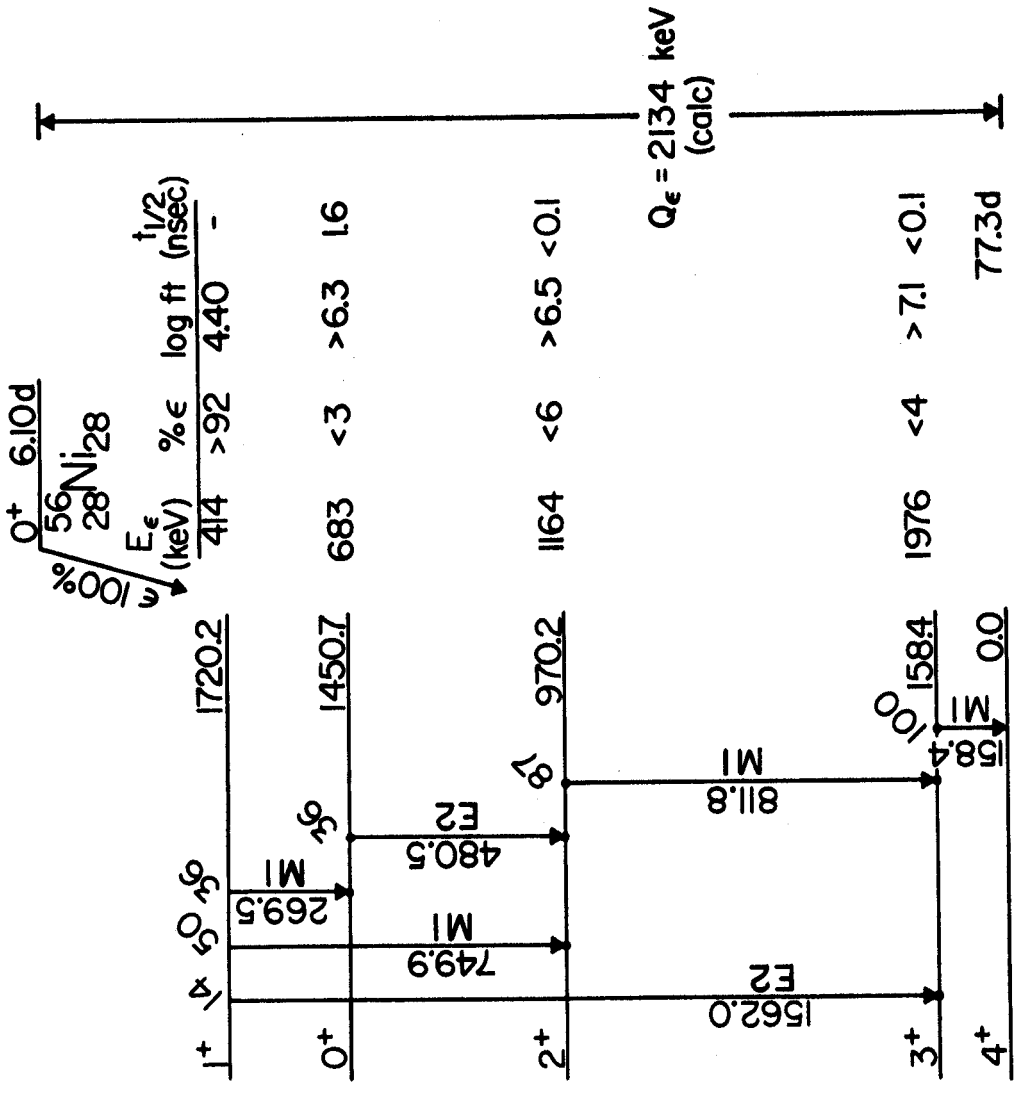
Q_ϵ = 2134 keV (calc)
$^{56}_{28}Ni_{28}$
0+ 6.10d
100%
E_ϵ (keV) 414
%ε >92
log ft 4.40
$t_{1/2}$ (nsec) -
683 <3 >6.3 1.6
1164 <6 >6.5 <0.1
1976 <4 >7.1 <0.1
77.3d
1720.2
1450.7
970.2
158.4
0.0
269.5 M1
480.5 E2
749.9 M1
811.8 M1
1562.0 E2
58.4 M1
1+
0+
2+
3+
4+
$^{56}_{27}Co_{29}$

Figure 3

decay to the ground state and the 158.4- and 970.2-keV states. However, no coincidences with the 511.0-keV annihilation radiation (other than chance) were observed in the ^{56}Ni decay (see Fig. 2). This fact supports the upper limit of 0.01 per decay for the relative intensity of positron emission reported by Sheline and Stoughton.[46]

Weak peaks seen at 427.9, 908.3, and 970.2 keV in the singles spectra taken with the ^{56}Ni sources at 5 cm and weak peaks seen at 428, 639, 908, 970, 1081, and 1292 keV in the γ-γ coincidence spectra, were concluded to be sum-coincidence peaks since they were only found to be in coincidence with appropriate members of the same γ-ray cascade and they all disappeared in singles spectra taken with the sources at 25 cm. (Observable intensities would have been expected if the peaks had been real.) Unfortunately, because of the longer counting time required, the possible 970.2-keV ground-state transition was masked somewhat in the 25 cm measurements by a 968.9-keV background γ radiation from the negatron decay of ^{228}Ac (from the ^{232}Th α-decay chain). However, the 970.2-keV peak apparently disappeared at the larger distance, since the centroid shifted between the 5 cm and the 25 cm measurements by the entire 1.3-keV difference between these two γ rays, and since the peak area at 25 cm was completely accounted for by taking the ratio (measured in the background spectrum) of the areas of the 968.9-keV peak and the slightly more intense 911.1-keV peak which branch from the same excited state in the ^{228}Th daughter.[5,47] There was no evidence to suggest changing the upper limits of 0.01 out of 100 ^{56}Ni decays reported by Piluso *et al.*[4] for the intensities of possible 970.2-, 1292.3-, 1450.7-, and 1720.2-keV γ rays.

A discussion of the 1451-keV excitation region is given in Section IV-H.

III. THE $^{56}Fe(p,n\gamma)^{56}Co$ REACTION

Four types of experiments were performed using the $^{56}Fe(p,n\gamma)^{56}Co$ reaction (Q = -5.357 MeV).[48] In the first type, γ-γ coincidences were measured with a Ge(Li)-Ge(Li) spectrometer for ^{56}Co excitations up to 2.85 MeV. These coincidences identified ^{56}Co γ rays and allowed placement in the excited-state decay scheme. Except for the special cases of ground-state transitions with no coincidences, this method was very powerful. In the second type of experiment, excitation functions of the various ^{56}Co γ rays were measured from below the (p,n) threshold up to 2.26 MeV of excitation. Individual spectra provided γ-ray branching ratios, while the excitation functions provided threshold information (and hence, evidence for γ-ray placement in the excited-state decay scheme), information on relative cross sections as a function of proton energy (and hence, evidence for spin assignments), and an indication of the level density and the degree of statistical averaging in the compound nucleus. In the third type of experiment, angular distributions of the various Co γ rays were measured for excitations up to 1.91 MeV. Beam energies were chosen, where possible, such that the state in question was not fed from above by γ-ray transitions. The γ-ray angular distributions provided information on spins, γ-ray multipole mixing ratios, and γ-ray branching ratios. In the fourth type of experiment, absolute cross sections for excitations of the first eight excited states of ^{56}Co were measured at a beam energy of 7.30 MeV. The experimental absolute cross sections offer direct comparisons with theoretical cross-section predictions of the statistical CN theory. In the following discussions, ^{56}Co γ rays and excited states are

referred to with energies measured using $^{56}Fe(p,n\gamma)^{56}Co$. In a few instances these energies are slightly different from ^{56}Ni decay values. The adopted energies appear in Section VI.

A. γ-γ Coincidences

Proton beams (all beam energies quoted in this paper are in the laboratory system) of 7.38 and 8.36 MeV (corresponding to excitations in ^{56}Co of about 1.89 and 2.85 MeV, respectively) were obtained from the MSU Cyclotron for the in-beam γ-γ coincidence measurements. The target was a 0.90 mg/cm^2 iron foil enriched to 99.4% ^{56}Fe. The 2.5%-efficient Ge(Li) detector (previously described) and a 7.4%-efficient Ge(Li) detector with a peak-to-Compton ratio of 25:1 and FWHM resolution of 3.5 keV were positioned as shown in Fig. 4. The lead block between the detectors has a 1.3 cm diameter hole drilled almost through it and served as a shielded beam stop as well as an attenuator for photons Compton scattered from one detector toward the other.

A typical two-parameter, fast-slow coincidence arrangement with constant-fraction timing discrimination was used. The single-channel analyzer window ($2\tau \cong 50$ nsec) set on the output from a time-to-amplitude converter was a few nanoseconds less than the interval between cyclotron beam bursts. The 77-day half life of the ^{56}Co ground state resulted in minimal radioactivity build-up in the target, and insured that most detected γ rays were from beam induced reactions. The coincidence events were stored on magnetic tape and later sorted off-line using background subtraction as described previously for the beta decay work. The 7.38-MeV spectra contain about 1 million coincidence events accumulated in 12 hours of counting, while the 8.36-MeV spectra contain close to 7 million coincidence events accumulated in 31 hours. Typical singles counting rates for both experiments were 7000 cts/sec in the 2.5%-efficient detector and 20,000 cts/sec

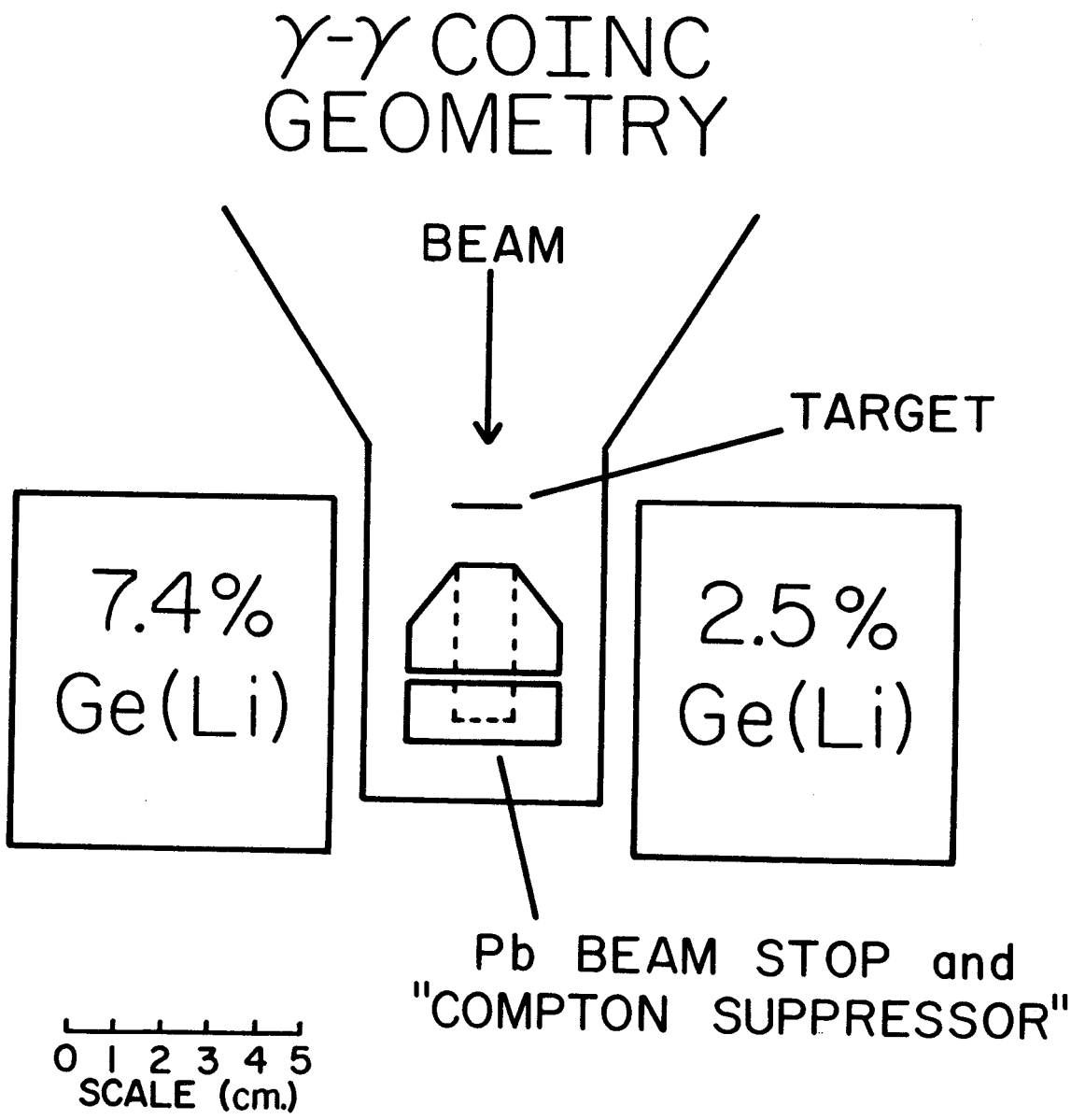

Figure 4. Geometry for the in-beam γ-γ coincidence measurements. The squares are not meant to represent the actual size of the Ge(Li) detectors, but only the approximate location of their cryostat caps.

in the 7.4%-efficient detector. The average beam current was about 7 nA.

The two integral spectra and some representative gated spectra from the experiment with E_p = 8.36 MeV are shown in Fig. 5. Thirty-five γ rays were definitely identified to be from ^{56}Co, and 6 others are possibly from the same nucleus. These include 21 γ rays previously reported by Del Vecchio *et al.*[24] to be in coincidence with neutrons from the same reaction. The energies (as determined below) of the ^{56}Co γ rays are listed in Table III; the coincidence relationships between these γ rays are listed in Table IV. (For brevity, the coincidence data taken at E_p = 7.38 MeV and many gated spectra taken at E_p = 8.36 MeV are not shown here. All the gated coincidence spectra from which the coincidence relationships were derived and from which energy calibrations were determined, can be found in an Appendix to Ref. 49.)

As a supplement to the coincidence experiments, the energies of those γ rays from the excited states of ^{56}Co up to and including the 1720.3-keV state (excluding the 1561.7-keV γ ray) were determined by taking a γ-ray singles spectrum of ^{56}Fe$(p,n\gamma)^{56}$Co at E_p = 7.30 MeV in the presence of the well-known γ-ray energy standards ^{22}Na, ^{75}Se, ^{88}Y, ^{118}Sn, and ^{137}Cs. The calibration energies assumed are presented in Table V. The remaining energies of the 1561.7-keV γ ray and the γ rays from the excited states of 1930.4 keV and above, were determined from the various γ-γ coincidence gated spectra. In both cases, prominent ^{56}Fe γ rays from the ^{56}Fe$(p,p'\gamma)$ reaction (see Table V) were used as sone of the energy standards. For the γ-ray energy determinations from the γ-ray singles data, a quadratic fit was made to the measured centroids (analyzed by SAMPO[34]) versus calibration

Figure 5. Integral coincidence and representative gated spectra from the $^{56}Fe(p,n\gamma\text{-}\gamma)^{56}Co$ γ-γ coincidence experiment at E_p = 8.36 MeV. γ-rays labeled with a question mark, although they appear to be in coincidence, could not be placed in the decay scheme. Peaks labeled in parenthesis are believed to be from chance coincidences or insufficient background subtraction.

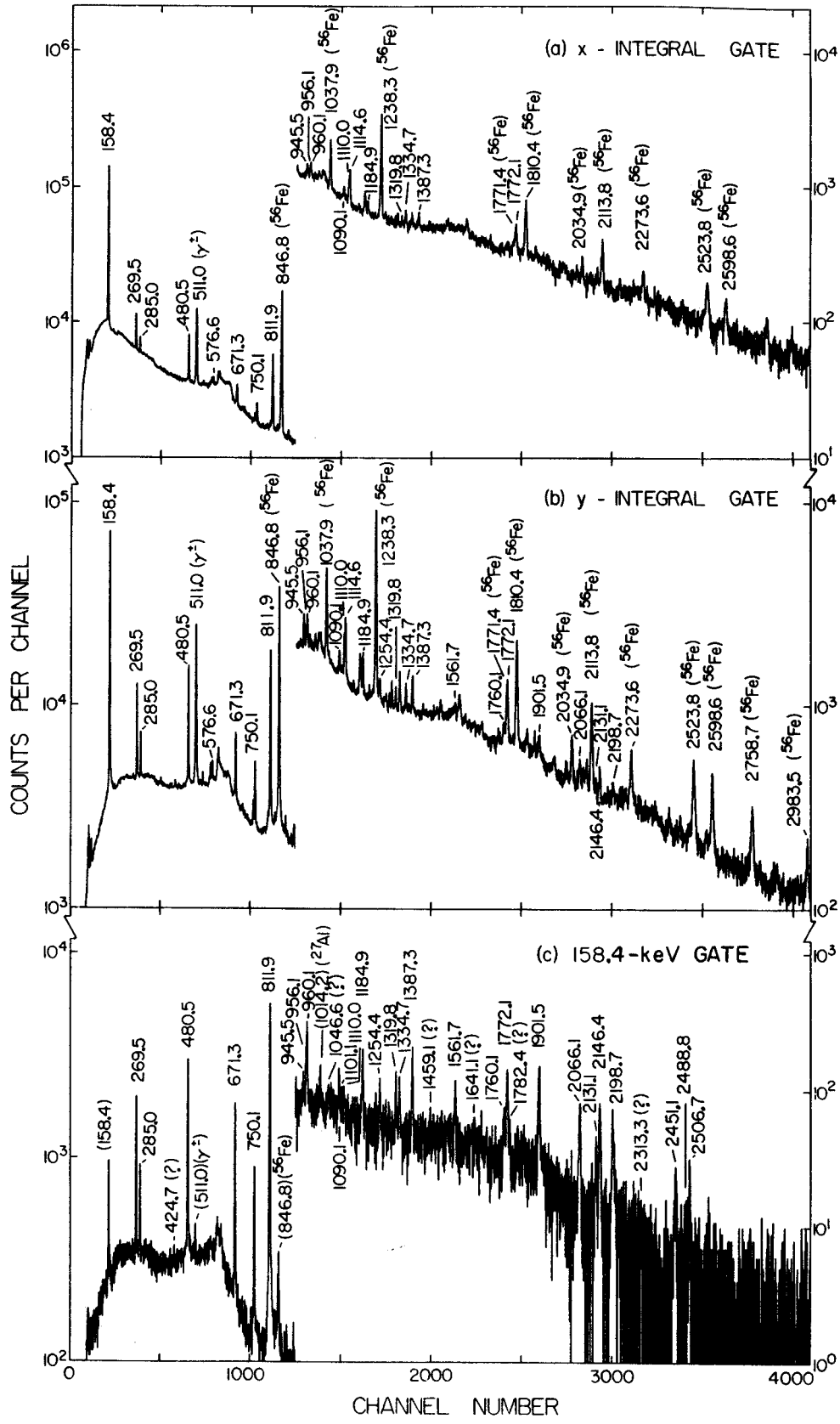
(a) x - INTEGRAL GATE
(b) y - INTEGRAL GATE
(c) 158.4-keV GATE
COUNTS PER CHANNEL
CHANNEL NUMBER
158.4
269.5
285.0
480.5
511.0 (y±)
576.6
671.3
750.1
811.9
846.8 (56Fe)
945.5
956.1
960.1
1037.9 (56Fe)
1090.1
1110.0
1114.6
1184.9
1238.3 (56Fe)
1319.8
1334.7
1387.3
1561.7
1760.1
1771.4 (56Fe)
1772.1
1810.4 (56Fe)
1901.5
2034.9 (56Fe)
2066.1
2113.8 (56Fe)
2131
2198.7
2273.6 (56Fe)
2523.8 (56Fe)
2598.6 (56Fe)
2758.7 (56Fe)
2983.5 (56Fe)
2146.4
(158.4)
424.7 (?)
(511.0)(y±)
(846.8)(56Fe)
1046.6 (?)
1101.1
1254.4
1459.1 (?)
1641.1 (?)
1782.4 (?)
2313.3 (?)
2451.1
2488.8
2506.7
(27Al)

Figure 5

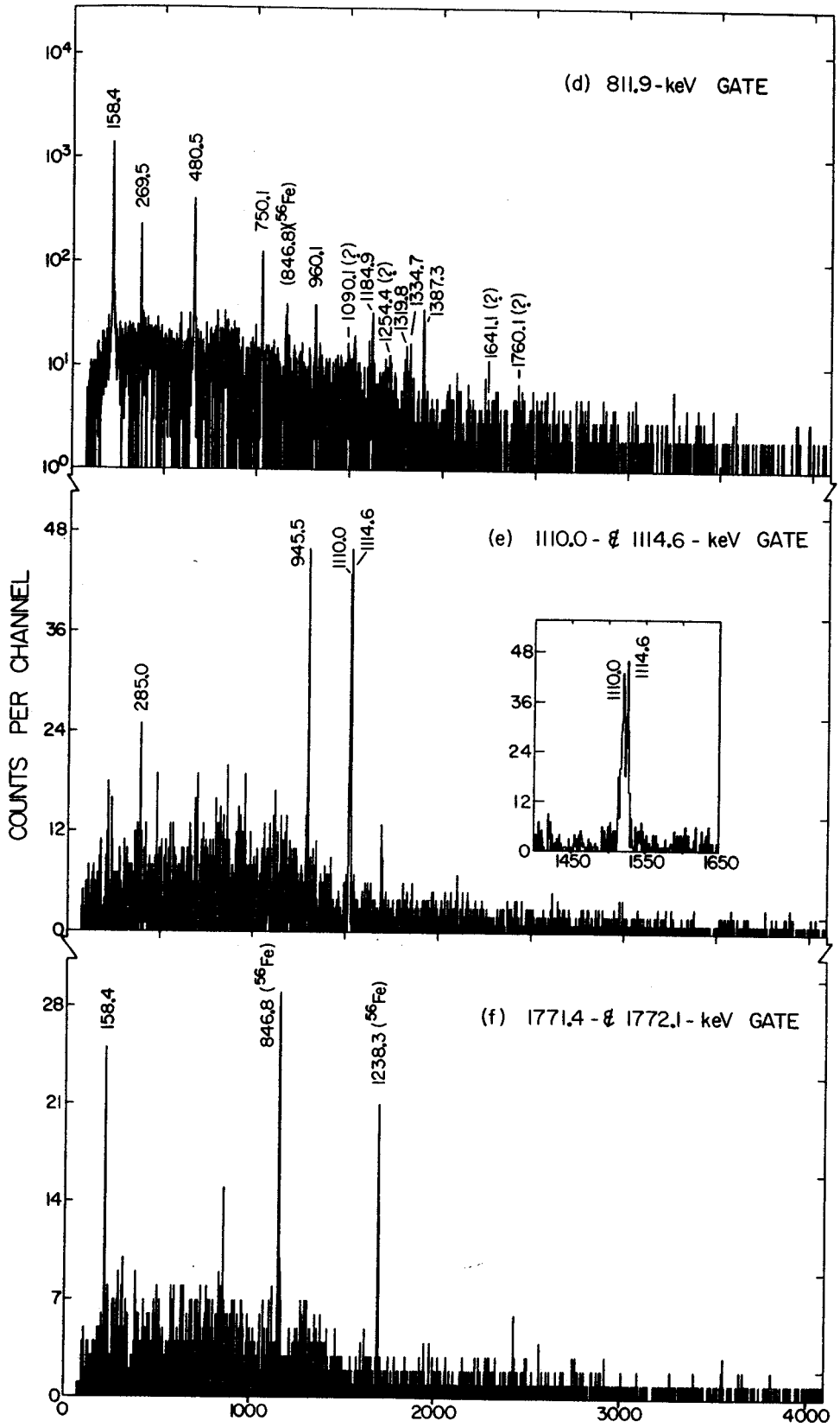

Figure 5 Continued

Table III. Energies of γ rays found in ^{56}Co at excitations up to 2.86 MeV from ^{56}Fe($p,n\gamma$)^{56}Co. Unless otherwise indicated, the identification of ^{56}Co γ rays are based upon both γ-ray excitation functions and γ–γ coincidences.

Transition energies (keV)			
Present work[a]	n–γ coincidence (Ref. 22)[b]	Present work[a]	n–γ coincidence (Ref. 22)[b]
158.4±0.1	158.5	1254.4±0.3[c]	
269.5±0.1	269.7	1319.8±0.3[c]	1317.9
285.0±0.1	284.7	1334.7±0.3[c]	
(424.7±0.2)[c]		1387.3±0.3[c]	1387.1
432.8±0.2		(1459.1±0.6)[c]	
480.5±0.1	480.4	1561.7±0.4	
576.6±0.1	576.4	(1641.1±0.7)[c]	
671.3±0.1	671.3	1760.1±0.5[c]	
750.1±0.1	750.0	1772.1±0.4[c]	1771.5
811.9±0.1	812.0	(1782.4±0.6)[c]	
829.8±0.1	830.0	1892.7±0.4[c]	
945.5±0.2	945.4	1901.5±0.4	1901.3
956.1±0.3		2066.1±0.4[c]	2066.5
960.1±0.2	959.6	2131.1±0.5[c]	2129.5
1009.2±0.1[d]	1009.3	2146.4±0.5[c]	2145.0
(1046.6±0.5)[c]		2198.7±0.5[c]	
1090.1±0.4[c]		(2313.3±0.9)[c]	
1101.1±0.5[c]		2451.1±0.7[c]	
1110.0±0.2		2488.8±0.7[c]	
1114.6±0.1	1114.6	2506.7±0.7[c]	
1184.9±0.2[c]			

[a] Those γ-ray energies presented in parentheses are from weak transitions believed to belong to ^{56}Co but which could not be placed in the decay scheme.

[b] The energy errors of all γ rays listed are ±0.5 keV.

[c] Identification was based upon γ–γ coincidences only.

[d] Identification was based upon γ-ray excitation functions only.

Table IV. Results of two parameter γ-γ coincidence experiments from $^{56}Fe(p,n\gamma\text{-}\gamma)^{56}Co$.

Gated γ ray (keV)	Coincident γ rays[a] (keV)
158.4	269.5(4.9), 285.0(1.8),(424.7)[b](0.45), 480.5 (20.), 671.3(21.), 750.1(12.), 811.9(≡100.), 945.5(0.74), 956.1(1.6), 960.1(5.3), (1046.6)[b] (0.97), 1090.1(2.1), 1101.1(1.1), 1110.0(1.1), 1184.9(4.7), 1254.4(2.1), 1319.8(3.0), 1334.7 (3.3), 1387.3(6.3), (1459.1)[b](1.2), 1561.7 (4.0), (1641.1)[b](1.1), 1760.1(2.7), 1772.1(8.0), (1782.4)[b](1.3), 1901.5(10.), 2066.1(7.0), 2131.1 (4.0), 2146.4(9.4), 2198.7(7.1), (2313.3)[b](0.89), 2451.1(2.7), 2488.8(1.0), 2506.7(3.1)
269.5	158.4(16.), 480.5(85.), 811.9(≡100.)
285.0	158.4(13.), 671.3(≡100.), 829.8(32.), 945.5(16.), 1110.0(23.)
480.5	158.4(16.), 269.5(17.), 811.9(≡100.), 1184.9(16.)
576.6	432.8(11.0), 1892.7(≡100.)
671.3	158.4(≡100.), 285.0(51.), (945.5)[c](24.)
750.1	158.4, 811.9
811.9	158.4(73.), 269.5(23.), 480.5(≡100.), 750.1(66.), 960.1(32.), (1090.1)[c], 1184.9(26.), (1254.4)[c], 1319.8(10.), 1334.7(13.), 1387.3(33.), (1641.1)[c], (1760.1)[c]
829.8	285.0
945.5	158.4(5.2), 285.0(12.), 671.3(23.), 1114.6(≡100.)
956.1 & 960.1	158.4, 811.9
1110.0 & 1114.6	285.0(7.1), 945.5(70.), 1110.0(≡100.), 1114.6(84.)
1090.1	158.4, 811.9
1184.9	158.4(65.), 480.5(≡100.), 811.9(67.)
1254.4	158.4, 811.9
1319.8	158.4, 811.9
1334.7	158.4, 811.9

Table IV (continued)

Gated γ ray (keV)	Coincident γ rays[a] (keV)
1387.3	158.4, 811.9
1561.7	158.4
1760.1	158.4, (811.9)[c]
1772.1	158.4
1782.4	(158.4)[c]
1901.5	158.4
2066.1	158.4
2131.1	158.4
2146.4	158.4
2198.7	158.4

[a]Numbers in parentheses following the γ-ray energies represent the γ-ray relative intensities (normalized to 100. for the most intense peak) observed in that particular gated spectrum. It should be carefully noted that since these numbers are highly geometry dependent (because of angular correlation effects), they are presented solely as a crude indication of the peak intensities that one might expect to observe in a similar experiment.

[b]These γ rays seem to be in coincidence with the gated γ ray but could not be placed explicitly in the excited-state decay scheme.

[c]These γ-ray peaks did not have sufficient statistics to warrant the claim of a definite coincidence.

Table V. γ-ray energy standards used as calibrations in the determination of ^{56}Co γ-ray energies from ^{56}Fe$(p,n\gamma)^{56}$Co. Those γ rays listed for the isotope ^{56}Fe appeared in the spectra from ^{56}Fe$(p,p'\gamma)$.

Isotope	Calibration energy (keV)	Reference	Isotope	Calibration energy (keV)	Reference
^{75}Se	121.113±0.010	a	^{56}Fe	1175.13±0.05	c
	135.998±0.010	a		1238.30±0.02	c
	264.651±0.015	a		1360.22±0.03	c
	279.525±0.012	a		1810.44±0.58	c
	400.640±0.015	a		2034.92±0.03	c
^{113}Sn	391.689±0.010	a		2113.81±0.15	c
^{137}Cs	661.635±0.076	b		2273.6 ±1.5	d
^{88}Y	898.04 ±0.04	b		2523.8 ±0.08	c
^{22}Na	1274.55 ±0.04	b		2598.58±0.03	c
^{56}Fe	846.79 ±0.08	c		2758.7 ±2.1	d
	1037.91 ±0.03	c		2983.5 ±1.6	d

[a] See Ref. 36.

[b] See Ref. 35.

[c] See Ref. 39; these calibration energies were determined in Ref. 39, using the decay of ^{56}Co.

[d] See Ref. 57; these calibration energies were determined in Ref. 57, using ^{56}Fe$(n,n'\gamma)$.

energies in one energy region (120-1300 keV). For the γ-ray energy determinations from the γ-γ coincidence data, a similar quadratic fit was made in one energy region (800-3000 keV). In the latter, the ^{56}Fe calibration peak centroids were determined from a spectrum gated on the intense 846.8-keV ^{56}Fe γ-ray peak. The ^{56}Co γ-ray energies were then calculated by computer using the appropriate calibration curve. The energies of six γ rays found in both the ^{56}Ni decay and the ^{56}Fe(p,$n\gamma$)^{56}Co reaction, agree to within the experimental errors (see Tables I and III). The adopted energies of these six γ rays are listed in Section VI.

The excited-state decay scheme in Fig. 6 is consistent with the coincidence data and the excitation function data (next section). Dots denote observed coincidence relationships between γ-ray transitions entering and leaving a state. The beam energies (and the corresponding maximum possible ^{56}Co excitations) at which the coincidence and angular distribution data were taken are shown on the right. The spin assignments for states up to and including the 1720.3-keV state, are based on the present experiments and will be discussed in detail later in Section IV. The spin and parity assignments to the states at 1930.4 keV and above are those of Schneider and Daehnik[15] and are consistent with these and other experiments.

The positive parities shown in Fig. 6, up to and including that for the 1720.3-keV state, could not be determined in the present work and are therefore assumed. This assumption is supported, however, by the even ℓ transfers observed in the (d,α) experiment of Schneider and Daehnik[15] and in the (p,^{3}He) experiment of Bruge and Leonard,[12] and by shell-model considerations.[30,50] In its simplest shell-model

Figure 6. The γ-ray decay scheme for excitations of ^{57}Co. The γ-ray energies and branching ratios were measured using ^{57}Fe$(p,n\gamma)^{56}$Co. The arrows on the right indicate the maximum possible excitations for the proton energies of the γ-γ coincidence and γ-ray angular distribution experiments. The spins, parities, and level energies labeled with an asterisk are from Ref. 15, while the remaining values were determined from ^{56}Fe$(p,n\gamma)^{56}$Co. Dots denote observed coincidence relationships between γ-ray transitions entering and leaving a state.

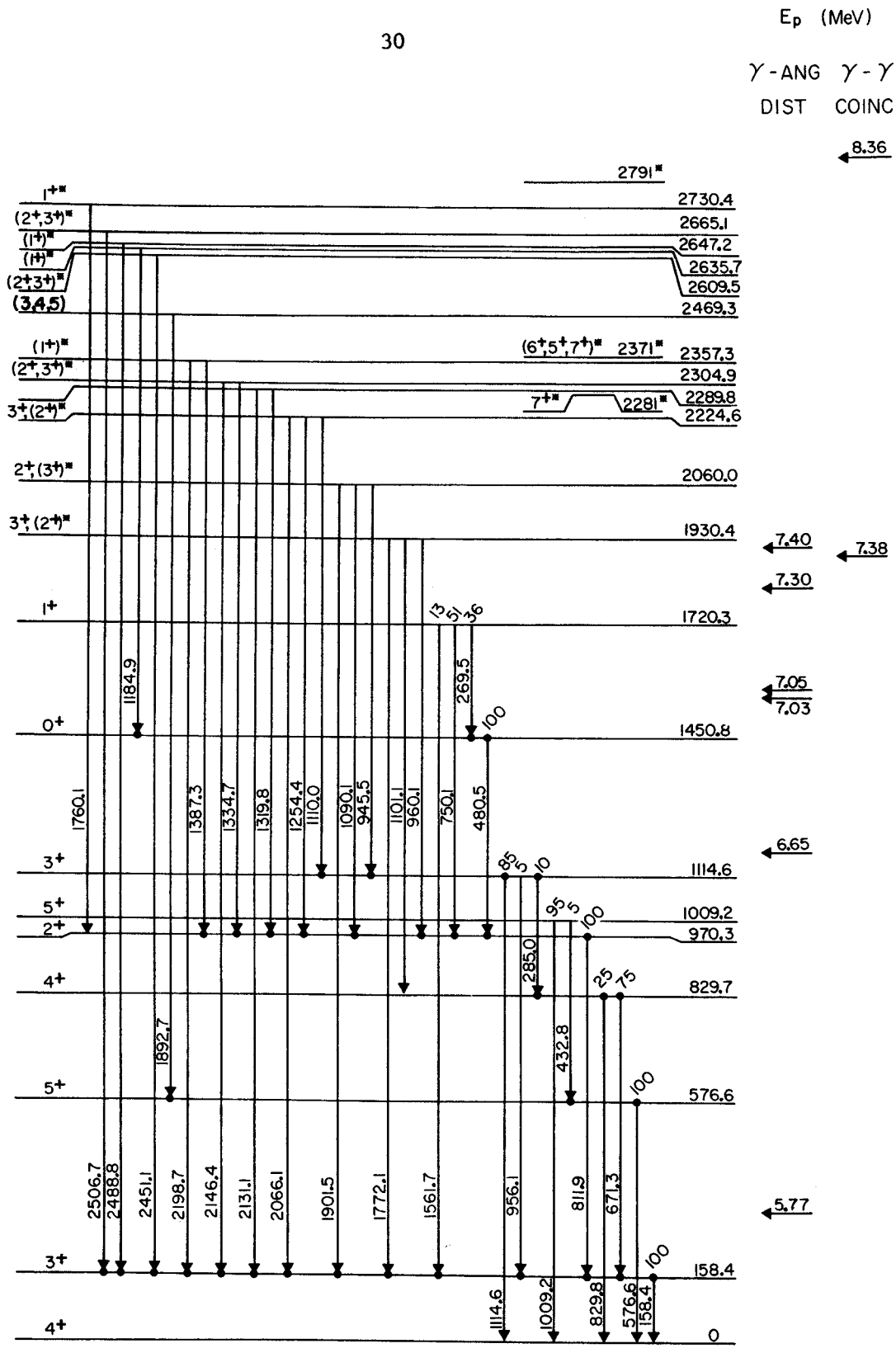

$^{56}_{27}Co_{29}$

Figure 6

configuration, ^{56}Co has two valence nucleons: a proton hole in the $f_{7/2}$ orbit and a neutron in the $p_{3/2}$ orbit. Since the three nearest orbits available for particle excitations ($p_{3/2}$, $f_{5/2}$, and $p_{1/2}$) have odd parities, all states formed with the required even number of valence nucleons will necessarily have a total even parity. The simplest shell-model states having odd parities that can be formed, have particle configurations $[(\pi d_{3/2})^{-1}(\nu p_{3/2})]$ and $[(\pi f_{7/2})^{-1}(\nu g_{9/2})]$. Because of the energy required for formation, such states would be expected at considerably higher excitations.

Because of the high Compton continuum and the large number of ^{56}Fe γ rays from the ^{56}Fe$(p,p'\gamma)$ reaction that occur in all singles spectra, ground-state transitions in ^{56}Co having no coincidences and having energies greater than 2 MeV are difficult to identify. Thus, although some such ground-state transitions would be expected from states excited in the present experiments, none were positively identified. Also, because of these same reasons, branching ratios for those states above 1.8 MeV of excitation could not be determined.

B. γ-Ray Excitation Functions

The γ-ray excitation functions were obtained with proton beams having energies ranging from 5.55 to 7.75 MeV. These beams were stepped in 100 keV intervals with the Western Michigan University Tandem Van de Graaff. The target was the same ^{56}Fe foil used in the coincidence studies and contributed approximately 40 keV to the energy spread of the proton beams. The γ rays from the $^{56}Fe(p,n\gamma)^{56}Co$ reaction were detected with the 2.5%-efficient Ge(Li) detector (previously described) at approximately 125° from the beam direction (to minimize angular distribution effects) and at 5 cm from the target.

Dead-time and amplifier pile-up corrections, as well as run-to-run normalizations, were made by using the digitized output from a beam current integrator to trigger a Berkley Nucleonics Corporation model #BH-1 Tail Pulse Generator. The pulser was in turn connected to the test input of the detector's preamplifier. The resulting pulser peak in the γ-ray spectrum was placed so as not to interfere with γ-ray peaks. Again, to preserve optimum resolution and symmetric peak shapes, an ORTEC model #450 Research Amplifier was direct coupled to a Northern Scientific 100-MHz ADC. The γ-ray spectra were stored in 4096 channels with approximately 0.5 keV per channel in the WMU on-line PDP-15 computer. Typical run times were 50 minutes with counting rates of less than 6000 cts/sec.

Typical γ-ray spectra which show the appearance and growth of the various ^{56}Co γ rays are shown in Fig. 7. In addition to seventeen ^{56}Co γ rays previously identified from the coincidence experiments, a 1009.2-keV ground-state transition was identified. The approximate

Figure 7. Typical γ-ray spectra from the excitation function measurements. the first appearances of the various ^{56}Co γ rays are labeled.

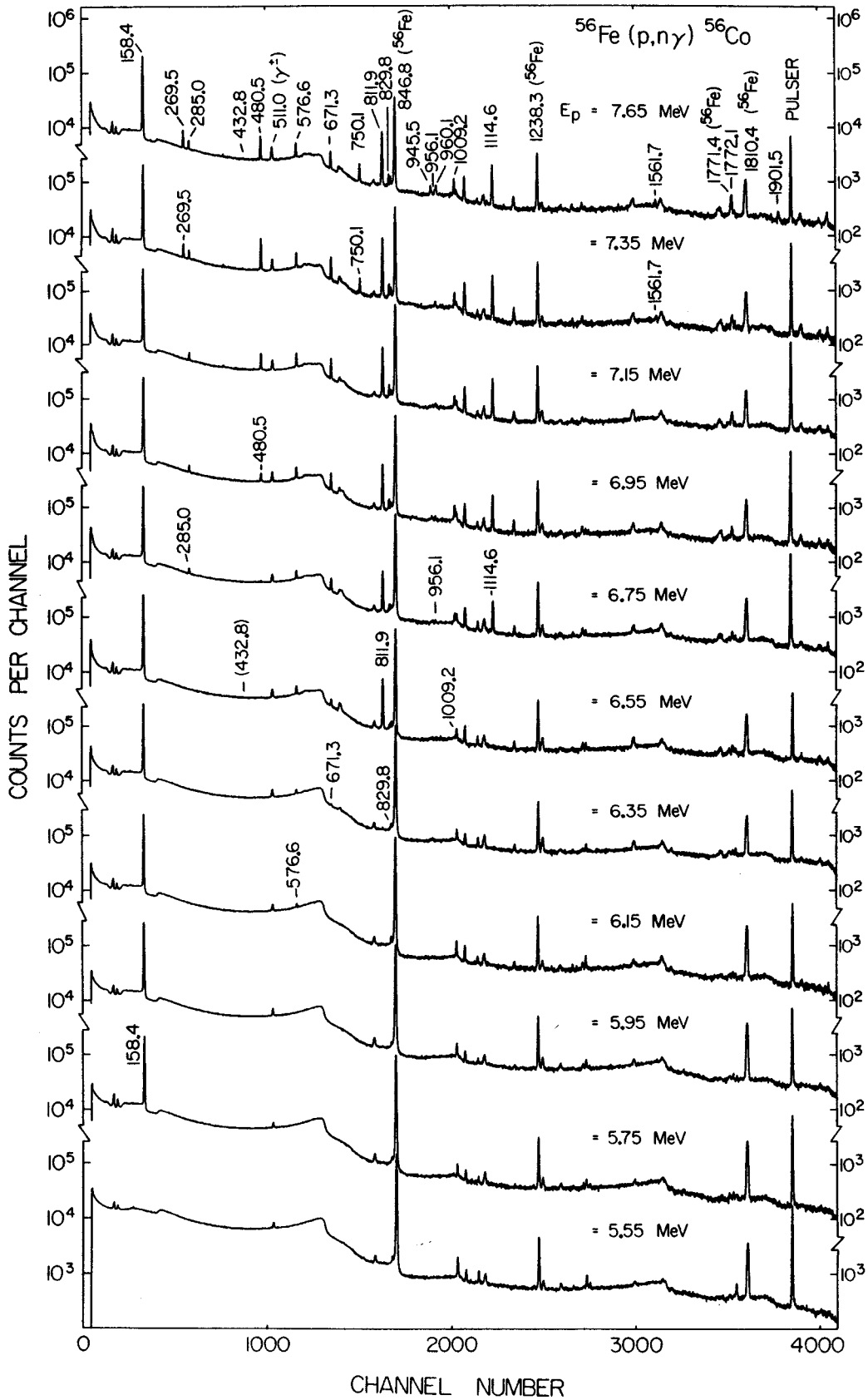
^{56}Fe (p,nγ) ^{56}Co
E_p = 7.65 MeV
158.4
269.5
285.0
432.8
480.5
511.0 (γ-)
576.6
671.3
750.1
811.9
829.8
846.8 (^{56}Fe)
945.5
956.1
960.1
1009.2
1114.6
1238.3 (^{56}Fe)
1561.7
1771.4 (^{56}Fe)
1772.1
1810.4 (^{56}Fe)
1901.5
PULSER
= 7.35 MeV
= 7.15 MeV
= 6.95 MeV
= 6.75 MeV
= 6.55 MeV
= 6.35 MeV
= 6.15 MeV
= 5.95 MeV
= 5.75 MeV
= 5.55 MeV
COUNTS PER CHANNEL
CHANNEL NUMBER
0
1000
2000
3000
4000

Figure 7

thresholds of the ^{56}Co γ rays were completely in agreement with their placement in the excited-state decay scheme.

The excitation functions for the first eight excited states of ^{56}Co, measured to a maximum excitation of 2.26 MeV, are shown in Fig. 8. For each data point the total neutron population of the state was determined by subtracting the intensities of all the γ rays feeding the state (where appropriate) from the intensities of all the γ rays deexciting the state. Internal-conversion corrections were neglected since they were small in comparison to other errors. (The largest correction would be 1% for the 158.4-keV M1 transition.[2]) The γ-ray intensities were determined from the peak areas obtained using SAMPO[34] and the detector's relative efficiency curve. The neutron population of each state at each beam energy was normalized by dividing by the pulser peak area.

The most noticeable features of the excitation functions are the large fluctuations. The maximum experimental error associated with any given point is 12% whereas the point-to-point fluctuations average 15% and some are as high as 100%. Since the fluctuations do not correlate in sign and magnitude from state to state, it is unlikely that they originate from an incorrect experimental technique. Hausman *et al.*[51] observed this same phenomenon in their low energy ^{48}Ti$(p,p'\gamma)$ experiment (there, a CN excitation of $\approx$11.7 MeV was achieved). Since their fluctuations persisted from angle to angle and were approximately 100-keV wide, they suggested that the peaks were neither due to Ericson-type fluctuations nor due to isolated resonances, but instead were caused by several overlapping resonances. Since the statistical CN excitation-function predictions agreed well, both in shape and in

Figure 8. Excitation functions for the first eight excited states of ^{56}Co. The units of the ordinate are arbitrary but are proportional to the absolute cross section. The data were taken at 125°, a zero of $P_2(\cos\theta)$, in order to minimize angular distribution effects. Neutron feedings were computed for each level from the γ-ray intensity imbalances, and then were normalized from run to run (as described in the text) to obtain the relative cross sections. The thresholds were calculated using Q = -5.357 MeV for the ground state (Ref. 48) and are connected to the first non-zero data points with dotted lines. Solid lines connect the data to guide the eye. Where not visible, error bars are smaller than the data-point symbol.

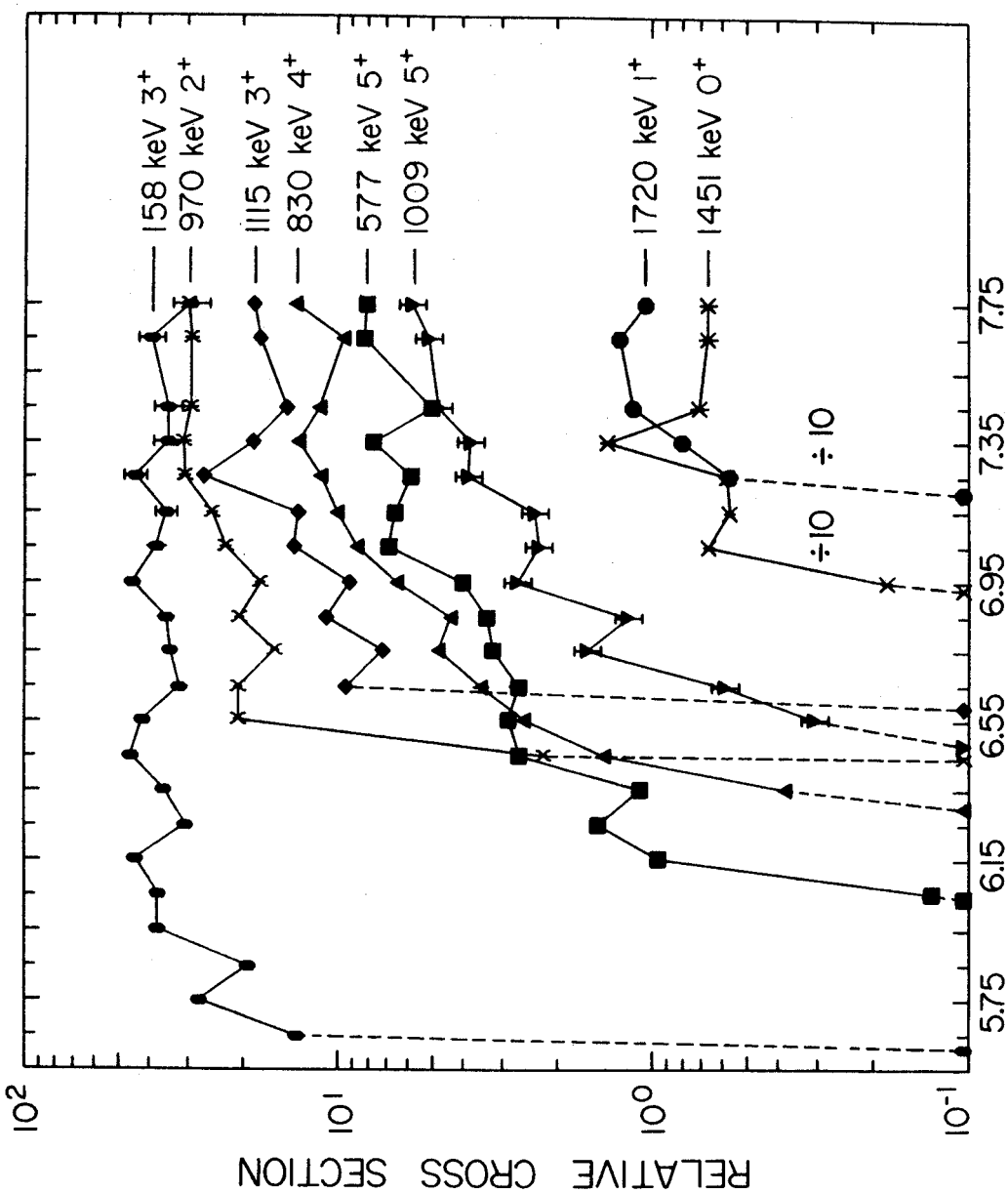
158 keV 3+
970 keV 2+
1115 keV 3+
830 keV 4+
577 keV 5+
1009 keV 5+
1720 keV 1+
1451 keV 0+
÷10
÷10
RELATIVE CROSS SECTION
10^2
10^1
10^0
10^-1
5.75
6.15
6.55
6.95
7.35
7.75
Ep (MeV)

Figure 8

absolute magnitude with their data averaged over 200-keV energy intervals, they further concluded that an experimental energy spread of 200 keV would have resulted in good statistical averaging whereas their actual 50-keV spread was too small.

In similar experiments with A ≈ 60 and CN excitations of 10-15 MeV, Lee *et al.*[52] observed fluctuations on the order of 2-3 times the experimental resolution. They suggested that the assumption of complete randomness of the statistical CN theory may be invalid and that some residual interactions may cause clustering of strong levels which give rise to the gross fluctuations. No conclusions can be drawn from the present experiment concerning the above suggestions other than to say that similar gross fluctuations have been observed.

From level-density studies by Huizenga and Katsonos,[53] the average level spacing in ^{57}Co (assuming similarity to ^{57}Fe for which empirical parameters are known) at a CN excitation of about 12 MeV (corresponding to a beam energy of about 6 MeV) is expected to be 0.03 keV. Thus, the energy spread of 40 keV is predicted to overlap ≈1300 CN states of mixed spin and parity in the present experiment. The overlap predicted for ^{49}V in the experiment of Hausman *et al.*,[51] was ≈1800 CN states Thus, the conclusion here is similar to that of Hausman *et al.*,[51] namely, that since the agreement between experimental and theoretical cross-section ratios and γ-ray angular distributions is so good (see below), the statistical CN theory reasonably describes the situation even though complete statistical averaging is not achieved.

In order to compare the excitation functions with the predictions

of the statistical CN theory, experimental and theoretical cross sections for the various excited states of ^{56}Co are plotted in Fig. 9 as ratios with respect to those for the 158.4-keV first excited state. As is shown in Fig. 9 the theoretically predicted cross sections vary as a function of the spin and parity of the final excited state. This fact can be seen most easily from the following expression for the total cross section:

$$\sigma = \frac{\lambda^2}{8\pi} \sum_{j_1, j_2} (2J+1)\tau$$

where λ is the wavelength of the incoming proton, J_1 is the spin of the intermediate state in the compound nucleus, and τ is the penetrability term. The penetrability τ is determined from the following expression:

$$\tau = \frac{T_{\ell_1 j_1}(E_1) T_{\ell_2 j_2}(E_2)}{\sum T_{\ell j}(E)}$$

where the $T_{\ell j}(E)$'s are the various particle transmission coefficients which depend upon the particle's center-of-mass energy, E, and orbital and total angular momentum, ℓ and j, respectively. The sum in the denominator extends over all open channels by which the intermediate CN state can decay.

The sum in the total cross-section expression is made over all possible values of j_1 and j_2, which are the total angular momentum of the incoming protons and outgoing neutrons, respectively. Since this sum involves the spin of the intermediate compound-nuclear state, parity conservation and the angular momentum coupling rules require

Figure 9. Experimental and theoretical cross-section ratios. The ratios are taken with respect to the 158.4-keV first excited state. Error bars identify the data (lines connecting the data are to guide the eye). MANDY predictions for selected beam energies are shown for $J^{\pi} = 0^{+},..,6^{+}$. A $J^{\pi} = 3^{+}$ for the 158.4 keV state was used as explained in the text. Straight lines connecting the theoretical points approximate expected smooth curves.

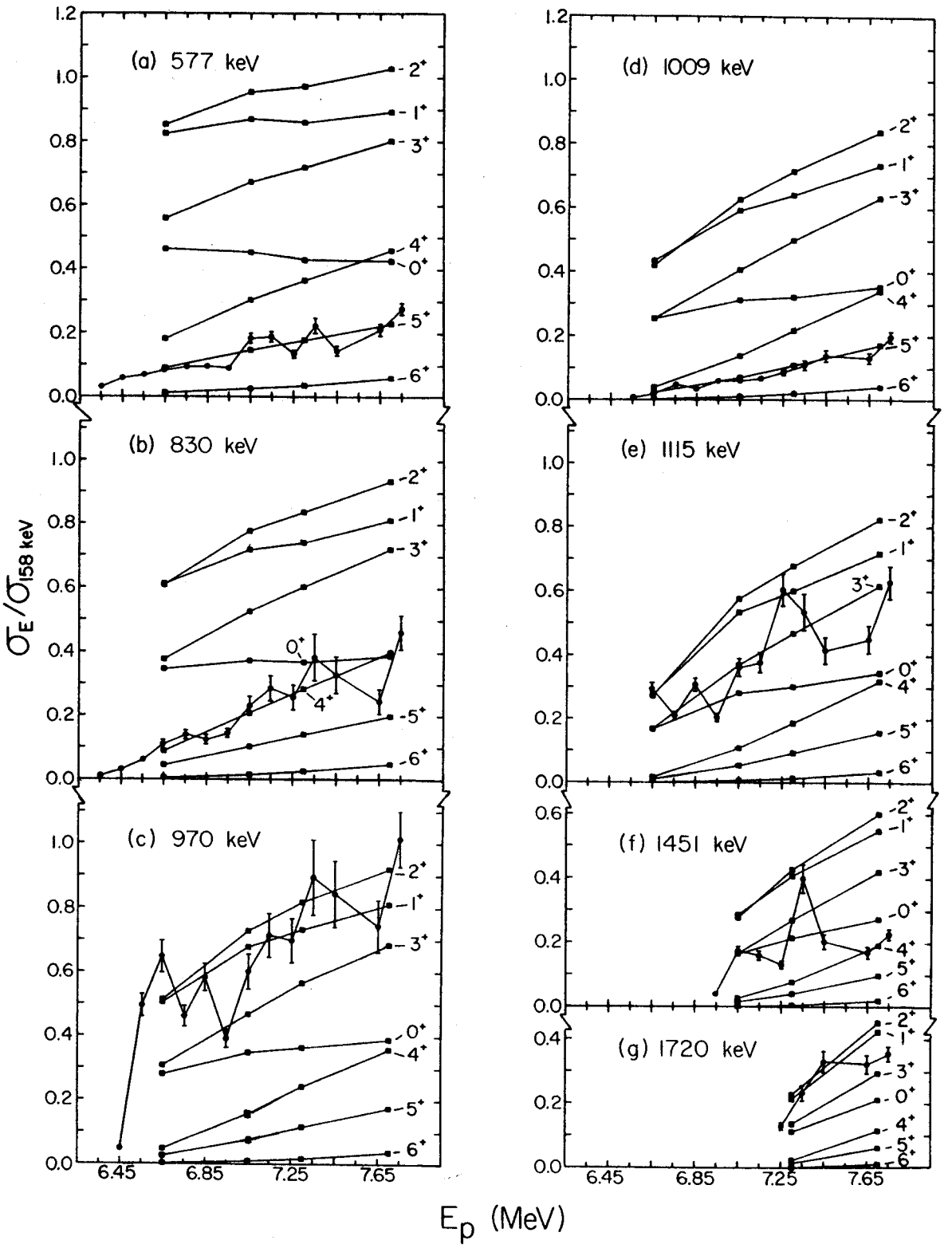
(a) 577 keV
(b) 830 keV
(c) 970 keV
(d) 1009 keV
(e) 1115 keV
(f) 1451 keV
(g) 1720 keV
$\sigma_E/\sigma_{158\ keV}$
E_p (MeV)
6.45
6.85
7.25
7.65

Figure 9

a different sum over the numerical τ-values for each possible final excited-state spin and parity. Since the target has $J^{\pi} = 0^{+}$ and since the outgoing neutrons are mostly $\ell = 0$, low (high) spin final states are reached predominantly through low (high) spin intermediate states which are in turn reached by low (high) angular momentum protons. At these bombarding energies (5.5 - 7.5 MeV), the incoming protons are predominantly $\ell=2$. Thus, the cross sections are expected to be largest for J values of 1, 2, or 3. The division of the cross section to each final state by that to the 158.4-keV state at the same proton energy, removes the absolute normalization and thus makes the comparison of the experimental and theoretical values quantitative. The interpretation of Fig. 9 in regard to spin assignments is discussed in Section IV.

The theoretical cross sections used above and the theoretical angular distribution parameters A_2^* and A_4^* were calculated using the statistical CN computer code MANDY written by Sheldon, Gantenbein, and Strang.[54] MANDY requires as input the transmission coefficients $T_{\ell j}(E)$ for all open entrance and exit channels. These coefficients were computed with a modified version of the optical-model code ABACUS - II.[55] For the real spin-independent pair of the nuclear potential, the usual Wood-Saxon form was used; for the imaginary part, the derivative of the Wood-Saxon form was used; and for the spin-orbit part, the Thomas form was used.

The proton transmission coefficients were calculated using the local optical-model parameters listed in Table VI. These parameters were determined by Perey[56] from elastic scattering data in the 9-22 MeV range. It was assumed that the explicit energy dependence would

Table VI. Form of the optical-model potential and parameters used in the calculations of transmission coefficients. The Coulomb potential, $V_c(r)$, is that due to a uniformly charged sphere of radius $1.25A^{1/3}$ [F]. The parameter E is the center-of-mass energy of the nucleon in MeV.

Nucleon	V_o (MeV)	W_D (MeV)	r_o (F)	r_o' (F)	a (F)	a' (F)	V_{so} (MeV)
Proton[a]	$46.7-0.32E + ZA^{-1/3}$	11	1.25	1.25	0.65	0.47	7.5
Neutron[b]	48.0 - 0.29E	10	1.25	1.25	0.65	0.47	7.5

$$V = V_c(r) - V_o \frac{1}{1 + e^{(r-R)/a}} + i W_D \frac{d}{dr} \frac{4a'}{1 + e^{(r-R')/a'}} + \left(\frac{h}{m_\pi c}\right)^2 \frac{V_{so}}{r} \ell \cdot \sigma \frac{d}{dr} \frac{1}{1 + e^{(r-R)/a}};$$

$$R = r_o A^{1/3}, \; R' = r_o' A^{1/3}$$

[a]The proton parameters, except V_{so}, are from Ref. 54.

[b]The neutron parameters and the proton V_{so} are from Ref. 55.

allow the use of these parameters at energies as low as 4 MeV. These same parameters were used quite successfully by Hausman *et al.*[51] in their ^{48}Ti study.

The neutron transmission coefficients were calculated using the local-equivalent optical model parameters of Perey and Buck[57] listed in Table VI. Again it was assumed that the explicit energy dependence would allow the use of these parameters at energies as low as 40 keV and as high as 1.8 MeV. These neutron and proton parameters were also used by Sheldon.[58] The depth of the real spin-orbit potential for both neutrons and protons was taken as 7.5 MeV which is the local equivalent to the non-local value used by Perey and Buck.

Fourteen inelastic proton channels and all known open neutron channels were included in each of the MANDY calculations. The spins and energies for the proton channels are from ^{56}Fe$(n,n'\gamma)$ work by Armitage *et al.*[59] There are many more open proton channels than were included; however, it was felt that they could be safely ignored, as the exit proton energies involved are well below the 5.35-MeV Coulomb barrier. These low energy protons also have much less phase space available to them. A comparison of predicted and measured absolute cross sections is made later in Section III-D.

Since the theoretical cross-section predictions involve the use of estimated optical-model parameters (in determining the penetrabilities), systematic errors in these predictions are possible. The internal consistency of the present experimental results and the agreement of some of the results with previously known quantities, indicate that these possible systematic errors are minimal. No attempt was made to vary any of the optical-model parameters in the theoretical calculations.

The errors assigned to the experimental points of Figs. 8 and 9 arise from uncertainties in three different quantities: (1) the γ-ray peak areas, (2) the detector relative γ-ray efficiency corrections, and (3) the run-to-run normalizations. The γ-ray peak area uncertainties result from the inherent statistical error associated with a nuclear decay process as well as from systematic analysis errors particularly in the determination of background. The latter is felt to be an often neglected but very important source of error. An estimate of the combined error (for each peak) was made by comparison with the γ-ray angular distribution data as described in the next section. (The γ-ray spectra of both experiments were quite similar.) The resulting estimated peak-area errors varied from 1.5 to 10% and in all cases were larger than the statistical errors. The uncertainties in the relative efficiency corrections were estimated to be between 3 and 5% (depending upon the γ-ray energy) by comparing graphically several possible fits to the experimental detector relative efficiency curve. Although systematic errors could enter here, they would be difficult to estimate. The uncertainties in the run-to-run normalizations were estimated to be between 0.5 and 1% (depending upon the pulser-peak area). Special care was taken to arrange the geometry to insure against any additional systematic errors associated with beam loss or secondary electron emission.

C. γ-Ray Angular Distributions

Proton beams of 5.77, 6.65, 7.03, 7.05, 7.30, and 7.40 MeV from the MSU cyclotron were used to bombard a piece of the previously described enriched ^{56}Fe foil. A thin strip of foil measuring 1 mm by 10 mm was carefully positioned on the axis of rotation of a high angular precision goniometer.[60] Thus, only when the beam passed through the axis of rotation could ^{56}Co γ rays be produced. A diagram of the scattering chamber geometry is shown in Fig. 10.

The 2.5%-efficient Ge(Li) detector was rigidly mounted on the goniometer arm with the face of the detector 12.7 cm from the target. The detector subtended approximately 10° of arc. A semicircle of 99.999% pure lead with a thickness of 0.419±0.013 mm was placed 5 cm from the target. Since this thickness of lead was capable of stopping 12-MeV protons, angular distributions all the way to 0° could be taken for all bombarding energies. Also, γ rays from reactions with the lead, although present, were minimal since the beam energies used were considerably below the 11.85-MeV Coulomb barrier for lead. As a precaution, all of the beam line near the detector was carefully lined with clean lead to eliminate any γ rays from beam-induced reactions with the aluminum beam pipe.

An electronic set-up similar to that used to take the excitation-function data was used to compensate for pile-up and dead-time effects caused by changing γ-ray counting rates due to beam current fluctuations and an increase of γ-ray and x-ray intensities from the lead beam stop as 0° was approached. Here the pulse generator was triggered by elastically scattered proton counts provided by a properly

Figure 10. Geometry for the in-beam γ-ray angular distribution measurements. The monitor and target angles were held fixed throughout all of the measurement.

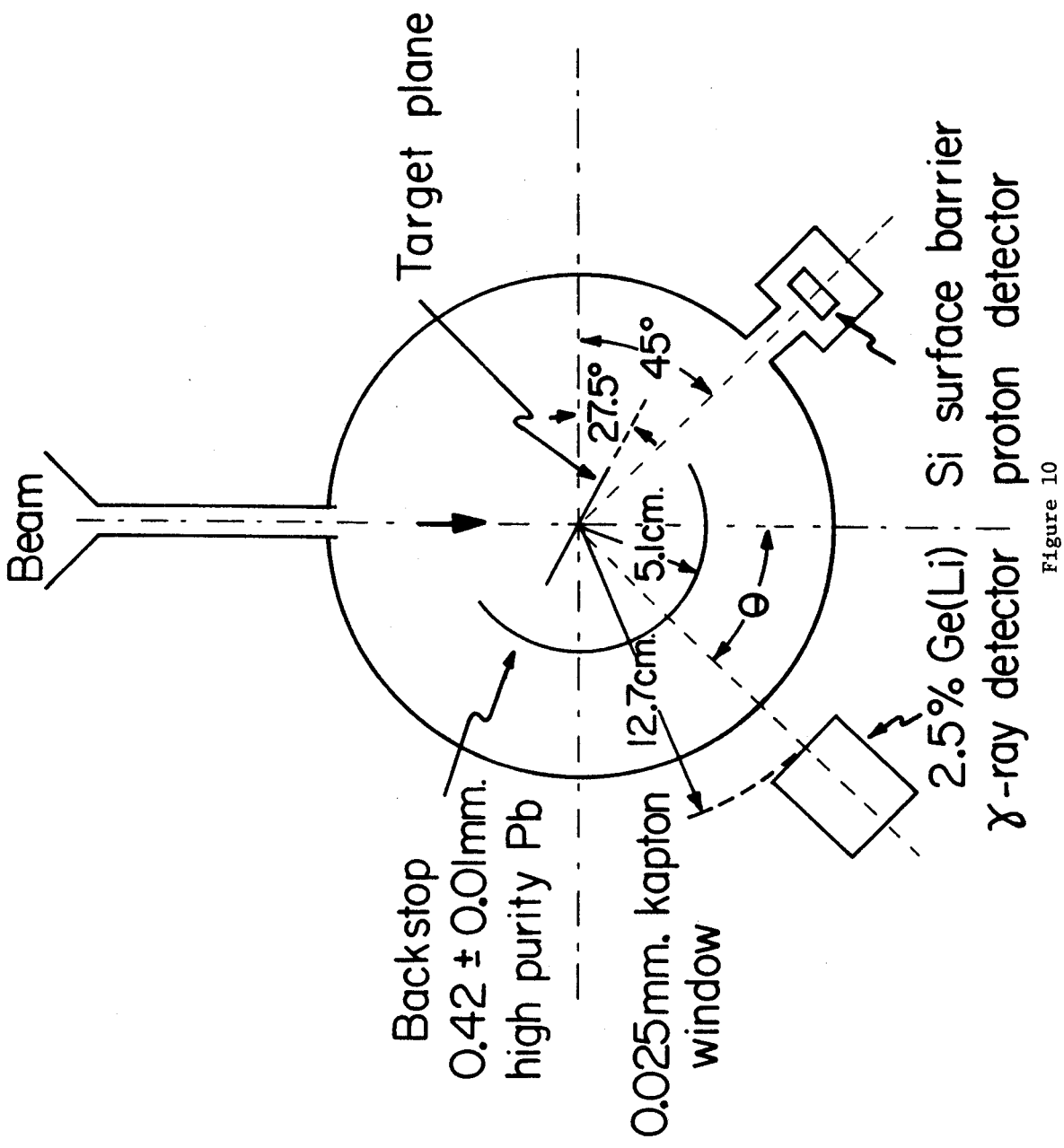
Beam
Target plane
27.5°
45°
5.1cm.
12.7cm.
θ
Backstop
0.42 ± 0.01mm.
high purity Pb
0.025mm. kapton
window
2.5% Ge(Li)
γ-ray detector
Si surface barrier
proton detector

Figure 10

collimated silicon surface-barrier detector held rigidly in place at -45° with respect to the beam direction. Since the total number of protons scattered into a given solid angle is directly proportional to the total integrated beam current that has passed through the target, correct normalization for the distributions taken at 5.77, 6.65, 7.05, and 7.40 MeV was then provided by simply dividing γ-ray peak areas by the pulser peak area. Once isotropy of the 480.5-keV γ-ray transition was well established in the 7.05- and 7.40-MeV angular distributions, this transition was used as an internal normalization for the angular distributions taken at 7.03 and 7.30 MeV (the tail pulse generator was not available).

The data were stored in 4096 channels with approximately 0.5 keV per channel through a Northern Scientific 50-MHz ADC interfaced to the MSU cyclotron's XDS Σ-7 computer.[33] The spectra (at the appropriate beam energies) are very similar to those presented in Fig. 7. Typically, spectra were accumulated for one hour between changes of angle and usually angular distributions contained 20 points in 10° intervals taken in random order over the angular range of 0° to 90°. Duplication of most points increased confidence in the data.

The spectra were analyzed off-line using the computer code SAMPO[34] which allowed γ-ray peaks of interest to be stripped from adjacent background peaks. After normalization of γ-ray peak areas, least squares fits to the experimental γ-ray angular distributions using the computer code GADFIT[61] were made to the equation:

$$W(\theta) = A_0[1 + A_2^* P_2(\cos\theta) + A_4^* P_4(\cos\theta)].$$

The parameters extracted from the fit are A_0, A_2^*, and A_4^* where A_0 is

the intensity integrated over all solid angles. By correcting these integrated intensities for the relative detector efficiency and absorption in the lead semicircle, branching ratios having all angular dependence removed were obtained. These branching ratios agree well with those obtained from the excitation function data. The branching ratios presented in Fig. 6 and listed in Table IX are averages of the two experiments. The effects on the angular distribution of the non-zero solid angular acceptance of the detector were found to be negligible. The γ-ray angular distributions taken at beam energies of 5.77, 6.65, 7.05, and 7.30 MeV and selected γ-ray angular distributions taken at 7.40 MeV are shown in Fig. 11, while the measured A_2^* and A_4^* values for all beam energies are listed in Table VII.

For each angular distribution measured, theoretical A_2^* and A_4^* coefficients as functions of the mixing ratio, δ, were generated from MANDY for a particular final spin, and an assortment of initial spins. An example of these δ-ellipses is shown in Fig. 12. The functional form of $W(\theta)$ using these predicted values of A_2^* and A_4^* (as a function of δ) was then compared with the experimental data to determine the chi-square (χ^2) per degree of freedom (reduced χ^2) for the fit. For reduced χ^2 to be meaningful, however, "accurate" uncertainties must be assigned to the data. Since two points were taken at each angle it was found that the purely statistical uncertainties rarely caused overlapping error bars. This fact would indicate that these uncertainties were underestimating the true uncertainties. For the γ-ray angular distribution measurements, the major uncertainties are in the γ-ray peak areas and the angle-to-angle normalizations (pulser peak areas). As indicated in the previous section, systematic errors (primarily in

Figure 11. Angular distributions of ^{56}Co γ rays taken at E_p = 5.77, 6.65, 7.05, 7.30, and 7.40 MeV. The solid lines through the data represent least squares fits using the equation for $W(\theta)$ given in the text. $W(\theta)$ has been normalized to 1 at 90°. Except for the E_p = 7.40 MeV case, two experimental points were taken at each angle; only their weighted average is presented.

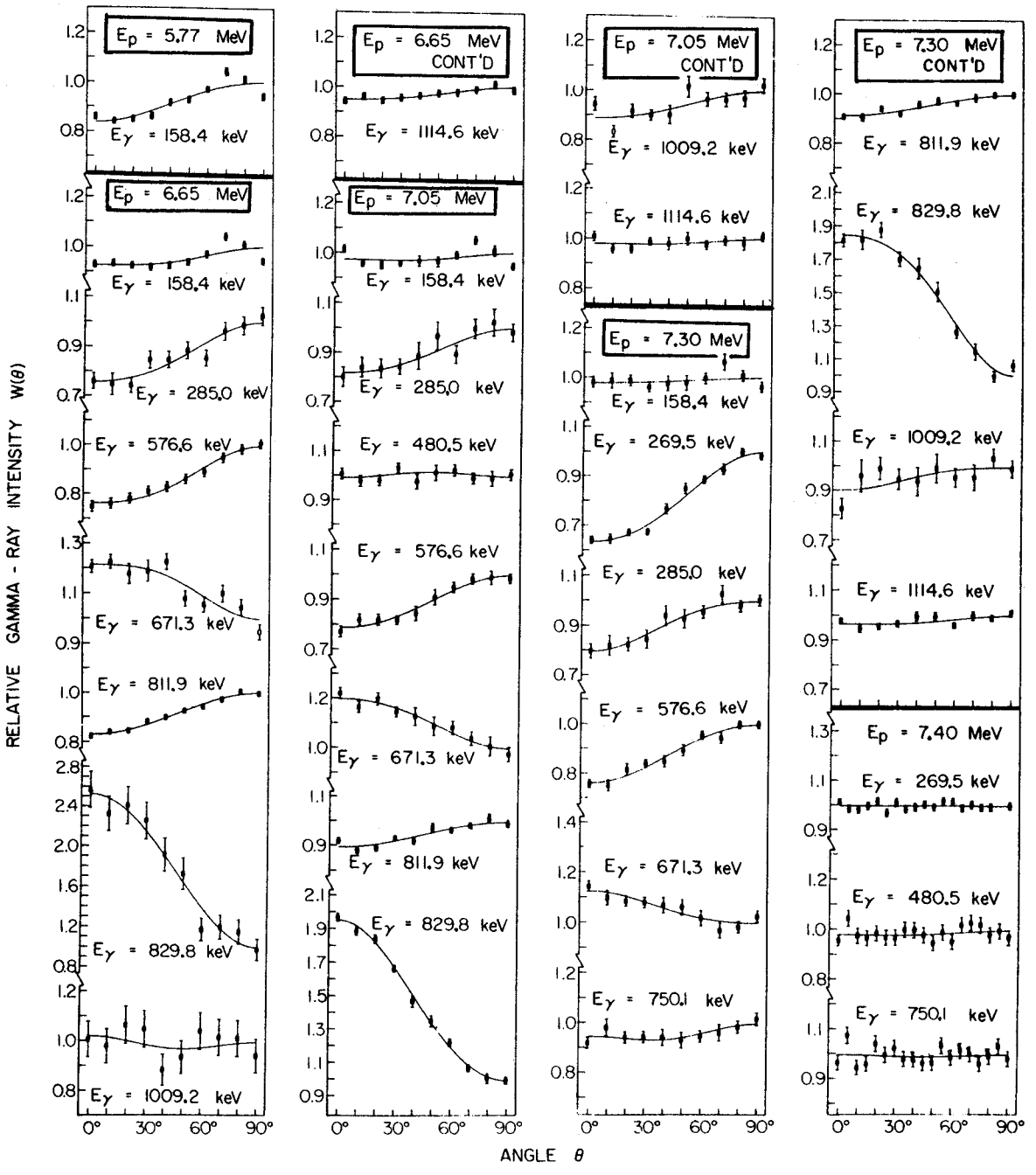
RELATIVE GAMMA - RAY INTENSITY W(θ)
ANGLE θ
Ep = 5.77 MeV
Eγ = 158.4 keV
Ep = 6.65 MeV
Eγ = 158.4 keV
Eγ = 285.0 keV
Eγ = 576.6 keV
Eγ = 671.3 keV
Eγ = 811.9 keV
Eγ = 829.8 keV
Eγ = 1009.2 keV
Ep = 6.65 MeV CONT'D
Eγ = 1114.6 keV
Ep = 7.05 MeV
Eγ = 158.4 keV
Eγ = 285.0 keV
Eγ = 480.5 keV
Eγ = 576.6 keV
Eγ = 671.3 keV
Eγ = 811.9 keV
Eγ = 829.8 keV
Ep = 7.05 MeV CONT'D
Eγ = 1009.2 keV
Eγ = 1114.6 keV
Ep = 7.30 MeV
Eγ = 158.4 keV
Eγ = 269.5 keV
Eγ = 285.0 keV
Eγ = 576.6 keV
Eγ = 671.3 keV
Eγ = 750.1 keV
Ep = 7.30 MeV CONT'D
Eγ = 811.9 keV
Eγ = 829.8 keV
Eγ = 1009.2 keV
Eγ = 1114.6 keV
Ep = 7.40 MeV
Eγ = 269.5 keV
Eγ = 480.5 keV
Eγ = 750.1 keV
0° 30° 60° 90°

Figure 11

Table VII. Experimental γ-ray angular distribution fitting parameters A_2^* and A_4^* and the associated γ-ray multipole mixing ratio, δ. The fitting parameters and mixing ratio are defined in the text. The errors assigned to both the A_2^* and A_4^* coefficients represent plus or minus one standard deviation. The ranges of δ were determined from these coefficients as described in the text.

E_p (MeV)	E_γ (keV)	A_2^*	A_4^*	δ
5.77	158.4	-0.110±0.018	-0.008±0.020	$-0.034 \leq \delta \leq -0.006$
6.65	158.4	-0.059±0.015	0.019±0.019	$-0.048 < \delta < -0.010$[a]
	285.0	-0.190±0.076	0.027±0.092	$-0.020 \leq \delta \leq 0.088$
	576.6	-0.191±0.042	0.037±0.053	$0.022 \leq \delta \leq 0.072$[a]
	671.3	0.146±0.060	-0.038±0.067	$0.221 \leq \delta \leq 0.304$[a]
	811.9	-0.121±0.010	0.001±0.012	$0.015 \leq \delta \leq 0.035$
	829.8	0.673±0.353	0.005±0.432	$-0.092 \leq \delta \leq 1.145$[a]
	1009.2	-0.002±0.346	0.035±0.410	$-0.024 < \delta < 0.361$
	1114.6	-0.038±0.025	-0.006±0.030	$-0.093 \leq \delta \leq -0.056$
7.03	158.4	-0.013±0.009	0.011±0.009	b
	285.0	-0.122±0.038	0.029±0.047	$-0.028 < \delta < 0.039$
	576.6	-0.178±0.016	0.023±0.023	$0.041 \leq \delta \leq 0.061$[a]
	671.3	0.141±0.023	-0.020±0.033	$0.253 \leq \delta \leq 0.290$[a]
	811.9	-0.066±0.010	0.003±0.012	
		-0.085±0.013[c]	0.004±0.015[c]	$0.005 < \delta < 0.040$[c]
	829.8	0.517±0.055	-0.086±0.068	d
	1009.2	-0.080±0.072	-0.006±0.089	$0.070 < \delta < 0.154$
	1114.6	-0.014±0.028	0.000±0.034	$-0.116 \leq \delta \leq -0.064$
7.05	158.4	-0.024±0.012	0.012±0.018	b
	285.0	-0.127±0.075	0.015±0.100	$-0.047 < \delta < 0.084$
	480.5	0.002±0.027	0.020±0.034	$\delta = 0.0$[e]
	576.6	-0.158±0.021	0.009±0.029	$0.050 < \delta < 0.076$[a]
	671.3	0.128±0.026	-0.014±0.031	$0.241 \leq \delta \leq 0.282$[a]
	811.9	-0.073±0.009	-0.001±0.011	
		-0.090±0.011[c]	-0.001±0.013[c]	$0.014 < \delta < 0.044$[c]
	829.8	0.475±0.043	0.038±0.061	$0.337 \leq \delta \leq 0.467$[a]
	1009.2	-0.082±0.069	0.008±0.088	$0.071 \leq \delta \leq 0.151$
	1114.6	-0.017±0.028	0.009±0.035	$-0.113 \leq \delta \leq -0.061$
7.30	158.4	-0.015±0.015	0.002±0.018	b
	269.5	-0.296±0.023	0.030±0.031	$\delta = 0.0$[e]
	285.0	-0.134±0.055	-0.025±0.076	$-0.022 < \delta < 0.088$
	576.6	-0.169±0.024	-0.008±0.032	$0.040 \leq \delta \leq 0.070$[a]
	671.3	0.074±0.030	0.014±0.038	$0.198 \leq \delta \leq 0.245$[a]

Table VII (continued)

E_p (MeV)	E_γ (keV)	A_2^*	A_4^*	δ
7.30	750.1	-0.053±0.043	0.033±0.055	$-22.7 \leq \delta \leq -2.91$[f] or $-0.041 \leq \delta \leq 0.251$
	811.9	-0.060±0.008	0.000±0.011	b
	829.8	0.453±0.071	-0.086±0.091	$0.142 \leq \delta \leq 0.715$[a]
	1009.2	-0.061±0.106	-0.017±0.144	$0.059 \leq \delta \leq 0.186$
	1114.6	-0.027±0.026	0.008±0.034	$-0.102 \leq \delta \leq -0.047$
	1561.7	0.082±0.742	-0.070±1.074	g
7.40	158.4	-0.028±0.009	0.016±0.009	b
	269.5	-0.018±0.025	0.006±0.029	$\delta = 0.0$[e]
	285.0	-0.066±0.142	-0.006±0.163	$-0.186 \leq \delta \leq 0.107$
	480.5	-0.002±0.006	-0.001±0.007	$\delta = 0.0$[e]
	576.6	-0.169±0.017	0.014±0.021	$0.044 \leq \delta \leq 0.065$
	671.3	0.087±0.021	-0.016±0.025	$0.215 \leq \delta \leq 0.248$[a]
	750.1	-0.006±0.034	0.007±0.040	$-4.30 \leq \delta \leq -1.95$[h] or, $-0.187 \leq \delta \leq 0.062$[h]
	811.9	-0.038±0.010	0.001±0.011	b
	829.8	0.504±0.064	-0.011±0.075	d
	1009.2	-0.090±0.078	0.012±0.096	$0.059 \leq \delta \leq 0.151$
	1114.6	-0.014±0.037	0.012±0.043	$-0.127 \leq \delta \leq -0.049$
	1561.7	0.020±0.724	-0.104±0.806	g

[a] The weak γ-ray feedings from higher lying states have been ignored in determining these mixing ratios.

[b] The γ-ray feedings from higher lying states for these cases could not be ignored, hence, no value for the mixing ratio could be determined.

[c] The γ-ray feeding from the higher lying 0^+ state at 1450.8 keV has been taken into account in these cases, hence, the corrected values for A_2^* and A_4^* and the corresponding range of the mixing ratio.

[d] The 4^+ δ-ellipse lies outside the ranges of A_2^* and A_4^* for these cases.

[e] See the text for discussion of the pure multipole order.

[f] This value is unlikely; see text for explanation.

[g] The errors on A_2^* and A_4^* for these cases are too large to allow a determination of the mixing ratio.

[h] The γ-ray angular distribution for this case has anomalously become isotropic for possible reasons discussed in the text. The possible ranges of δ given may therefore not be valid.

Figure 12. Representative plot of MANDY predictions for the A_2^* and A_4^* coefficients as a function of γ-ray mixing ratio, δ. (Definitions are presented in the text.) This plot is for the case of the 158.4-keV γ ray at E_p=5.77 MeV. A spin of 4 for the final state was assumed; the spins and parities of the initial state label their appropriate δ-ellipses. Representative values of δ are also labeled. The experimental A_2^* and A_4^* coefficients including uncertainties are shown as a rectangle in approximately the center of the plot.

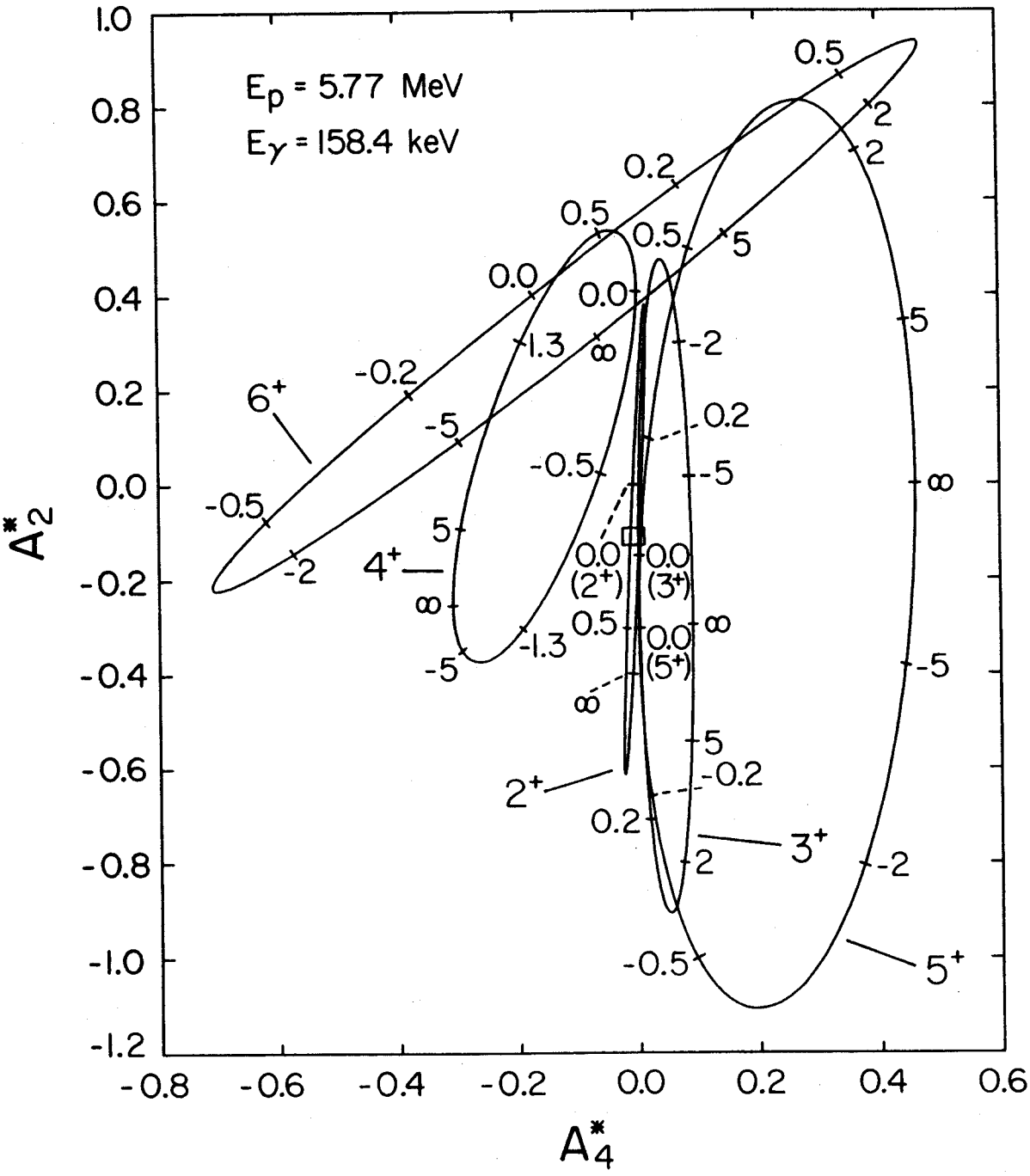
E_p = 5.77 MeV
E_γ = 158.4 keV
A_2^*
A_4^*
1.0
0.8
0.6
0.4
0.2
0.0
-0.2
-0.4
-0.6
-0.8
-1.0
-1.2
-0.8
-0.6
-0.4
-0.2
0.0
0.2
0.4
0.6
6^+
4^+
2^+
3^+
5^+
(2^+)
(3^+)
(5^+)
0.0
0.0
0.0
0.5
0.5
0.5
0.2
0.2
0.2
-0.2
-0.2
-0.2
-0.5
-0.5
-0.5
1.3
-1.3
2
2
2
-2
-2
-2
5
5
5
-5
-5
-5
∞
∞
∞

Figure 12

the background determination) are very important in the case of the γ-ray peak areas. Since it was felt that these systematic errors could not be "accurately" estimated *a priori*, the following approach was taken.

The uncertainties for each of the data points were adjusted during the determination of the experimental A_2^* and A_4^* coefficients to make the reduced χ^2 for the best fit to be approximately one. This condition yields accurate uncertainties provided the form of the fitting function $W(\theta)$ is correct. Since direct interaction effects are expected to be small at the beam energies used, the even-order Legendre polynomial series used is probably valid. The uncertainties determined in this manner varied from 1.5 to 10%. In all cases these uncertainties were larger than the combined statistical errors of the γ-ray peak areas and the pulser peak areas.

The values of reduced χ^2 were determined from the theoretical A_2^* and A_4^* coefficients, the experimental γ-ray angular distribution, and the data uncertainties determined as described above, and were plotted against arctan δ. Some representative plots are shown in Fig. 13. (Again, the remaining plots can be found in Ref. 49.) All relevant spin and parity values have been included in the plots, although in each case several of them can be eliminated on the basis of cross-section ratios as discussed in the next section. The ordinate is labeled "relative χ^2" instead of "reduced χ^2" because of the manner in which the uncertainties were determined. It should be noted that a pronounced minimum in relative χ^2 will only be approximately one if the theoretical δ-ellipse passes through the experimental range of the A_2^* and A_4^* coefficients. It should also be noted that the 0.1%

Figure 13. Representative relative χ^2 versus arctan δ plots for angular distributions of each of the ^{56}Co γ rays. J^{π} values for the initial states label each curve. The J value assumed for the final state was that previously assigned in this work.

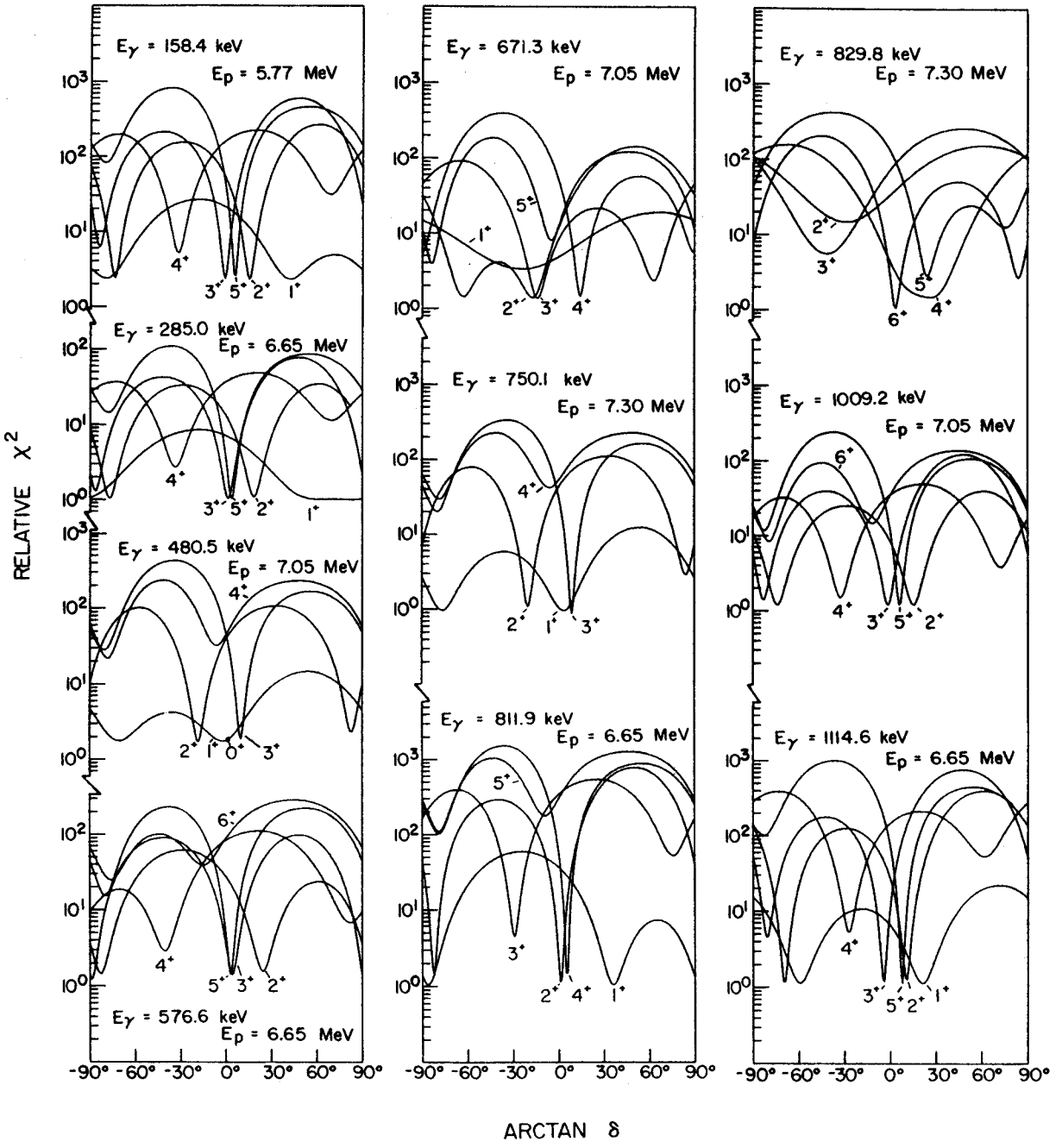
Eγ = 158.4 keV
Ep = 5.77 MeV
Eγ = 285.0 keV
Ep = 6.65 MeV
Eγ = 480.5 keV
Ep = 7.05 MeV
Eγ = 576.6 keV
Ep = 6.65 MeV
Eγ = 671.3 keV
Ep = 7.05 MeV
Eγ = 750.1 keV
Ep = 7.30 MeV
Eγ = 811.9 keV
Ep = 6.65 MeV
Eγ = 829.8 keV
Ep = 7.30 MeV
Eγ = 1009.2 keV
Ep = 7.05 MeV
Eγ = 1114.6 keV
Ep = 6.65 MeV
RELATIVE χ²
ARCTAN δ
-90° -60° -30° 0° 30° 60° 90°

Figure 13

confidence limit here is at reduced $\chi^2 = 2.27$, provided that the assigned uncertainties are "accurate". Finally the uncertainties of the A_2^* and A_4^* coefficients were almost independent of the errors assigned to the individual data points and were therefore essentially determined by the data-point scatter about the fit. Because the angular distributions usually included 20 points, these uncertainties can be assumed to be approximately one standard deviation errors.

The measured mixing ratios are presented in Table VII. The ranges were determined from the one standard deviation errors in the A_2^* and A_4^* coefficients. (In virtually every case, the appropriate δ-ellipse passed through a sufficient portion of the A_2^* and A_4^* range to allow the quoted range of mixing ratio to reflect the experimental error.) When more than one measurement of δ exists, an average of the several values was made. More weight was given to those cases with smaller errors in the A_2^* and A_4^* coefficients. The final averaged values suggested for the mixing ratios of the various ^{56}Co γ rays measured in the present work are given in Table IX.

D. Total Absolute Cross Sections at E_p = 7.30 MeV

A 7.30-MeV proton beam from the MSU cyclotron was used to bombard the ^{56}Fe foil which was placed at 55° with respect to the beam direction. The 2.5%-efficient Ge(Li) detector was positioned with its face 12.7 cm from the center of the target and at 90° to the beam. Dead-time and amplifier pile-up corrections were made as described for the excitation function measurements. The charge was collected in a shielded 200-cm long, 8.3-cm diameter piece of lead-lined aluminum beam pipe and integrated. The 0.90±0.09 mg/cm^2 target thickness was determined by measuring the energy loss of 5.48-MeV alpha particles from an ^{241}Am source. The target was placed 15 cm in front of the Faraday cup described above. Since the root-mean-square angle for beam scattering from the target is approximately 1°, all of the charge should have entered the charge-collecting section of the beam pipe. The absolute normalization of the counting efficiency curve was determined for the geometry used by counting ^{57}Co, ^{137}Cs, ^{54}Mn, and ^{60}Co intensity standards. The precision quoted for the standards was ±5%.[62] Care was taken to place the standards as closely as possible to the position of the beam spot on target. Corrections for γ-ray angular distribution effects were included in the analyses, but corrections for internal conversion and target self-absorption were neglected since these were expected to be small in comparison to experimental errors.

Major experimental uncertainties lie in the target thickness (estimated uncertain by ±10%, including non-uniformities), the integrated charge (estimated at ±5%), the absolute normalization for the

efficiency curve (approximately ±10%, including uncertainty in source positioning), and the γ-ray peak areas (±2 to ±7%). The total error associated with the measurement is then approximately ±15%.

The neutron feeding to each state was determined from the absolute γ-ray intensities as described in the excitation function work. The (p,n) cross sections were finally calculated using these neutron feedings. The results are listed in Table VIII. Included in the table are the total absolute cross-section predictions of MANDY for E_p = 7.30 MeV as well as a comparison of the relative cross sections normalized to that of the 158.4-keV first excited state. The theoretical total cross sections listed are for the J^π values suggested by this work. Because of the fluctuations in the excitation functions, the total cross sections measured here are expected to deviate randomly from the theoretically predicted values. However, except for the cross section to the 1450.8-keV state, which appears to have a maximum in this energy region (see Fig. 8), the measured total cross sections are on the average 30% below the theoretically predicted values. Accurate quantitative comparison cannot be made between these measurements and the excitation function data because the experiments were performed with different accelerators, and the beam energy of the MSU cyclotron has not been calibrated precisely at these low energies. The nominal beam energies of the two accelerators are expected to be within a few kilovolts, however.

Four possible explanations can be suggested for the 30% discrepancy. First, an unknown systematic error could have caused the experiment to yield incorrect results. Second, the transmission coefficients used in the MANDY calculations, although good enough to

Table VIII. $^{56}Fe(p,n)^{56}Co$ total cross sections at E_p = 7.30 MeV.

Excitation energy (keV)	Experimental		Theoretical[a]		
	σ (mb)	σ_{rel}[b]	σ (mb)	σ_{rel}[b]	J^{π}
158.4	50.7±7.8	≡1.000	81.3	≡1.000	3^+
576.6	8.9±1.2	0.175	14.4	0.177	5^+
829.7	18.5±2.6	0.366	23.1	0.284	4^+
970.3	46.9±6.7	0.925	66.4	0.814	2^+
1009.2	6.2±0.9	0.122	8.8	0.108	5^+
1114.6	23.8±3.3	0.471	38.1	0.469	3^+
1450.8	23.9±3.3	0.472	17.5	0.215]	0^+
1720.3	14.0±2.0	0.277	17.3	0.213	1^+

[a]Theoretical total cross sections are only presented for those values of J^{π} suggested by this work

[b]$\sigma_{rel} = \sigma/\sigma_{158.4}$.

yield reasonable γ-ray angular distribution and relative cross-section predictions, could yield inaccurate absolute cross sections. Third, the calculations included all open neutron exit channels but were restricted to 14 proton exit channels. The open proton channels used corresponded to a maximum excitation in ^{56}Fe of about 4 MeV. With 7.28 MeV of incident proton energy, an excitation of about 7.15 MeV is expected. Thus, a multitude of open proton channels in this additional 3-MeV excitation range were not taken into account. Although inclusion of these additional channels would reduce the predicted cross sections, the effect could not be large since, as mentioned earlier, the limited phase space available to such low energy particles and the 5.39-MeV Coulomb barrier both act to reduce the transmission coefficients considerably. The absolute cross-section predictions presented in Table VIII, using 14 open proton exit channels, were on the average 7% smaller than the results of a similar calculation using 8 open proton exit channels. Finally, the Moldauer level-width fluctuation correction[63] was not included in this calculation. This correction would reduce slightly the magnitude of the total absolute cross sections but would have a pronounced effect only at much lower bombarding energies.

IV. DISCUSSION OF INDIVIDUAL LEVELS

Excluding the ground and first excited states, the spin assignments resulting from the present work are based upon cross-section ratios taken with respect to that of the 158.4-keV first excited state, upon γ-ray angular distributions, and where necessary, upon previous internal-conversion electron and lifetime measurements. Spins eliminated by the comparisons of the cross-section ratios to the theoretical predictions of MANDY are not to be considered as choices in the analyses of the γ-ray angular distributions. Other J^{π} values have been included in the relative χ^2 plots in Fig. 13 to emphasize the difficulty of making J^{π} assignments to states of ^{56}Co solely on the basis of γ-ray angular distributions. Throughout the following discussions it is assumed that only even parity states exist below 1.8 MeV of excitation in ^{56}Co.

A. Ground State, $J^{\pi} = 4^{+}$

The ground-state spin is not directly measured in this experiment but is important since it in part determines the A_2^* and A_4^* coefficients for the γ-ray angular distributions of the five ground-state transitions. Fortunately, the ground-state J^{π} has been previously determined to be 4^{+} by such diverse methods as γ-γ angular correlation,[1,3] hyperfine structure in paramagnetic resonance,[64] several different particle-transfer and charge-exchange reactions (references listed earlier), and inference from the log ft data for its decay to states in ^{56}Fe.[65] It should be noted that consistencies in the present work support this assignment.

B. E_x = 158.4 keV, 3^+

The plot in Fig. 13 for the ground-state transition from this state shows pronounced minima in relative χ^2 for the J^π possibilities of 1^+, 2^+, 3^+ and 5^+. A less pronounced minimum is exhibited for $J^\pi = 4^+$ suggesting this choice is less likely. A careful study of Fig. 12 shows that $J^\pi = 6^+$ can be eliminated. Since the angular distribution of the 158.4-keV γ ray is not isotropic (see Fig. 11 and Table VII), $J^\pi = 0^+$ can also be eliminated.

Previous internal-conversion electron measurements by Menti,[66] Jenkins and Meyerhof,[2] and Ohnuma *et al.*,[3] as well as lifetime measurements by Wells *et al.*,[1] have shown that the 158.4-keV transition is predominately M1 in character. This fact rules out the $J^\pi = 1^+$ possibility since either a 45% M3 + 55% E4 or 3% M3 + 97% E4 transition is required to be consistent with the two minima observed for $J^\pi = 1^+$ in relative χ^2. Similarly, the $J^\pi = 2^+$ possibility is ruled out since a 93.2% E2 + 6.8% M3 or 7.6% E2 + 92.4% M3 transition is required.

The $J^\pi = 4^+$ and 5^+ possibilities can be eliminated by comparing the changes in the theoretically predicted cross section as a function of beam energy with the measured excitation function for this state. (See Fig. 8.) The experimental cross section changes at most by a factor of 2 from a beam energy of 5.77 to 7.30 MeV, while the change predicted by MANDY is a factor of 7.4 for $J^\pi = 4^+$ and 6.0 for $J^\pi = 5^+$. The change predicted for $J^\pi = 3^+$ is 1.4.

Thus, $J^\pi = 3^+$ is the only value consistent with the known M1 character of the 158.4-keV γ ray and with the results of the present experiment. From its angular distribution, an M1 transition with a

0.01 to 0.09% E2 admixture is indicated for the 158.4-keV γ ray. A mixing ratio $-0.04 \leqslant \delta \leqslant -0.06$ (see Tables VII and IX) is in excellent agreement with the value $-0.045 \leqslant \delta \leqslant 0.014$ measured by Ohnuma *et al.*[3] and the value $-0.33 \leqslant \delta \leqslant 0.00$ measured by Wells *et al.*,[1] both using γ–γ angular correlations in the decay of ^{56}Ni.

The 158.4-keV γ-ray angular distribution reported by Menti[66] using the $(p,n\gamma)$ reaction is in complete disagreement with the present experiment. Menti's measurement of $A_2^* = 0.258\pm0.027$ and $A_4^* = -0.125\pm 0.028$ at $E_p = 5.8$ MeV is not consistent with our values of $A_2^* = -0.110\pm0.018$ and $A_4^* = -0.008\pm0.020$ at $E_p = 5.77$ MeV. This was the only ^{56}Co γ-ray angular distribution reported by Menti. The internal consistency of our data and their agreement with other types of experiments suggests that the coefficients reported by Menti are in error.

C. $E_x = 576.6$ keV, 5^+

The cross-section ratio plot in Fig. 9, shows an unambiguous choice of $J^\pi = 5^+$ for this state. A pronounced minimum in relative χ^2 is observed for $J^\pi = 5^+$ in the plot of Fig. 13 for the ground-state transition from this state. An M1 transition with 0.04 to 0.49% E2 admixture is indicated for this γ ray.

D. $E_x = 829.7$ keV, 4^+

The cross-section ratio plot in Fig. 9, shows an unambiguous choice of $J^\pi = 4^+$ for this state. Both γ-ray branches from this state have analyzable angular distributions. It should be noted that for

all of the γ-ray angular distribution measurements in which the 829.7-keV state was excited, it was also fed from above by a weak 285.0-keV γ-ray transition. The feeding intensity was never more than 17% of the total intensity from the 829.7-keV state and was found to cause changes in the A_2^* and A_4^* coefficients that were much less than the quoted errors. The feeding was therefore ignored in the following analysis.

The angular distribution of the 671.3-keV γ ray yields a pronounced minimum in relative χ^2 for $J^\pi = 4^+$ in the plot of Fig. 13. A predominantly M1 transition with 4.6 to 7.8% E2 admixture is indicated for this γ ray.

The 829.8-keV γ-ray angular distribution shows somewhat anomalous behavior. The experimental A_2^* for every beam energy is consistently large and positive. Only large error bars in three cases allow intersection with the 4^+ δ-ellipse. (The δ-ellipses for this case are very similar to those of Fig. 12.) The δ-ellipse is approached more closely as the beam energy increases, however. A possible explanation is that since the peak is very weak, systematic errors are allowed to enter during the critical background subtraction process. The background exhibits a large anisotropy with $A_2^* = 0.26\pm0.01$ and $A_4^* = -0.07\pm0.01$ in this region of the γ-ray energy spectrum. A diffuse minimum is observed in relative χ^2 for $J^\pi = 4^+$ in the plot of Fig. 13. A predominantly M1 transition with 1.2 to 37% E2 admixture is possible for this γ ray.

E. E_x = 970.3 keV, 2^+

The choice of J^π from the cross-section ratio plot in Fig. 9 for this state is ambiguous since the points scatter equally as well about the 1^+, 2^+ and, less likely, 3^+ theoretical lines. A γ-ray transition of 811.9 keV to the 3^+ first excited state is the only γ ray observed to deexcite this state. The depths of the minima in relative χ^2 in the plot of Fig. 13 for the angular distribution of this γ ray, eliminate the $J^\pi = 3^+$ possibility but leave both the 1^+ and 2^+ choices. Internal-conversion electron measurements by Ohnuma *et al.*[3] have shown that the 811.9-keV γ ray is predominately M1. This fact rules out the $J^\pi = 1^+$ possibility since either an 65% E2 + 35% M3 or 0.5% E2 + 99.5% M3 transition is required.

Thus, $J^\pi = 2^+$ is the only value consistent with the known M1 character of the 811.9-keV γ ray and with the results of the present experiment. Two pronounced minima in relative χ^2 are observed for $J^\pi = 2^+$. One minimum requires a 1.7% M1 + 98.3% E2 transition. Since this multipole mixing is inconsistent with the M1 character of this γ-ray, it can be discarded. The other minimum requires an M1 transition with 0.02 to 0.12% E2 admixture. A mixing ratio $0.015 \leqslant \delta \leqslant 0.035$ (see Tables VII and IX) is in excellent agreement with the value $-0.025 \leqslant \delta \leqslant 0.12$ measured by Ohnuma *et al.*[3] using γ-γ angular correlations in the decay of ^{56}Ni.

F. E_x = 1009.2 keV, 5^+

The cross-section ratio plot in Fig. 9 shows an unambiguous

choice of $J^\pi = 5^+$ for this state. Although two γ-ray branches are observed for this state, only the 1009.2-keV ground-state transition is strong enough to allow an angular distribution analysis. A pronounced minimum in relative χ^2 in the plot of Fig. 13, is observed for the 5^+ choice. An M1 transition with a 0.49 to 2.5% E2 admixture is indicated for the 1009.2-keV γ ray.

G. E_x = 1114.6 keV, 3^+

The cross-section ratios for this state (Fig. 9) are scattered about the $J^\pi = 3^+$ theoretical line with other possible, but less likely, choices being 0^+ or 1^+. Three γ-ray branches are observed for this state with two, the 285.0- and 1114.6-keV γ rays, having analyzable angular distributions. The asymmetric 285.0-keV γ-ray angular distributions shown in Fig. 11 rule out $J^\pi = 0^+$. The $J^\pi = 1^+$ possibility cannot be ruled out on the basis of the γ-ray angular distributions, however, since pronounced minima in relative χ^2 in the plots of Fig. 13, are observed for $J^\pi = 1^+$ for both γ rays.

This level does not deexcite as would be expected for a 1^+ state. The lowest multipole order possible for the γ-ray branches to the two 4^+ states fed would be M3. Assuming the B(M3)'s of these transitions to be comparable in magnitude, the energy dependence of the transition probability alone would require the 1114.6-keV transition to be 10^4 times as intense as the 285.0-keV transition. The measured value is only 8.5. Also, the 956.1-keV γ-ray branch to the first excited 3^+ state would be an E2 transition. The lifetime against such an E2 decay is 10^7 (Weisskopf estimate) times smaller than that

for an M3 decay. The fact that this branch is so weak (5% of the decays) would be inexplicable without a remarkable accidental cancellation of matrix elements.

Finally, a $J^{\pi} = 1^{+}$ assignment would open up the possibility of feeding from the decay of ^{56}Ni, the possibility of γ-ray feeding from both the higher lying 0^{+} and 1^{+} states at 1450.8 keV and 1720.3 keV, respectively, and the possibility of γ-ray decay to the lower lying 2^{+} state at 970.3 keV. None of these phenomena are observed. A $J^{\pi} = 1^{+}$ assignment is therefore highly unlikely and only $J^{\pi} = 3^{+}$ remains.

Pronounced minima in relative χ^2 in the plot of Fig. 13 for $J^{\pi} = 3^{+}$ are observed for both the 285.0- and 1114.6-keV γ rays. An M1 transition with a 0.04 to 0.64% E2 admixture is indicated for the 285.0-keV γ ray, and an M1 transition with a 0.01 to 0.25% E2 admixture is indicated for the 1114.6-keV γ ray.

H. E_x = 1450.8 keV, 0^{+}

The cross-section ratios for this state (Fig. 9) are scattered about the $J^{\pi} = 0^{+}$ theoretical line with other choices of 3^{+} or 4^{+} seemingly possible. A γ-ray transition of 480.5 keV to the 2^{+} fourth excited state at 970.3 keV is the only γ ray observed to deexcite this state. The angular distribution for this 480.5-keV γ ray is isotropic (see Fig. 11). The isotropy is a necessary (although insufficient) condition for a spin zero assignment. A pronounced minimum in relative χ^2 in the plot of Fig. 13 is not observed for $J^{\pi} = 4^{+}$ and clearly eliminates this possibility. However, a pronounced minimum is observed for $J^{\pi} = 3^{+}$. Conversion-electron measurements by Jenkins and

Meyerhof,[2] and by Ohnuma *et al.*,[3] as well as lifetime measurements by Wells *et al.*,[1] have shown that this transition is largely E2. The necessary mixing ratio for the $J^{\pi} = 3^{+}$ possibility, however, is $0.16 \leqslant \delta \leqslant 0.20$, giving at most a 96.2% M1 + 3.8% E2 transition. A $J^{\pi} = 0^{+}$ assignment on the other hand requires the 480.5-keV γ-ray transition to be pure E2. Thus, $J^{\pi} = 0^{+}$ is the only value consistent with the known E2 character of the 480.5-keV γ ray and with the results of the present experiment.

Because of the abnormally long half life of this state (1.6±0.1 nsec),[1] a supplementary experiment was performed to investigate possible nuclear hyperfine interaction effects caused by the expected large internal magnetic field (≈333 koe)[67] in the vicinity of the target nuclei in the ^{56}Fe target. A proton beam of 7.52 MeV was used to bombard a 0.02 mg/cm^2 stainless steel target. In this stainless steel target the magnetic field in the vicinity of the nuclei is minimal, thus, angular distribution "wash-out" due to precession of the magnetic moment should be greatly reduced. Partial angular distributions (10 data points) clearly showed an isotropic distribution for the 480.5-keV γ ray ($A_2^* = 0.01\pm0.02$ and $A_4^* = 0.00\pm0.03$). Other ^{56}Co γ-rays preserved their previous behavior observed in the ^{56}Fe foil target (e.g. the 269.5-keV transition had $A_2^* = -0.30\pm0.10$ and $A_4^* = 0.01\pm0.13$).

As discussed earlier, J^{π} assignments of 1^{-} and $2^{\pm}$ have been suggested for this state. These suggestions are incompatible with the measured cross-section ratios. The odd parity possibilities, which are not shown on the plot of Fig. 9, require, for example, cross-section ratios of 0.543 for $J^{\pi} = 1^{-}$ and 0.573 for $J^{\pi} = 2^{-}$ at $E_p = 7.68$ MeV. These values are very close to the $J^{\pi} = 1^{+}$ and 2^{+} theoretical

points and are about 2.5 times the average of the two closest measured ratios, 0.198. The $J^{\pi} = 0^{+}$ assignment suggested in this work was essentially eliminated in the γ-γ angular correlation analyses by Wells *et al.*[1] and Ohnuma *et al.* [3](using the decay of ^{56}Ni) on the basis of their error assignments to the angular correlation coefficients. An increase to two standard deviations in their reported errors would have resulted in compatibility with the $J^{\pi} = 0^{+}$ assignment.[6]

The additional suggestion that two states exist in this region of excitation with $J^{\pi} = 0^{+}$ and 1^{-} is also incompatible with the present work. From the γ-ray singles and γ-γ coincidences measured using the ^{56}Ni decay, no evidence could be found for γ rays deexciting a second state near 1451 keV. The full width at half maximum (FWHM) for both the 269.5- and 480.5-keV γ-ray peaks (exciting and deexciting the 1450.8-keV state, respectively) as determined by SAMPO,[34] were predicted to within 0.9 and 0.4%, respectively, using a least squares linear fit to the FWHM values and energies of the seven other most prominent γ-ray peaks (other than the 511.0-keV annihilation radiation peak) in the spectrum of Fig. 1. Assuming doublet members with approximately the same intensity, an increase in the FWHM value of 5% corresponds to a centroid difference of only 0.02 keV. Similarly, from γ-ray singles and γ-γ coincidences measured using the ^{56}Fe$(p,n\gamma)$-^{56}Co reaction, no evidence could be found for γ rays deexciting an additional state in this region. Here, as opposed to the β decay, all existing states are expected to be excited. Since the additional state is suggested to have $J^{\pi} = 1^{-}$, a large predicted cross section should produce a reasonably large γ-ray peak or peaks. As before, the FWHM

for both the 269.5- and 480.5-keV peaks (from a randomly chosen excitation function spectrum) were predicted within 3.2 and 2.2%, respectively. If the 1450.8-keV state were really a very close-lying doublet with both members deexciting via a 480.5-keV γ ray, the cross-section ratios should be $\simeq$3.5 times the measured values. In view of the internal consistency of the present data, this value is a much larger inconsistency than would be expected.

Finally, the energies of the 269.5- and 480.5-keV γ rays were measured independently to be the same within the experimental errors of $\pm$0.1 keV using both the ^{56}Ni decay and ^{56}Fe$(p,n\gamma)^{56}$Co. Thus, it is concluded that there is strong evidence that only one state exists in ^{56}Co in the region of 1451 keV of excitation, namely, at 1450.8 keV and the state has $J^{\pi} = 0^{+}$.

I. E_x = 1720.3 keV, 1^+

The cross-section ratios for this state show a scatter of points about the $J^{\pi} = 1^{+}$ and 2^{+} theoretical lines and in close proximity to the 0^{+} and 3^{+} lines. Three γ-ray branches are observed for this state with two, the 269.5- and 750.1-keV γ rays, having analyzable angular distributions. The J = 0 possibility is eliminated by the anisotropic distributions of both γ rays (see Fig. 11). The relative χ^2 plot for the 750.1-keV γ ray sheds little light on possible J^{π} assignments since all the remaining choices have pronounced minima.

The 269.5-keV γ-ray angular distribution is more illuminating, however. Since this transition goes to a spin zero state, the $\delta = 0$ requirement yields theoretical angular distribution coefficients that

are unique (i.e. it must be a pure multipole transition). The coefficients predicted by MANDY at E_p = 7.30 MeV for $J^\pi = 1^+$ are A_2^* = -0.218 and A_4^* = 0.000, for $J^\pi = 2^+$ are A_2^* = 0.517 and A_4^* = -0.302, and for $J^\pi = 3^+$ are A_2^* = 0.842 and A_4^* = 0.136. The measured values of A_2^* = -0.296±0.023 and A_4^* = 0.030±0.031 at E_p = 7.30 MeV are compatible only with $J^\pi = 1^+$ since $J^\pi = 2^+$ and 3^+ require large positive values of A_2^*. The measured value of A_2^* is, however, still almost four standard deviations more negative than the predicted value. Najam *et al.*[68] observed this same type of behavior for a 1^+ state in a $^{66}Zn(p,n\gamma)^{66}Ga$ experiment at a proton beam energy of approximately 6.50 MeV. They attribute this behavior to a direct reaction component for the $(p,n\gamma)$ reaction.

To further investigate this somewhat anomalous behavior an additional γ-ray angular-distribution measurement was made with the beam energy increased by just 100 keV (from 7.30 MeV to 7.40 MeV). The angular distribution for the 269.5-keV γ ray obtained at the new energy was, very surprisingly, isotropic with A_2^* = -0.018±0.025 and A_4^* = 0.016±0.029. The angular distributions for all the other γ rays, except the 750.1-keV γ ray which had also become isotropic, remained virtually unchanged (see Table VII). The following possible explanation, given below, for this strange behavior supports the $J^\pi = 1^+$ assignment.

Anisotropic γ-ray angular distributions result from alignment of the excited residual nuclei with respect to the beam direction. The addition of angular momentum from the incident proton causes the original alignment of the compound nucleus which then, after neutron decay, results in alignment of the excited residual nucleus. Assuming s-wave

exit neutrons, $\ell_n = 0$ (expected near threshold), a final state with spin 1 can only be reached with s-, p-, and d-wave protons, $\ell_p = 0$, 1, and 2, since the ^{56}Fe target nuclei have $J^\pi = 0^+$. The parity selection rule, $\pi_f = \pi_i$ for $\ell_p + \ell_n$ = even, further requires ℓ_p = even only, since $\pi_f = \pi_i = +1$ and $\ell_n = 0$. This restriction eliminates the participation of p-wave protons. Thus, the final state of $J^\pi = 1^+$ can only be reached with s-wave protons going through $1/2^+$ compound-nuclear states and d-wave protons going through $3/2^+$ compound-nuclear states. No other combinations are allowed.

States of residual nuclei reached with s-wave entrance protons and s-wave exit neutrons through $1/2^+$ compound nuclear states can have no alignment since the proton imparts no orbital angular momentum to the compound nucleus and the spin of the neutron can be oriented in any direction. On the other hand, states of residual nuclei reached through $3/2^+$ compound nuclear states created by d-wave entrance protons have some alignment. The exit neutron in this case can "wash out" the alignment but cannot destroy it. Resulting γ-ray angular distributions in the former case must be isotropic from the lack of nuclear alignment but in the latter case can be anisotropic. Because of the extremely restricted number of possibilities, a dominance in the compound nucleus (in either cross section or density of states) of one spin over the other can greatly affect the magnitude of the subsequent γ-ray anisotropy. MANDY predicts a maximum possible value of $A_2^* = -0.5$ for the case of only $3/2^+$ states in the compound nucleus and $A_2^* = 0.0$ for the case of only $1/2^+$ states. This behavior is restricted to spin 1 states since residual states of spin greater than 1 can always be reached by more than one pathway in which nuclear alignment is preserved,

even if only one type of spin state is available in the compound system.

Thus, $J^{\pi} = 1^{+}$ for the 1720.3-keV state, is the only value consistent with the results of this experiment and with the above discussion. The 269.5-keV γ ray is thus pure M1 which is consistent with the internal-conversion electron measurements by Jenkins and Meyerhof[2] and Ohnuma *et al.*[3] A mixing ratio of $-0.04 \leqslant \delta \leqslant 0.25$ or $-22.7 \leqslant \delta \leqslant -2.9$ is indicated for the 750.1-keV γ ray. The former value (i.e. an M1 transition with a 0.16 to 5.9% E2 admixture) is in reasonable agreement with the value $-0.20 \leqslant \gamma \leqslant 0.09$ measured by Ohnuma *et al.*[3] using γ-γ angular correlation in the decay of ^{56}Ni. The mostly M1 character is further supported by the internal-conversion electron measurements of Ohnuma *et al.*[3] The 1561.7-keV γ-ray branch from this state to the 3^{+} first excited state at 158.4 keV, must be an E2 transition by virtue of the angular momentum change between these states.

J. Higher Excited States

Excitation functions and γ-ray angular distributions were not measured for any of the higher states. An increasingly complex γ-ray spectrum and rapidly decreasing detector efficiency with the increasing energies of newly encountered γ-rays, would have made such measurements difficult. In addition, for the case of the γ-ray angular distributions, increasing beam energies resulted in higher levels of radiation from the lead beam stop. For these same reasons, no ground-state transitions were identified from these states in singles experiments.

Some comments can be made, however, about the γ-ray transitions from these states observed in the γ-γ coincidence measurement at E_p = 8.36 MeV. All of the spins suggested for these higher states by Schneider and Daehnik[15] (marked with asterisks in Fig. 6) from $^{58}Ni(d,\alpha)^{56}Co$, are compatible with the assumption that there is at most a spin change of two between states connected by γ-ray transitions. This assumption suggests a spin 1 or 2 for the 2635.7-keV state by virtue of its 1184.9-keV γ-ray transition to the 0^+ state at 1450.8 keV. No γ-ray transitions from the known states (see Ref. 15) at 2281 keV (7^+) and 2371 keV (6^+, 5^+, 7^+) were observed, presumably because the low energy (p,n) cross sections to such high spin states are very small. Thus, the spin of the 2469.3-keV state must surely be 3, 4, or 5 by virtue of its observable 1892.7-keV γ-ray transition to the 5^+ state at 576.6 keV. This 2469.3-keV state may be a 4^+ state predicted in this energy region by McGrory.[30] (See Fig. 14.) The lack of observed γ-ray transitions from the known state (see Ref. 15) at 2791 keV may be simply due to a low cross section caused by low exit neutron energy and not to high spin. The existence of a state at 2289.8 keV suggested by Del Vecchio *et al.*[24] is confirmed.

V. COMPARISONS WITH SHELL MODEL CALCULATIONS FOR ^{56}Co.

The ^{56}Co nucleus has one neutron outside and one proton hole inside an otherwise closed $f_{7/2}$ shell. It thus lends itself quite nicely to shell-model calculations. McGrory[30] has recently performed a calculation in which ^{56}Co was represented as a ^{40}Ca core plus 14 or 15 nucleons in the $f_{7/2}$ orbit and the remainder in the $p_{3/2}$, $f_{5/2}$, or $p_{1/2}$ orbits. He used single-particle energies which best reproduced the ^{57}Ni spectrum and Kuo-Brown matrix elements for the effective two-body Hamiltonian. He then used the resulting ^{56}Co wave functions to calculate the reduced transition probabilities, B(M1) and B(E2), for all possible M1 and E2 γ-ray decay channels for each of the predicted states. For the B(M1)'s the bare M1 operator was used while for the B(E2)'s an effective charge of 0.5 was used.[69] These reduced transition probabilities are compared below with lifetime measurements by Wells *et al.*[1] and with the γ-ray multipole mixing ratios and branching ratios measured in this experiment. The same ^{56}Co wave functions used in these calculations were quite successful in predicting strengths for deuteron pickup in a recent ^{58}Ni$(d,\alpha)^{56}$Co experiment by Schneider and Daehnik.[15]

The spins, parities, and energies of the ^{56}Co states predicted by McGrory and the corresponding experimental assignments of the present work are shown in Fig. 14. As can be seen, the agreement between theory and experiment is quite remarkable for the states below 2 MeV of excitation. Only the second 5^+ state and the 0^+ state are predicted too high in energy and even these discrepancies are no more than 450 keV.

Figure 14. Comparisons of level spins, parities, and energies of the present experiment and from Ref. 15 (asterisked values), with the predictions of McGrory (Ref. 30). Dashed lines indicate tentative correlations. For excitations above 3 MeV, see Ref. 15.

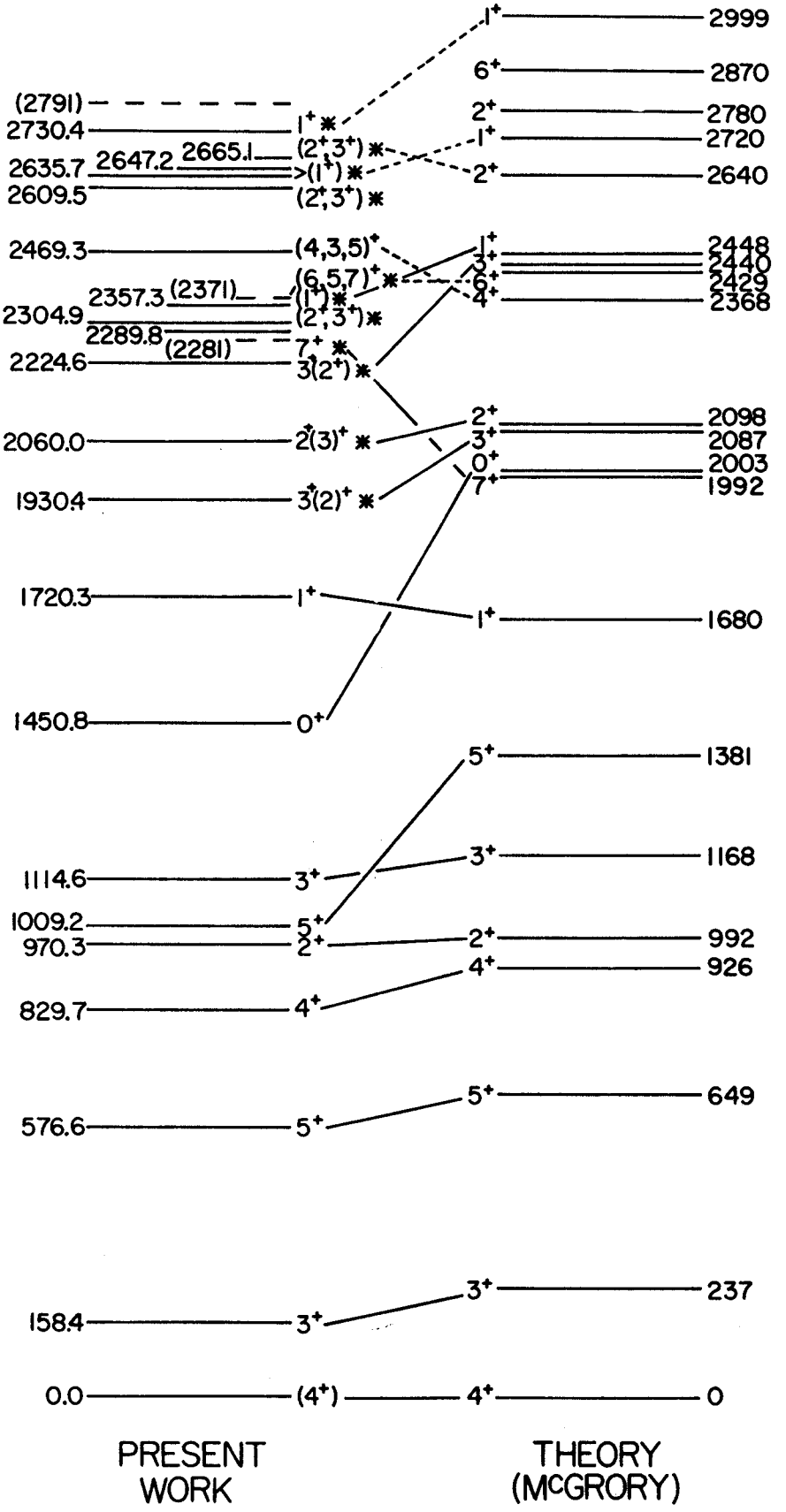
(2791)
2730.4
2635.7
2647.2
2665.1
2609.5
2469.3
2357.3
(2371)
2304.9
2289.8
(2281)
2224.6
2060.0
1930.4
1720.3
1450.8
1114.6
1009.2
970.3
829.7
576.6
158.4
0.0
1+
(2+,3+)
(1+)
(2+,3+)
(4,3,5)+
(6,5,7)+
1+
(2+,3+)
7+
3(2+)
2+(3)+
3+(2)+
1+
0+
5+
3+
5+
2+
4+
5+
3+
(4+)
2999
2870
2780
2720
2640
2448
2440
2429
2368
2098
2087
2003
1992
1680
1381
1168
992
926
649
237
0
PRESENT WORK
THEORY (McGRORY)

Figure 14

For the following discussion, the M1 and E2 transition probabilities, W(M1) and W(E2), were calculated from the B(M1)'s and B(E2)'s computed by McGrory and presented in Table IX, according to,[70]

$$W(M1) = 1.7588 \times 10^{+13} \; E_\gamma^{\,3} \; B(M1), \qquad [Sec^{-1}]$$

and

$$W(E2) = 1.2258 \times 10^{+9} \; E_\gamma^{\,5} \; B(E2), \qquad [Sec^{-1}]$$

where E_γ = the experimental γ-ray energy in MeV,

$B(M1)$ = the M1 reduced transition probability in nuclear magnetons squared, $\mu_0^{\,2}$,

and $B(E2)$ = the E2 reduced transition probability in e^2F^4.

The predicted half lives are then the reciprocals of the transition probabilities multiplied by ln2.

The calculated B(E2)'s range from 0.01 to 100 e^2F^4 and the B(M1)'s from 0.002 to 2.5 $\mu_0^{\,2}$. Thus, in light of the above equations, all γ-ray transitions with energies less than 1 MeV should be predominantly M1 except for the rare case of accidental matrix-element cancellation or where M1 transitions are not allowed by angular momentum selection rules.

The latter is the case for the 0^+ state at 1450.8 keV. If this state is 0^+, no M1 decay is possible and, in fact, only one E2 channel, that to the 2^+ state at 970.3 keV, is open. McGrory's predicted half life against this E2 decay is 2.12 nsec (see Table X). The only γ-ray decay observed for the 1450.8-keV state is that to the 970.3-keV state and it has a measured half life of 1.6±0.1 nsec.[1] Even with the factor of 1.3 discrepancy (completely accountable by the somewhat arbitrary choice of 0.5 for the effective charge in the

Table IX. Reduced transition probabilities, B(M1) and B(E2), calculated by McGrory[a] and comparisons of the shell-model results with experimental γ-ray multipole mixing ratios, δ, and γ-ray branching ratios from $^{56}Fe(p,n\gamma)^{56}Co$. The experimental transition energies were used when calculating the theoretical mixing and branching ratios (necessary formulas are presented in the text).

Transition $J_i^\pi \rightarrow J_f^\pi$	E_γ[b] (keV)	B(M1) (μ_o^2)	B(E2) (e^2F^4)	δ_{th}[c]	δ_{exp}	Theoretical branching ratios[d] (%)	Experimental branching ratios[d,e] (%)
$3_1^+ \rightarrow 4_1^+$	158.4	1.60	74.1	+0.012	$-0.04 \leq \delta \leq -0.006$	100.	100.
$5_1^+ \rightarrow 3_1^+$	(418.2)	---	11.9	---		<0.5	<3.
$5_1^+ \rightarrow 4_1^+$	576.6	0.350	34.6	+0.048	$0.04 \leq \delta \leq 0.07$	≈100	100.
$4_2^+ \rightarrow 5_1^+$	(253.1)	0.0560	36.2	+0.054		21.3	<0.7
$4_2^+ \rightarrow 3_1^+$	671.3	0.0155	27.1	+0.234	$0.22 \leq \delta \leq 0.28$	66.5	75.3±1.3
$4_2^+ \rightarrow 4_1^+$	829.8	0.0020	16.2	-0.623	$(0.15 \leq \delta \leq 0.70)$[f]	12.2	24.7±1.3
$2_1^+ \rightarrow 4_2^+$	(140.6)	---	0.0150	---		<0.05	<0.3
$2_1^+ \rightarrow 3_1^+$	811.9	0.704	8.48	+0.024	$0.01 \leq \delta \leq 0.04$	99.8	100.
$2_1^+ \rightarrow 4_1^+$	(970.3)	---	9.77	---		0.2	<0.7
$5_2^+ \rightarrow 4_2^+$	(179.5)	0.609	77.1	+0.002		1.0	<2.
$5_2^+ \rightarrow 5_1^+$	432.8	0.0536	0.0032	-0.001	g	1.2	5.2±1.6
$5_2^+ \rightarrow 3_1^+$	(850.8)	---	1.04	---		<0.05	<7.
$5_2^+ \rightarrow 4_1^+$	1009.2	0.329	14.9	+0.057	$0.06 \leq \delta \leq 0.15$	97.7	94.8±1.6

Table IX (continued)

Transition $J_i^\pi \rightarrow J_f^\pi$	E_γ[b] (keV)	B(M1) (μ_o^2)	B(E2) (e^2F^4)	δ_{th}[c]	δ_{exp}	Theoretical branching ratios[d] (%)	Experimental branching ratios[d,e] (%)
$3_2^+ \rightarrow 5_2^+$	(105.4)	---	0.0116	---		<0.05	<0.3
$3_2^+ \rightarrow 2_1^+$	(144.3)	0.0168	3.83	+0.006		<0.05	<0.4
$3_2^+ \rightarrow 4_2^+$	285.0	0.792	59.0	+0.021	$-0.02 \leq \delta \leq 0.08$	24.6	10.1±2.0
$3_2^+ \rightarrow 5_1^+$	(538.0)	---	1.07	---		<0.05	<1.
$3_2^+ \rightarrow 3_1^+$	955.9	0.0189	4.76	+0.127	g	22.5	5.0±0.5
$3_2^+ \rightarrow 4_1^+$	1114.6	0.0282	2.84	-0.093	$-0.11 \leq \delta \leq -0.06$	52.8	84.9±1.9
$0_1^+ \rightarrow 2_1^+$	480.5	---	10.4	E2	E2	100.	100.
$1_1^+ \rightarrow 0_1^+$	269.5	2.49	---	M1	M1	93.3	36.4±5.3
$1_1^+ \rightarrow 3_2^+$	(605.7)	---	1.42	---		<0.05	<3.
$1_1^+ \rightarrow 2_1^+$	750.1	0.0068	0.438	+0.050	$-0.04 \leq \delta \leq 0.25$	5.5	51.0±4.5
$1_1^+ \rightarrow 3_1^+$	1561.7	---	0.967	---	g	1.2	12.6±1.2

[a] See Ref. 30.

[b] The energies shown in parentheses are possible transitions that have not been observed and whose magnitudes have been calculated using the measured level energies.

[c] The signs on δ_{th} are the relative phases predicted by McGrory, (Ref. 30).

[d] The branching ratio is the fraction of all γ-ray decays from the initial state proceeding by the transition considered.

[e] Branching ratios sum to 100. for all observed transitions from each state. Upper limits are shown for all unobserved transitions.

[f] This range of mixing ratio for the 829.8-keV γ ray is suspect as outlined in the text.

[g] Because of poor peak statistics, γ-ray angular distributions for these transitions could not be measured.

Table X. Shell-model predictions by McGrory[a] of the half lives of the first eight excited states of ^{56}Co. Only observed transitions were included in these calculations. Internal-conversion effects were not included.

Excitation energy (keV)	$T_{1/2th}$[a] (psec)	$T_{1/2exp}$[b] (psec)
158.4	10.9	<100
576.6	0.586	
829.8	6.03	
970.3	0.105	<100
1009.2	0.115	
1114.6	0.529	
1450.8	2.12×10^3	$(1.6 \pm 0.1) 10^3$
1720.3	0.753	

[a] See Ref. 30.

[b] See Ref. 1.

E2 operator), this is remarkable agreement.

Only two additional states, at 158.4 keV and 970.3 keV, have previously measured lifetimes.[1] Upper limits for the half lives of these states were set at 100 psec. The half lives predicted by McGrory for these states are 10.9 and 0.105 psec, respectively. The very short half life predicted for the 970.3-keV state accounts for the lack of an observable 970.3-keV E2 γ-ray branch to ground.

The predicted multipole mixing ratios presented in Table IX were calculated from the equation

$$\delta^2 = \frac{W(E2)}{W(M1)} .$$

The predicted relative phases of δ presented are those of McGrory. Except for the 829.8-keV transition whose anomalous behavior was discussed previously, the agreement between the theoretical and experimental mixing ratios is quite good. A particular case is the 671.3-keV transition from the first excited 4^+ state to the first excited 3^+ state. Here, compared to the E2 admixtures of other predominantly M1 transitions, a sizeable E2 strength (5.9±1.4 percent) is both predicted and observed. The rather small B(M1) predicted for this transition causes enhancement of the theoretical E2 strength (5.2 percent). Some quantitative agreement between theory and experiment is therefore indicated.

The theoretical and experimental γ-ray branching ratios are presented in Table IX. In general, agreement is very good.

The shell-model calculations show that the predominant γ-ray decay mode for the excited states of ^{56}Co below 2 MeV of excitation is

through M1 transitions. This supports those J^{π} assignments that were based in part on the prevalence of M1 decay.

VI. SUMMARY AND CONCLUSIONS

The γ-ray decays of the excited states of ^{56}Co below 2.85 MeV of excitation have been studied via the electron-capture decay of ^{56}Ni and the ^{56}Fe$(p,n\gamma)^{56}$Co reaction. The adopted energies (in keV) of the six γ rays common to both studies are: 158.4±0.1, 269.5±0.1, 480.5±0.1, 750.0±0.1, 811.9±0.1, and 1561.9±0.2. The Ge(Li)-Ge(Li) γ-γ coincidence technique used both on and off line, was extremely useful in the placement of γ rays in the decay schemes. In particular, high-energy γ rays (greater than 1500 keV) could be separated in the in-beam spectra from otherwise overwhelming Compton backgrounds. In fact, the high Compton background and diminishing detector efficiency for high energy γ rays forced an end to the excitation function and γ-ray angular distribution measurements at about 2 MeV of excitation in ^{56}Co. Since the statistical compound nuclear theory appears still valid at these excitations, these background problems are the only hindrance to a continuation of these measurements to higher excitations.

The combined use of cross-section ratios and γ-ray angular distributions proved very potent in determining unique spin assignments. The experimental errors of the γ-ray angular distributions and the experimental errors and fluctuations of the cross-section ratios were, however, greater than the sensitivities required to make parity determinations. Thus, it is necessary to assume all parities even based upon previous experimental results and shell-model considerations. Spin and parity assignments (in parenthesis) were thus made for the following ^{56}Co states (energies in keV): 158.4(3^+), 576.6(5^+), 829.7(4^+), 970.3(2^+), 1009.2(5^+), 1114.6(3^+), 1450.8(0^+), and 1720.3(1^+).

Comparisons of the experimental cross-section ratios and γ-ray angular distributions with the predictions of the statistical CN theory (via the code MANDY) showed remarkable agreement, with two notable exceptions. First, gross fluctuations, often 15% in magnitude and 40-100 keV in width (roughly 1-3 times the target thickness) were observed in the excitation function measurements. These fluctuations also manifested themselves in the cross-section ratios as scattering about the predicted values. Second, otherwise anisotropic angular distributions (both predicted and observed) for two γ-ray decays of the 1720.3-keV 1^+ state became isotropic when the beam energy was increased by 100 keV to 7.40 MeV. It would be interesting to know if the same behavior under similar conditions is observed for 1^+ states in other nuclei as would be predicted by the possible explanation offered in the text. These two exceptions indicate partial breakdown in the statistical assumption of large numbers of overlapping CN states of random spin and parity. A satisfying explanation for the gross fluctuations would be interesting and useful information.

No evidence was found in the present work for the existence of an additional level near the 1450.8-keV state. The cross-section ratio comparisons and the angular distributions of both the 480.5-keV γ ray deexciting the level and the 269.5-keV γ ray feeding it were uniquely compatible with a $J^\pi = 0^+$ assignment to a single state.

The shell-model calculations of McGrory[30] are in excellent agreement with the measured level energies and spins. Although spins were only measured in the present work to 1.8 MeV of excitation, the

apparent agreement of the results of other experiments indicates that his calculations can be extended quite satisfactorily to higher excitations. McGrory's calculations of the B(M1)'s and B(E2)'s agree, in general, with the γ-ray measurements reported here. Lifetime measurements for these states are needed for more direct comparisons with the predicted transition probabilities.

BIBLIOGRAPHY

References

[1]D. O. Wells, S. L. Blatt, and W. E. Meyerhof, Phys. Rev. 130, 1961 (1963).

[2]R. C. Jenkins and W. E. Meyerhof, Nucl. Phys. 58, 417 (1964).

[3]Hajime Ohnuma, Yoshio Hashimioto, and Isao Tomita, Nucl. Phys. 66, 337 (1965).

[4]C. J. Piluso, D. O. Wells, and D. K. McDaniels, Nucl. Phys. 77, 193 (1966).

[5]C. M. Lederer, J. M. Hollander, and I. Perlman, Table of Isotopes (John Wiley and Sons, Inc., New York, 1967), 6th ed.

[6]M. N. Rao, Nucl. Data Sheets B3 (No. 3-4), 43 (1970).

[7]R. G. Miller and R. W. Kavanagh, Nucl. Phys. A94, 261 (1967).

[8]T. A. Belote, W. E. Dorenbusch, and J. Rapaport, Nucl. Phys. A109, 666 (1968).

[9]J. M. Laget and J. Gastebois, Nucl. Phys. A122, 431 (1968).

[10]C. Shin, B. Pooh, K. Schadewalt, and J. P. Wurm, Phys. Rev. Letters 22, 1124 (1969).

[11]C. C. Lu, M. S. Zisman and B. G. Harvey, Phys. Rev. 186, 1086 (1969).

[12]G. Bruge and R. F. Leonard, Phys. Rev. C 2, 2200 (1970).

[13]J. M. Bjerregaard, P. F. Dahl, O. Hansen, and G. Sidenuis, Nucl. Phys. 51, 641 (1964).

[14]S. A. Hjorth, Arkiv Fysik 33, 147 (1966).

[15]M. J. Schneider and W. W. Daehnik, Phys. Rev. C 4, 1649 (1971).

[16]J. D. Anderson, C. Wong and J. W. McClure, Nucl. Phys. 36, 161 (1962).

[17]J. W. Nelson, H. S. Plendl, and P. H. Davis, Phys. Rev. 125, 2005 (1962).

[18]F. D. Becchetti, Jr., D. Dehnhard, and T. G. Dzubay, in Proceedings of the Second Conference on Nuclear Isospin, Asilomar-Pacific Grove, California, 1969, edited by J. D. Anderson, S. D. Bloom, J. Cerny and W. W. True (Academic Press, Inc., New York, 1969), p. 171.

[19]P. G. Roos and C. D. Goodman, in Proceedings of the Second Conference on Nuclear Isospin, Asilomar-Pacific Grove, California, 1969, edited by J. D. Anderson, S. D. Bloom, J. Cerny, and W. W. True (Academic Press, Inc., New York, 1969), p. 297.

[20]G. Bruge, A. Chaumeaux, Ha Duc Long, P. Roussel, and L. Valentin, Bull. Am. Phys. Soc. 15, 1208 (1969).

[21]T. G. Dzubay, R. Sherr, F. D. Becchetti, and D. Dehnhard, Nucl. Phys. A142, 488 (1970).

[22]D. O. Wells, Nucl. Phys. 66, 562 (1965).

[23]A preliminary account of this work was given by L. E. Samuelson, R. A. Warner, W. H. Kelly, R. R. Todd, and Wm. C. McHarris, Bull. Am. Phys. Soc. 16, 12 (1971); and L. E. Samuelson, R. A. Warner, W. H. Kelly, and F. M. Bernthal, Bull. Am. Phys. Soc. 17, 584 (1972).

[24]R. DelVecchio, R. F. Gibson, and W. W. Daehnik, Phys. Rev. C 5, 446 (1972).

[25]L. Wolfenstein, Phys. Rev. 82, 690 (1951).

[26]W. Hauser and H. Feshbach, Phys. Rev. 87, 366 (1953).

[27]L. C. Biedenharn and M. E. Rose, Rev. Mod. Phys. 25, 729 (1953).

[28]G. R. Satchler, Phys. Rev. 94, 1304 (1954); 104, 1198 (1956); erratum in Phys. Rev. 111, 1747 (1958).

[29]E. Sheldon and D. M. Van Patter, Rev. Mod. Phys. 38, 143 (1966).

[30]J. B. McGrory, private communication.

[31]K. A. Kraus and F. Nelson in Proceedings of the International Conference on the Peaceful Uses of Atomic Energy - Geneva, 1955, (United Nations Publication) p. 113.

[32]A. D. Horton, "Nickel, Spectrophotometric Di Methyl Glyoxime - Bromine Oxidation Method", Method Nos. 1 215411 and 9 00715411 (11-9-56), ORNL Master Analytical Manual, TID-7015, sec. 1 (April 1958).

[33]POLYPHEMUS, computer code written by R. Au, Michigan State University Cyclotron Laboratory, unpublished.

[34]J. T. Routti and S. G. Prussin, Nucl. Instr. and Meth. 72, 125 (1969).

[35]J. B. Marion, Nuclear Data A4, 301 (1968).

[36]R. C. Greenwood, R. G. Helmer, and R. J. Gehrke, Nucl. Instr. and Meth. 77, 141 (1970).

[37]A. J. Haverfield, F. M. Bernthal, and J. M. Hollander, Nucl. Phys. A94, 337 (1967).

[38]S. M. Brahmavar, J. H. Hamilton, A. V. Ramaygs, E. E. F. Zganjar, and C. E. Benris, Jr., Nucl. Phys. A125, 217 (1969).

[39]D. C. Camp and G. L. Meredith, Nucl. Phys. A166, 349 (1971).

[40]EVENT, computer code written by D. Bayer, Michigan State University Cyclotron Laboratory, unpublished.

[41]EVENT RECOVERY, computer code written by D. B. Beery and G. C. Giesler, Michigan State University Cyclotron Laboratory, unpublished.

[42]W. B. Ewbank and S. Raman, Nucl. Data Sheets B3 (No. 3-4), 187 (1970).

[43]P. Goode and L. Zanúk, Phys. Rev. Letters 22, 958 (1969).

[44]S. D. Bloom, L. G. Mann, and J. A. Miskel, Phys. Rev. 125, 2021 (1962).

[45]H. Daniel, Rev. of Mod. Phys. 40, 659 (1968).

[46]R. K. Sheline and R. W. Stoughton, Phys. Rev. 87, 1 (1952).

[47]H. Maria, J. Dalmasso, G. Ardisson, and C. Ythier, Compt. Rend. B271, 165 (1970).

[48]C. Maples, G. W. Goth, and J. Cerny, Nuclear Reaction Q-values, (University of California, Berkeley, 1966); UCRL-16964 (1966).

[49]L. E. Samuelson, Ph.D. Thesis, Michigan State University, (1972).

[50]J. Vervier, Nucl. Phys. 78, 497 (1966).

[51]H. J. Hausman, R. M. Humes, and R. G. Seyler, Phys. Rev. 164, 1407 (1967).

[52]L. L. Lee, Jr., and J. P. Schiffer, Phys. Letters 4, 104 (1963).

[53]J. R. Huizenga and A. A. Katsanos, Nucl. Phys. A98, 614 (1967).

[54]E. Sheldon and P. Gantenbein, J. Appl. Math. Phys. (ZAMP) 18, 397 (1967); E. Sheldon and R. M. Strang, Comp. Phys. Comm. 1, 35 (1969).

[55]E. H. Auerbach, "ABACUS-II", Brookhaven National Laboratory Preprint BNL-6562 (undated, unpublished).

[56]F. Perey, Direct Interactions and Nuclear Reaction Mechanisms, (Gordon and Breach Science Publishers Inc., New York, 1963).

[57]F. Perey and B. Buck, Nucl. Phys. 32, 353 (1962).

[58]E. Sheldon, Rev. Mod. Phys. 35, 795 (1963).

[59]B. H. Armitage, A. T. G. Ferguson, G. C. Neilson, and W. D. N. Pritchard, Nucl. Phys. A133, 241 (1969).

[60]K. M. Thompson and C. R. Gruhn, Nucl. Inst. and Meth. 74, 309 (1969).

[61]GADFIT, computer code written by R. A. Warner, Michigan State University Cyclotron Laboratory, unpublished.

[62]The absolute intensity standards were obtained from the Radiation Materials Corporation of Waltham, Massachusetts.

[63]P. A. Moldauer, Phys. Rev. 123, 968 (1961); 135, B642 (1964); Rev. Mod. Phys. 36, 1079 (1964).

[64]R. V. Jones, W. Dbrowalski, and C. D. Jeffries, Phys. Rev. 102, 738 (1956).

[65]A. H. Sher and B. D. Pate, Nucl. Phys. A112, 85 (1968), and references cited therein.

[66]Walter Menti, Helv. Phys. Acta, 40, 981 (1967).

[67]S. S. Hanna, J. Heberle, C. Littlejohn, G. J. Perlow, R. S. Preston, and D. H. Vincent, Phys. Rev. Letters 4, 177 (1960).

[68]M. R. Najam, W. F. Davidson, W. M. Zuk, L. E. Carlson, and M. A. Awal, Nucl. Phys. A173, 577 (1971).

[69]E. C. Halbert, J. B. McGrory, B. H. Wildenthal, and S. P. Pandya, in Advances in Nuclear Physics, edited by E. Vogt and M. Baranger (Plenum Press, Inc., New York, 1971), Vol. 4.

[70]Emilio Segrè, Nuclei and Particles, (W. A. Benjamin, Inc.), New York 1965).

APPENDICES

APPENDIX A

Separation of Nickel from Irradiated Iron Shimstock

1. Dissolve sample in HCl.
2. Add Mn and Ni hold-back carriers.
3. Adjust acidity to 1M with HCl.
4. Precipitate CuS by adding thioacetamide sparingly.
5. Remove precipitate by centrifugation and discard precipitate.
6. Boil supernatant with concentrated nitric acid and bromine water to destroy hydrogen sulfide and colloidal metal sulfides. (This step is extremely important.)
7. Precipitate iron hydroxides with 15M aqueous ammonia.
8. Remove precipitate by centrifugation and discard precipitate.
9. Precipitate Ni in supernatant with dimethylglyoxime (DMG).
10. Remove precipitate by centrifugation and discard supernatant.
11. Dissolve precipitate in HCl and add Co carrier.
12. Reprecipitate Ni DMG by the addition of NH_4OH.
13. Remove precipitate by centrifugation and discard supernatant.
14. Rinse precipitate twice with distilled H_2O using centrifugation and discarding supernatant each time.
15. Finally, dissolve precipitate in HCl and transfer to a small plastic vial for counting.

APPENDIX B

Integral Coincidence and Gated Spectra from the $^{56}Fe(p,n\gamma\text{-}\gamma)^{56}Co$ Reaction at E_p=7.38 and 8.36 MeV.

Figure 15. Integral coincidence and gated spectra from the $^{56}Fe(p,n\gamma)^{56}Co$ Reaction at E_p = 7.38 and 8.36 MeV. The x-axis is from the 2.5% detector while the y-axis is from the 7.4% detector. Background subtraction using the adjacent continuum has been included. Peaks labeled in parenthesis are believed to be from chance coincidences or insufficient background subtraction. More details are given in the text.

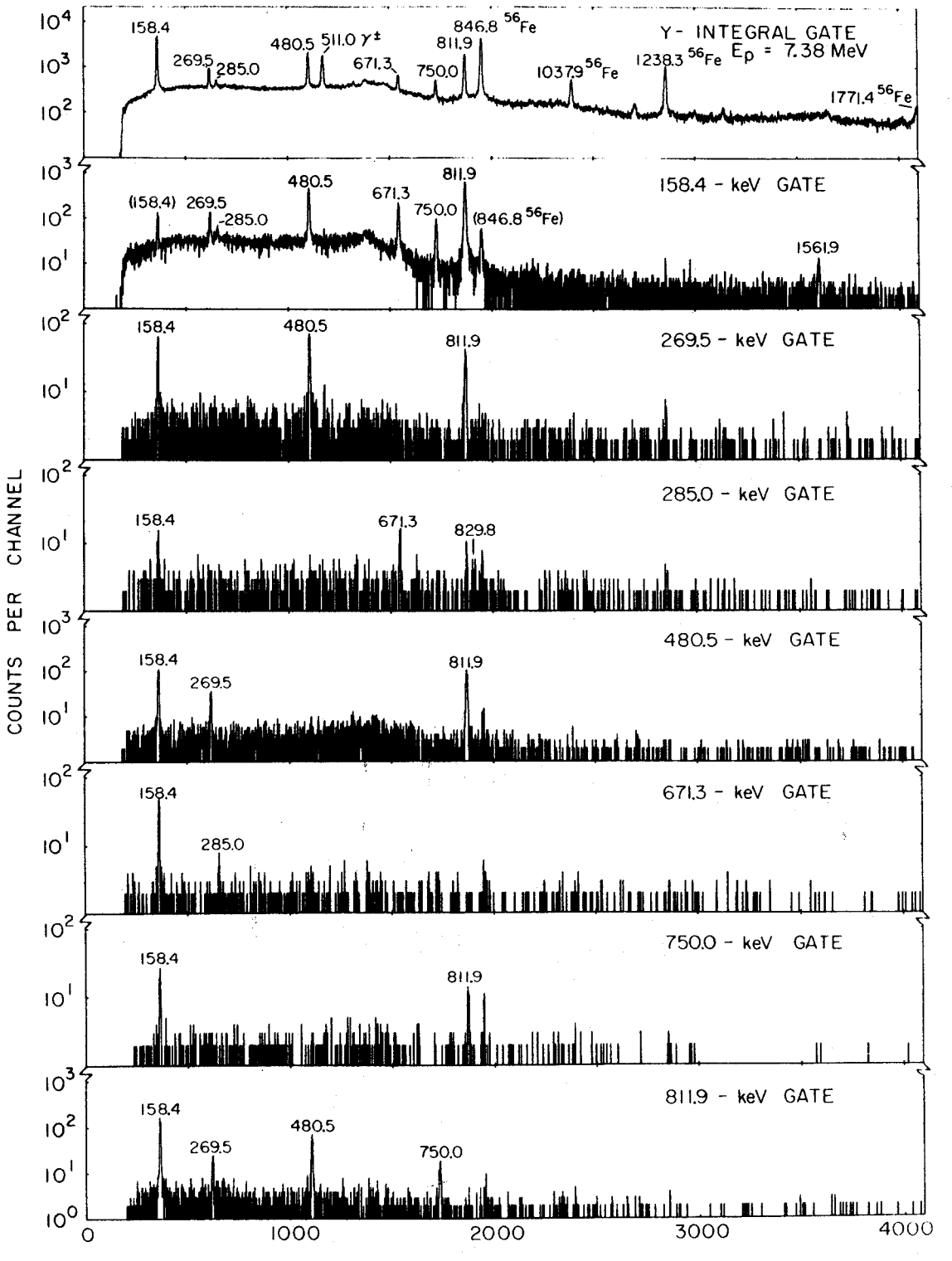

Figure 15 - continued.

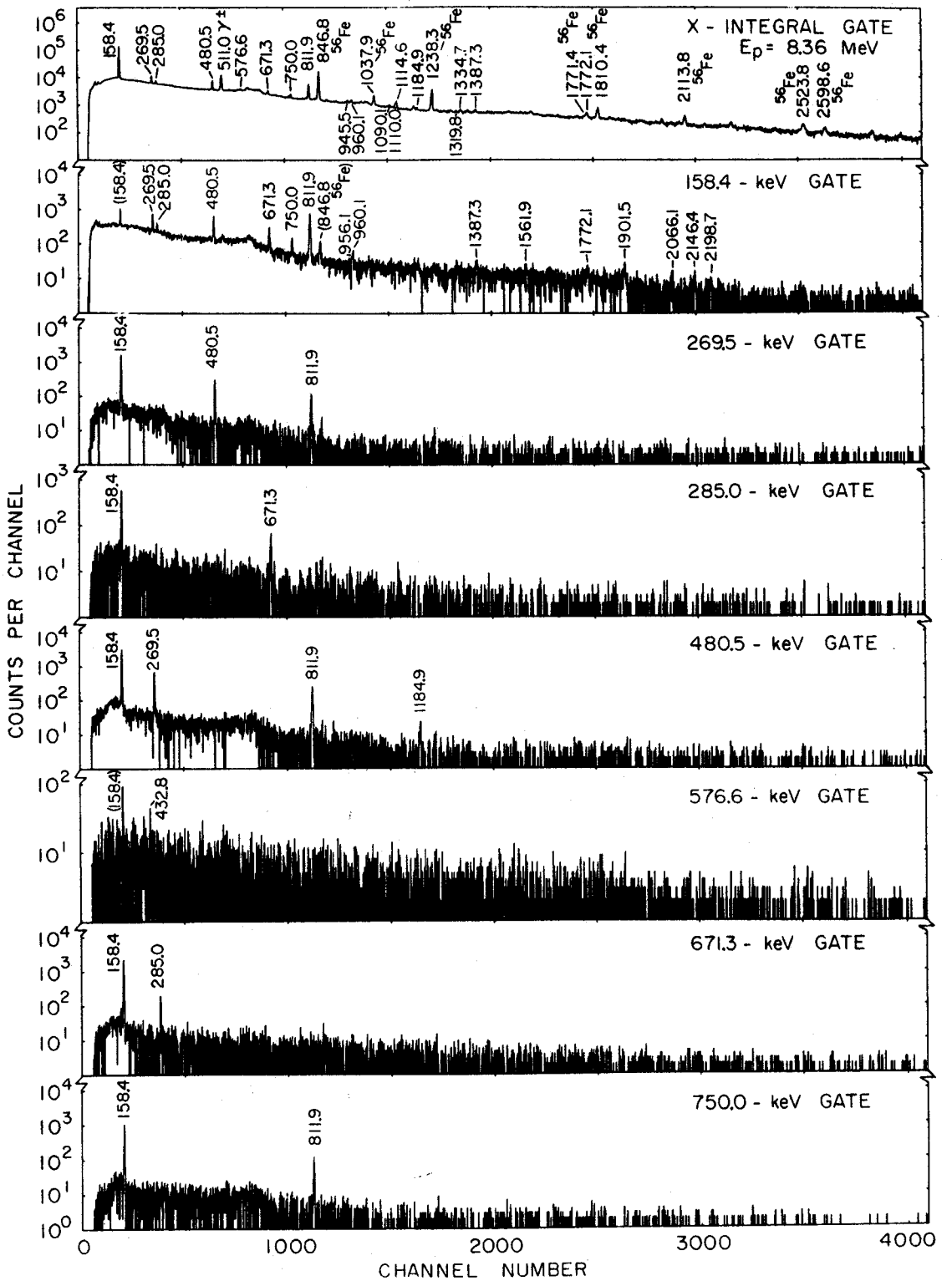

Figure 15 - continued.

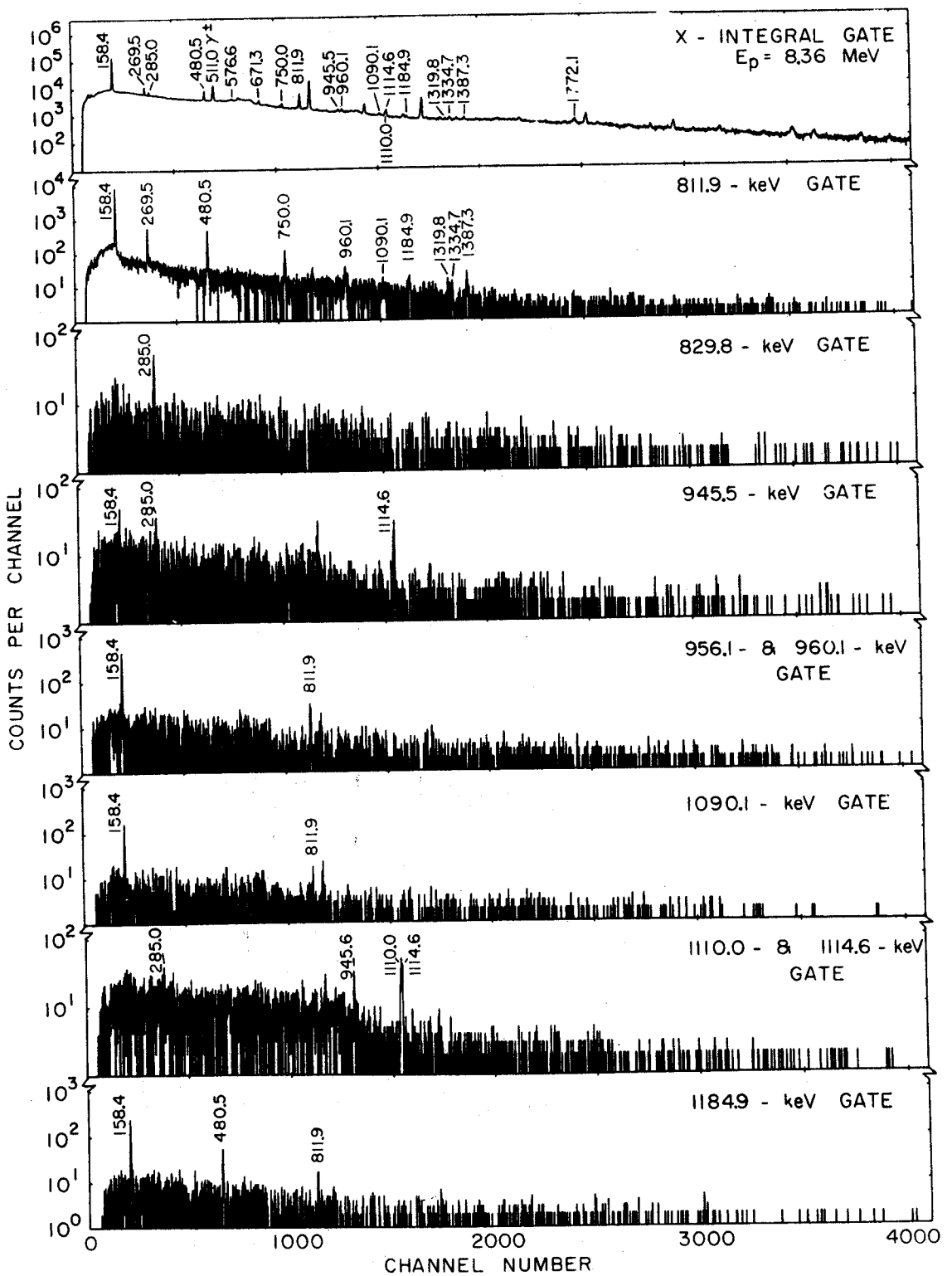

Figure 15 - continued.

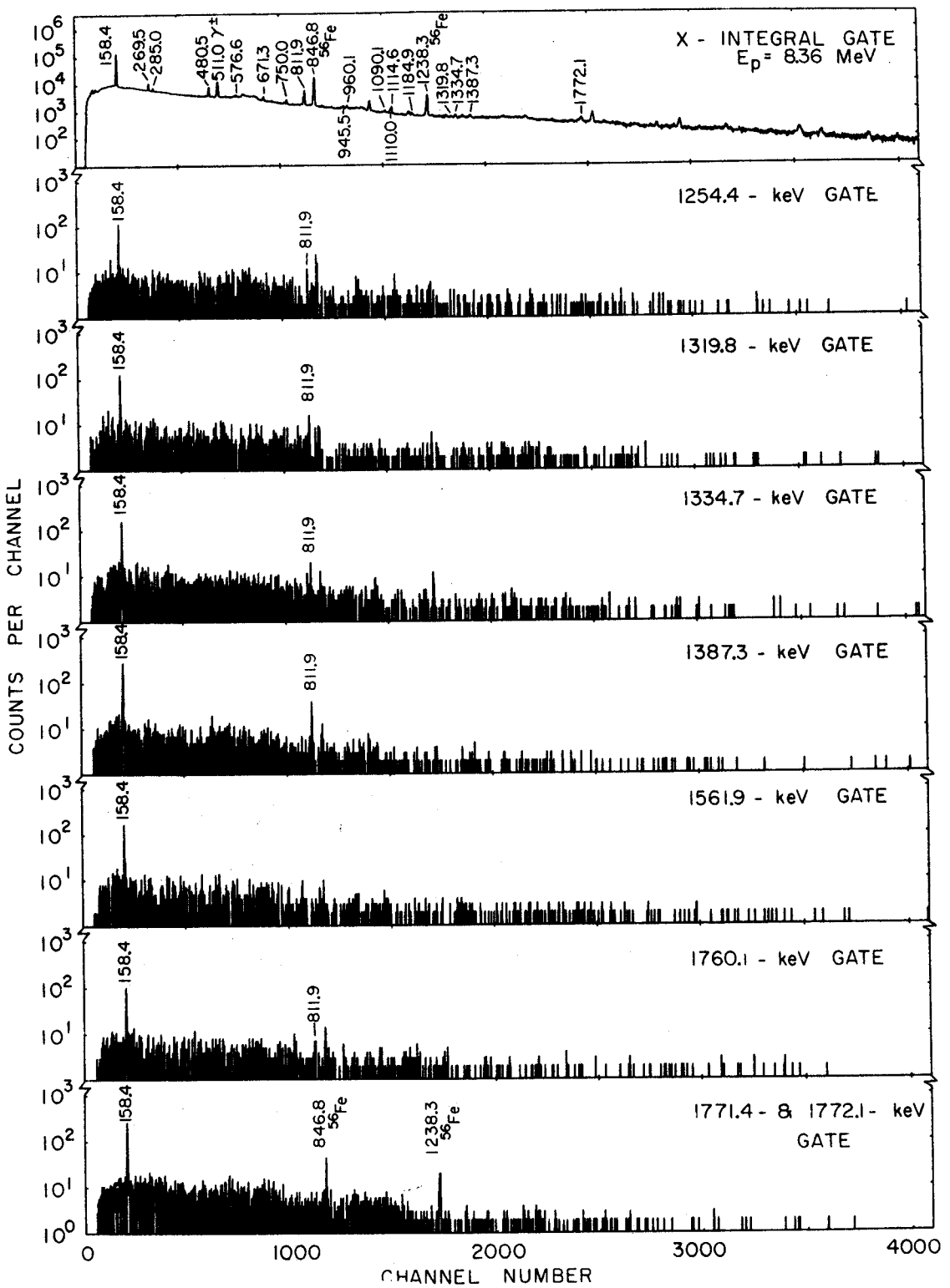

Figure 15 - continued

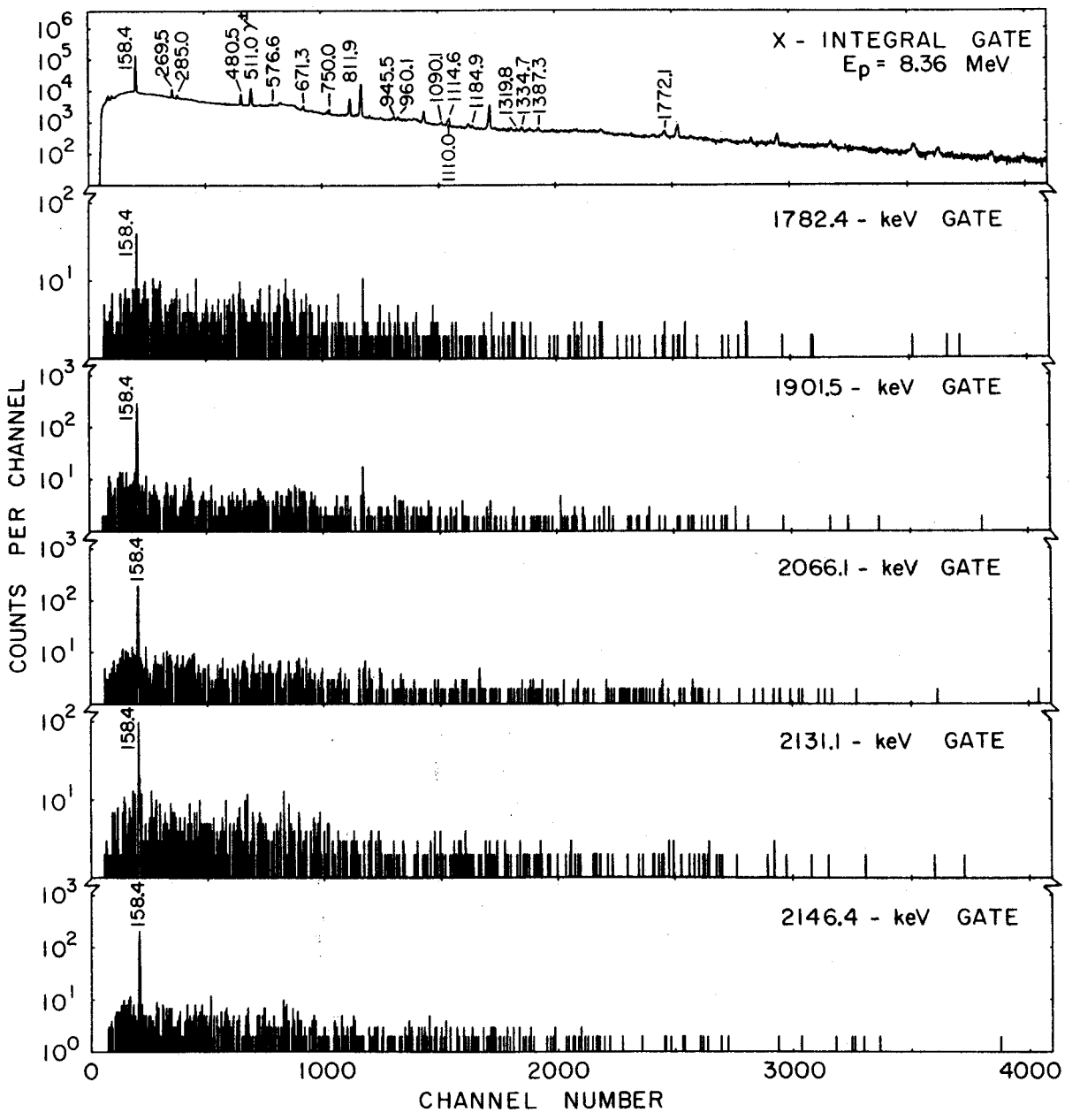

Figure 15 - continued.

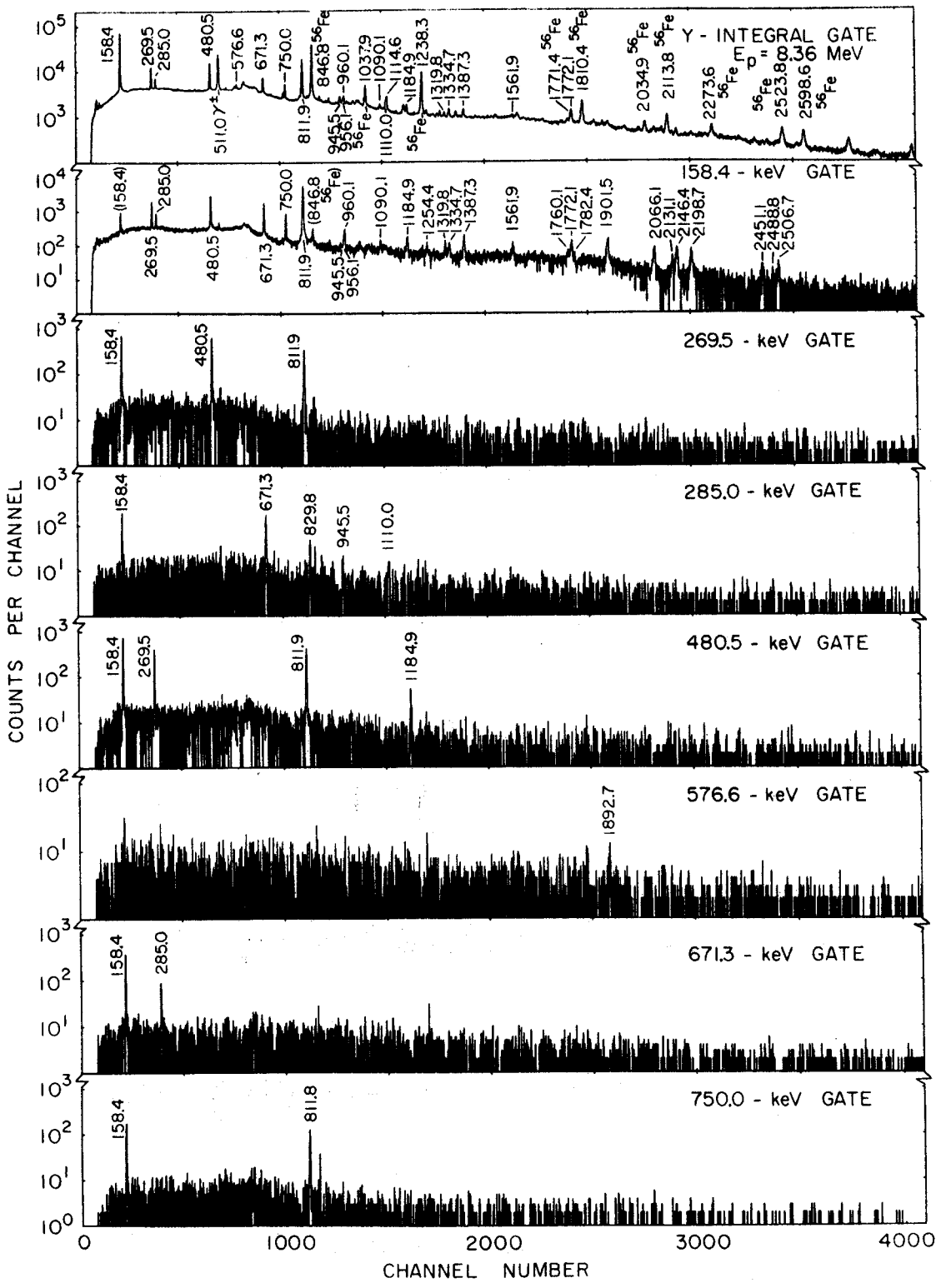

Figure 15 - continued.

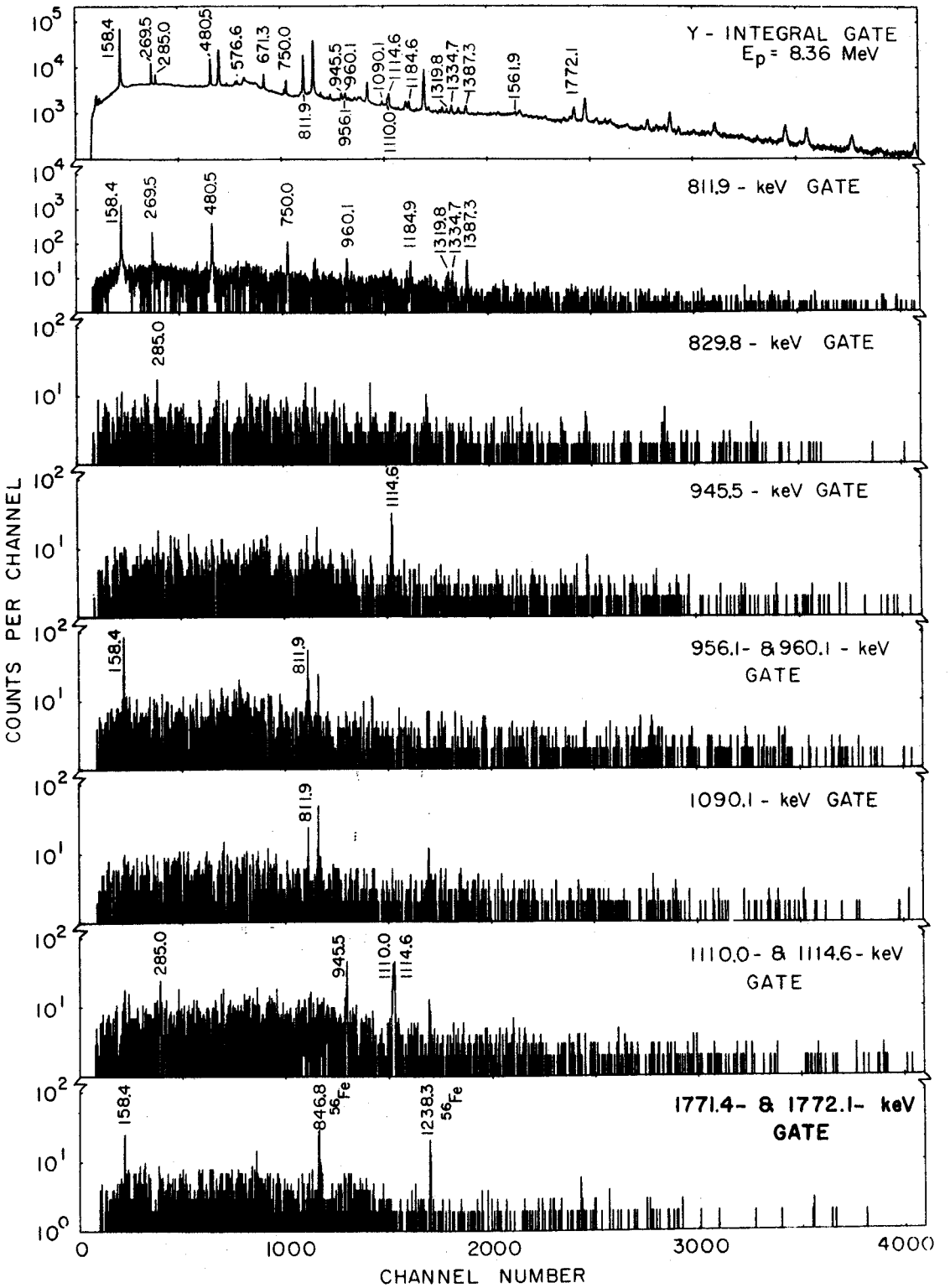

Figure 15 - continued.

APPENDIX C

γ-ray Angular Distributions from the $^{56}Fe(p,n\gamma)^{56}Co$ Reaction at E_p = 5.77, 6.65, 7.03, 7.05, 7.30, and 7.40 MeV.

Figure 16. γ-ray Angular Distributions from the $^{56}Fe(p,n\gamma)^{56}Co$ Reaction at E_p = 5.77, 6.65, 7.03, 7.05, 7.30, and 7.40 MeV. The solid lines through the data represent least squares fits using the equation for $W(\theta)$ given in the text. $W(\theta)$ has been normalized to 1 at 90°. Except for the E_p = 7.40 MeV case, two experimental points were taken at each angle; only their weighted average is presented. The assignment of errors is outlined in the text.

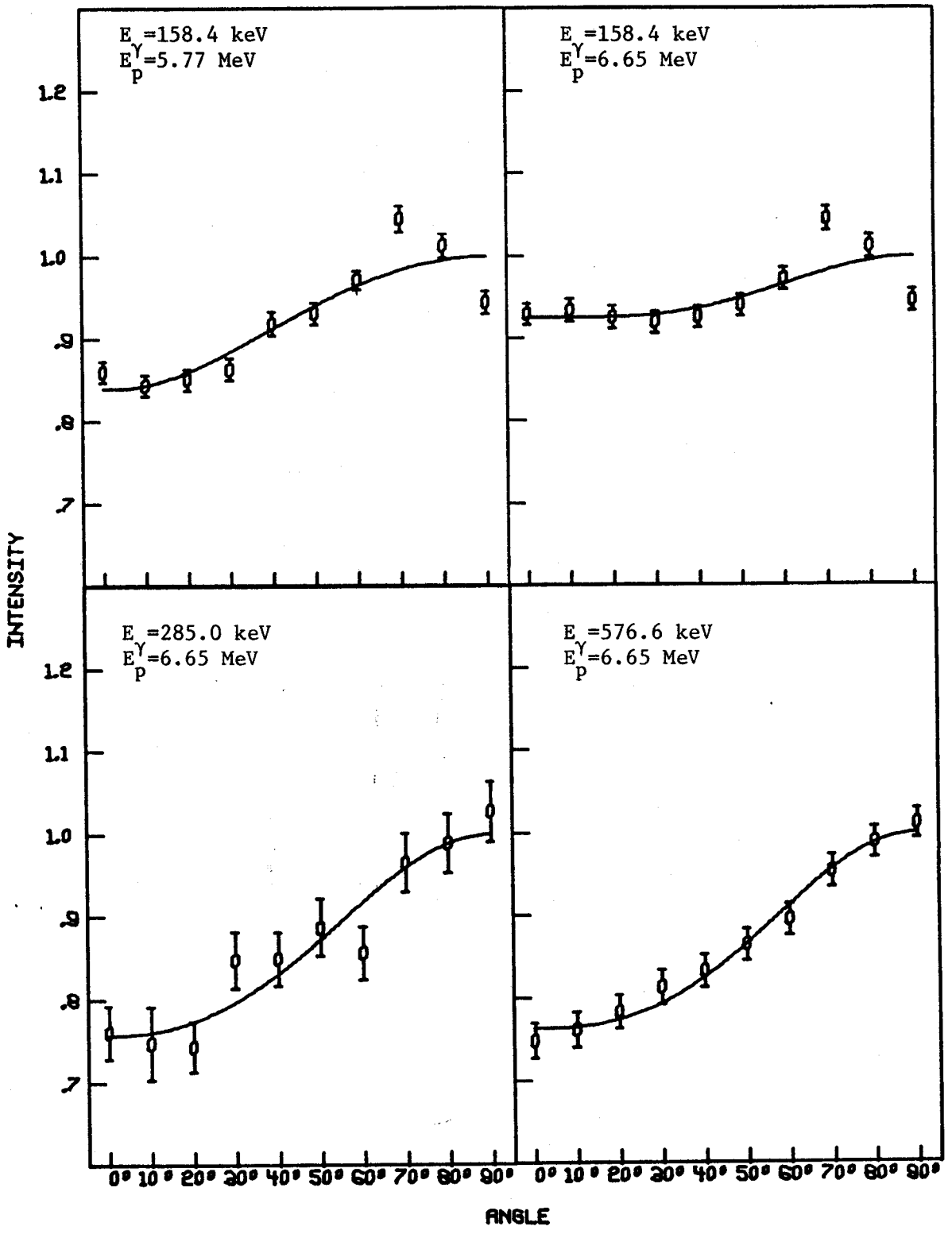
E_γ=158.4 keV
E_p=5.77 MeV
E_γ=158.4 keV
E_p=6.65 MeV
E_γ=285.0 keV
E_p=6.65 MeV
E_γ=576.6 keV
E_p=6.65 MeV
INTENSITY
1.2
1.1
1.0
.9
.8
.7
0° 10° 20° 30° 40° 50° 60° 70° 80° 90°
ANGLE

Figure 16.

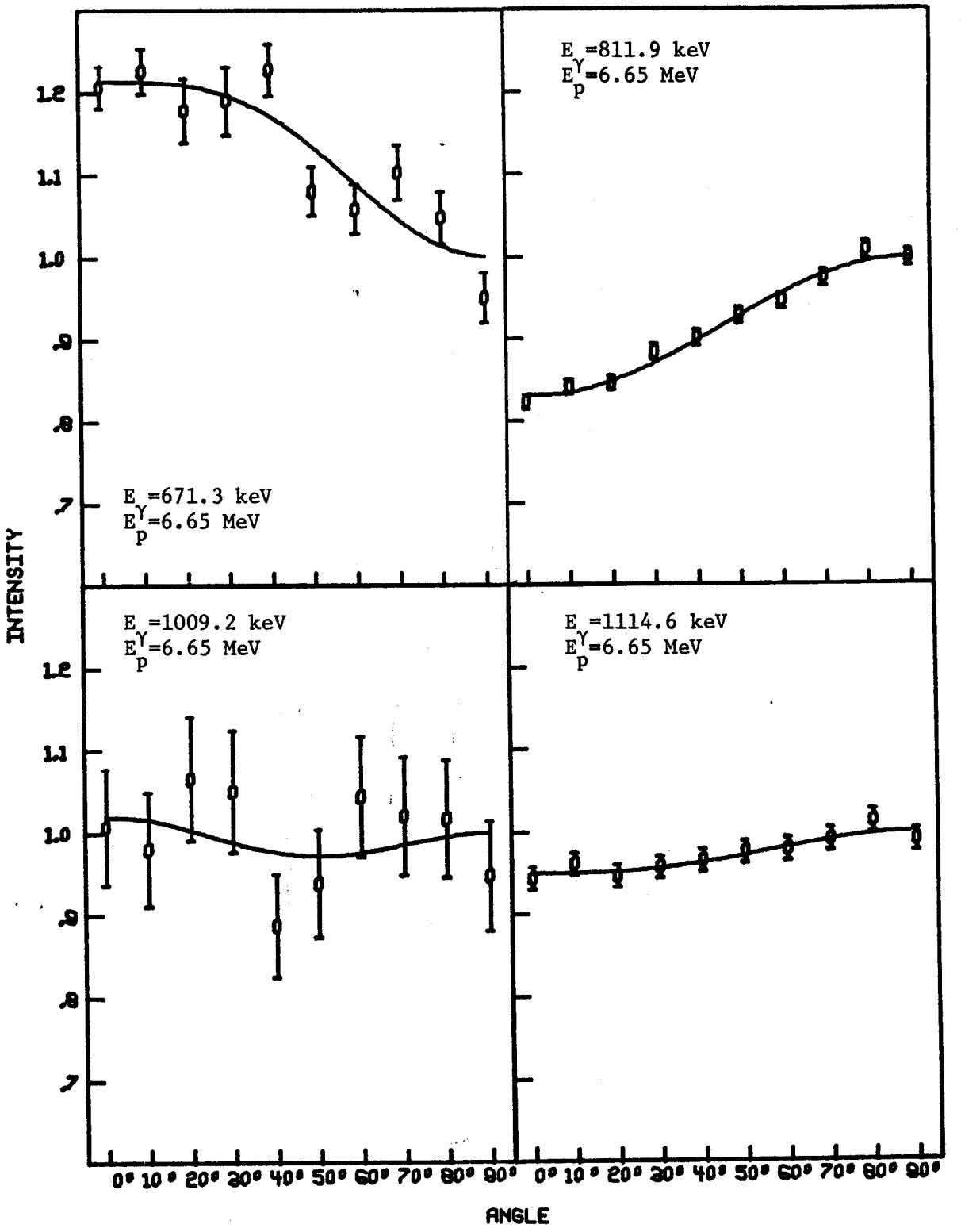

Figure 16 - continued.

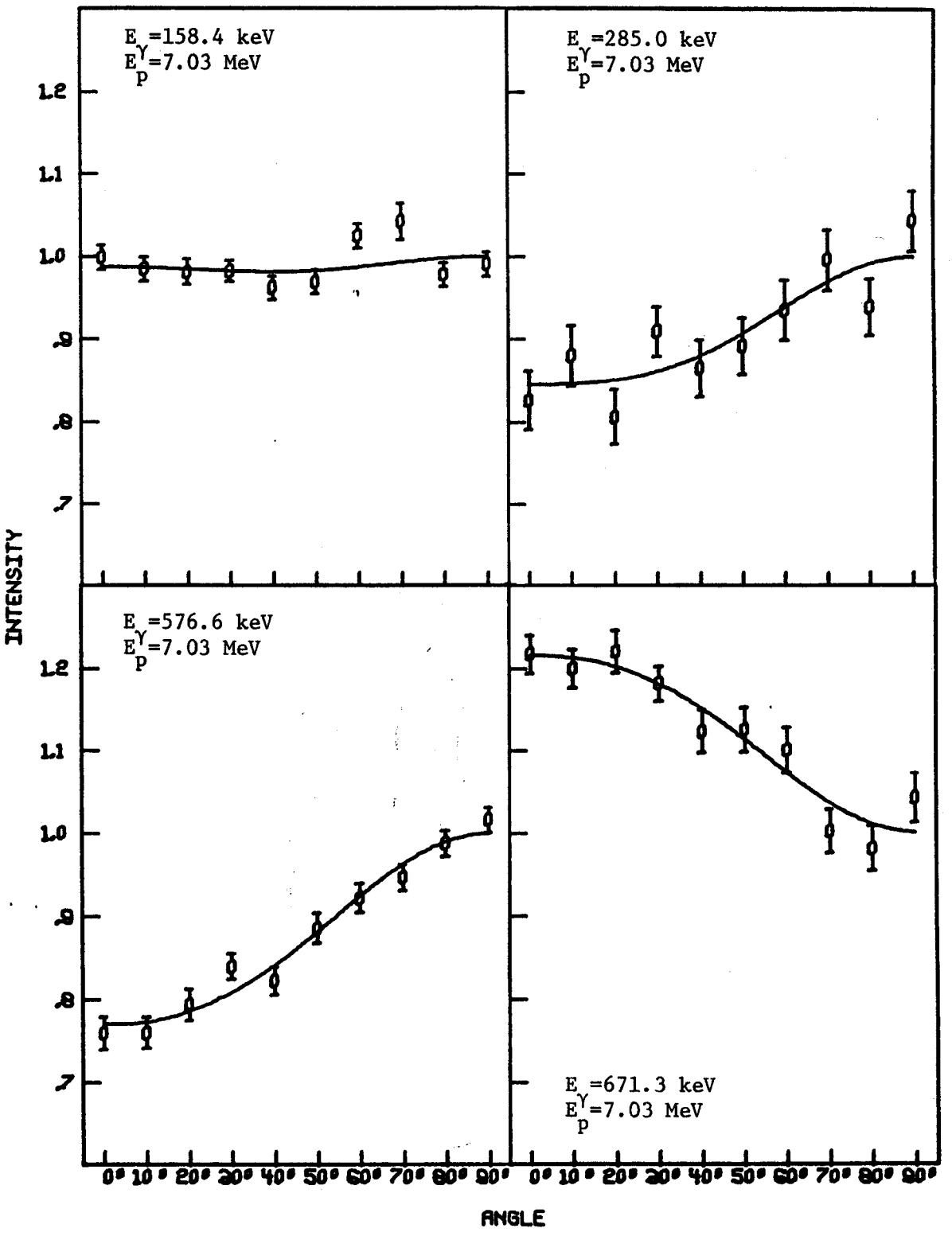

Figure 16 - continued.

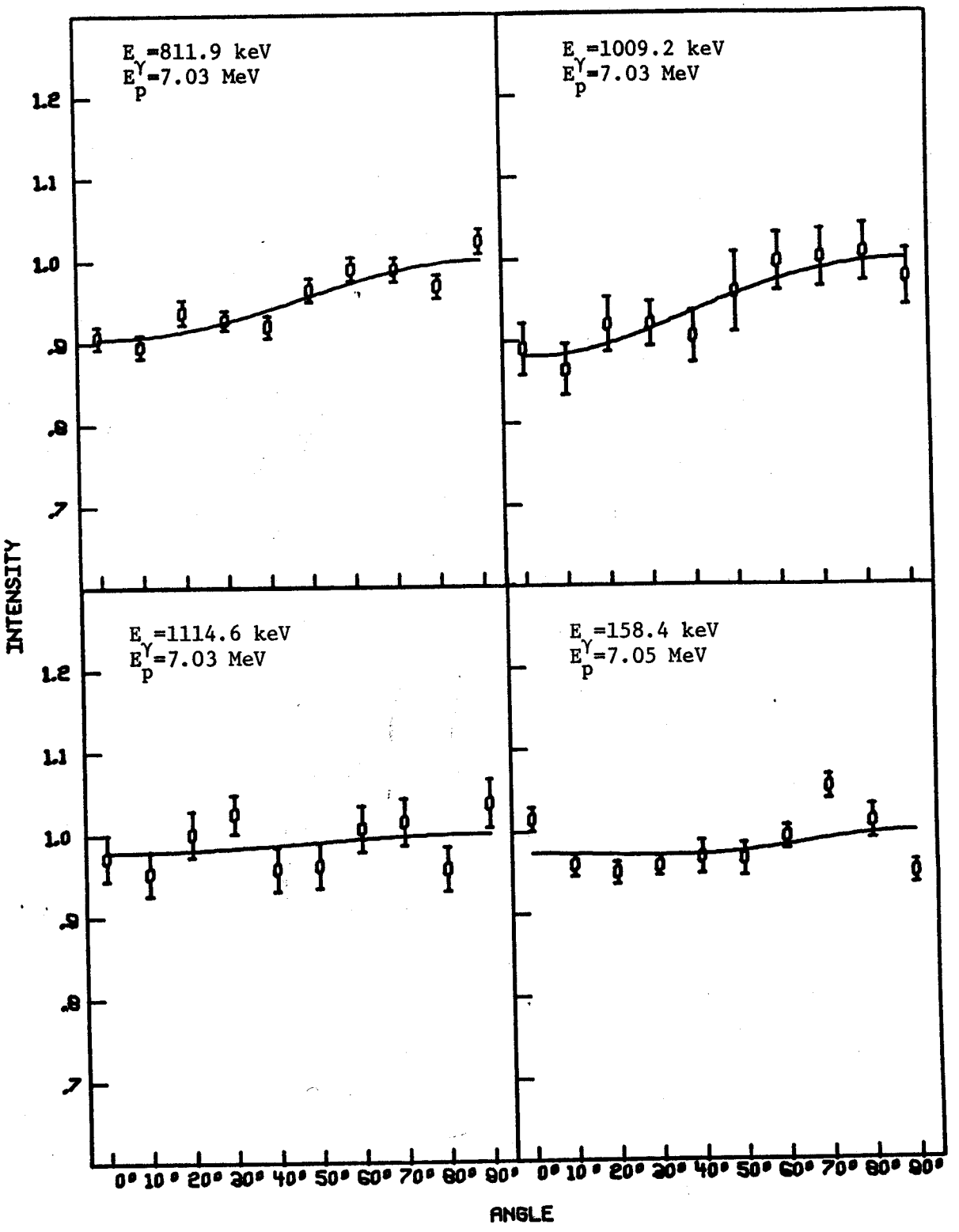

Figure 16 - continued.

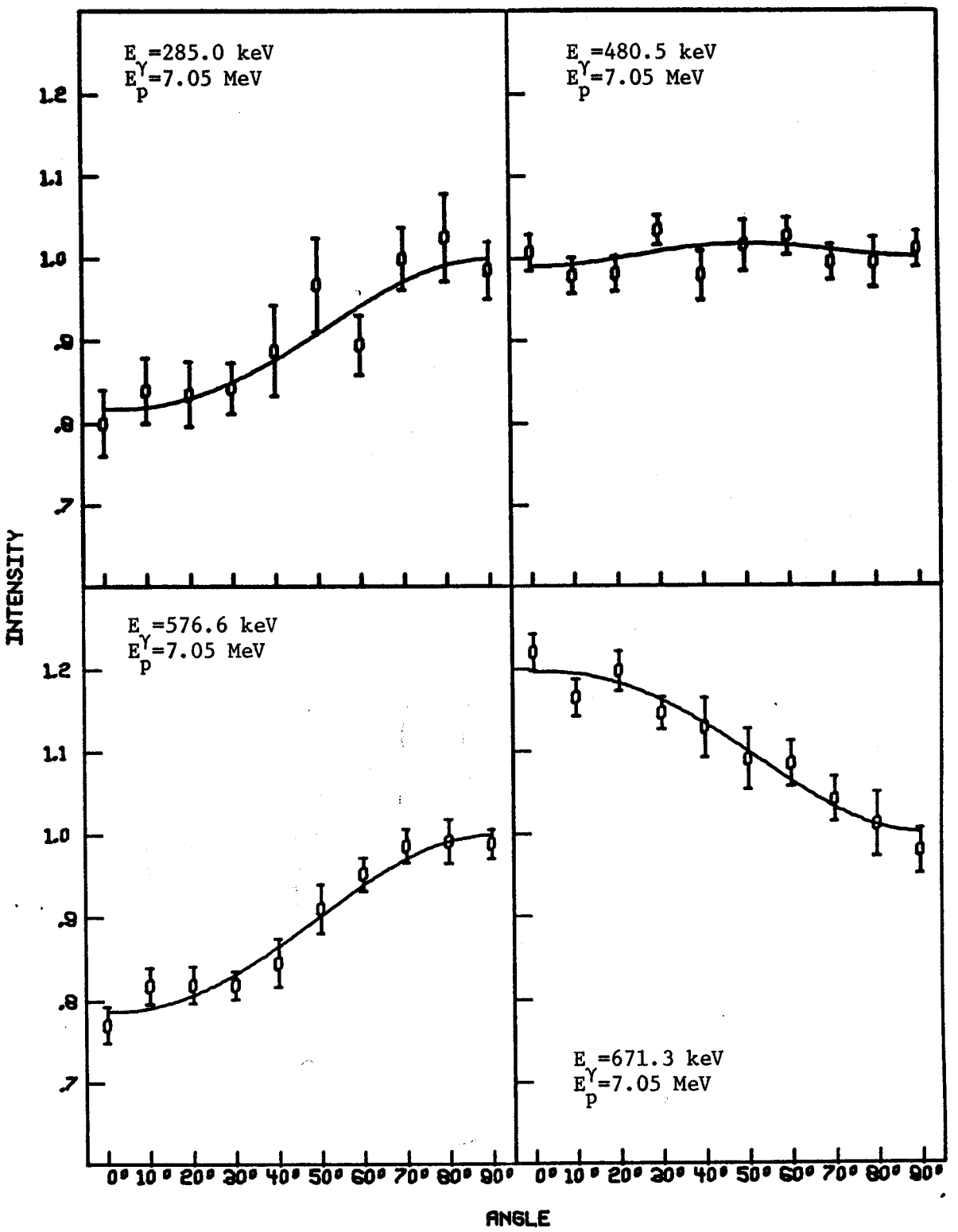

Figure 16 - continued.

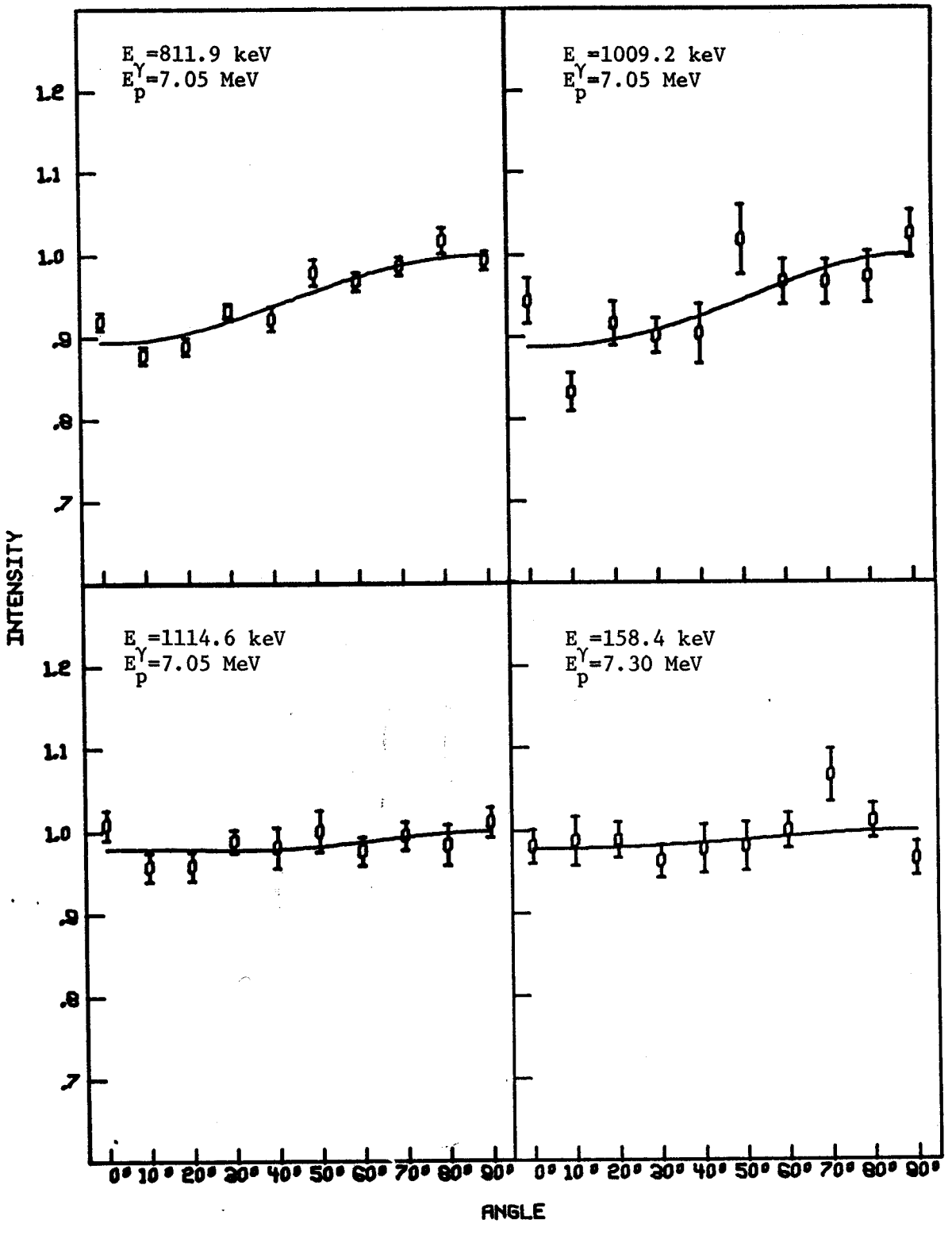

Figure 16 - continued.

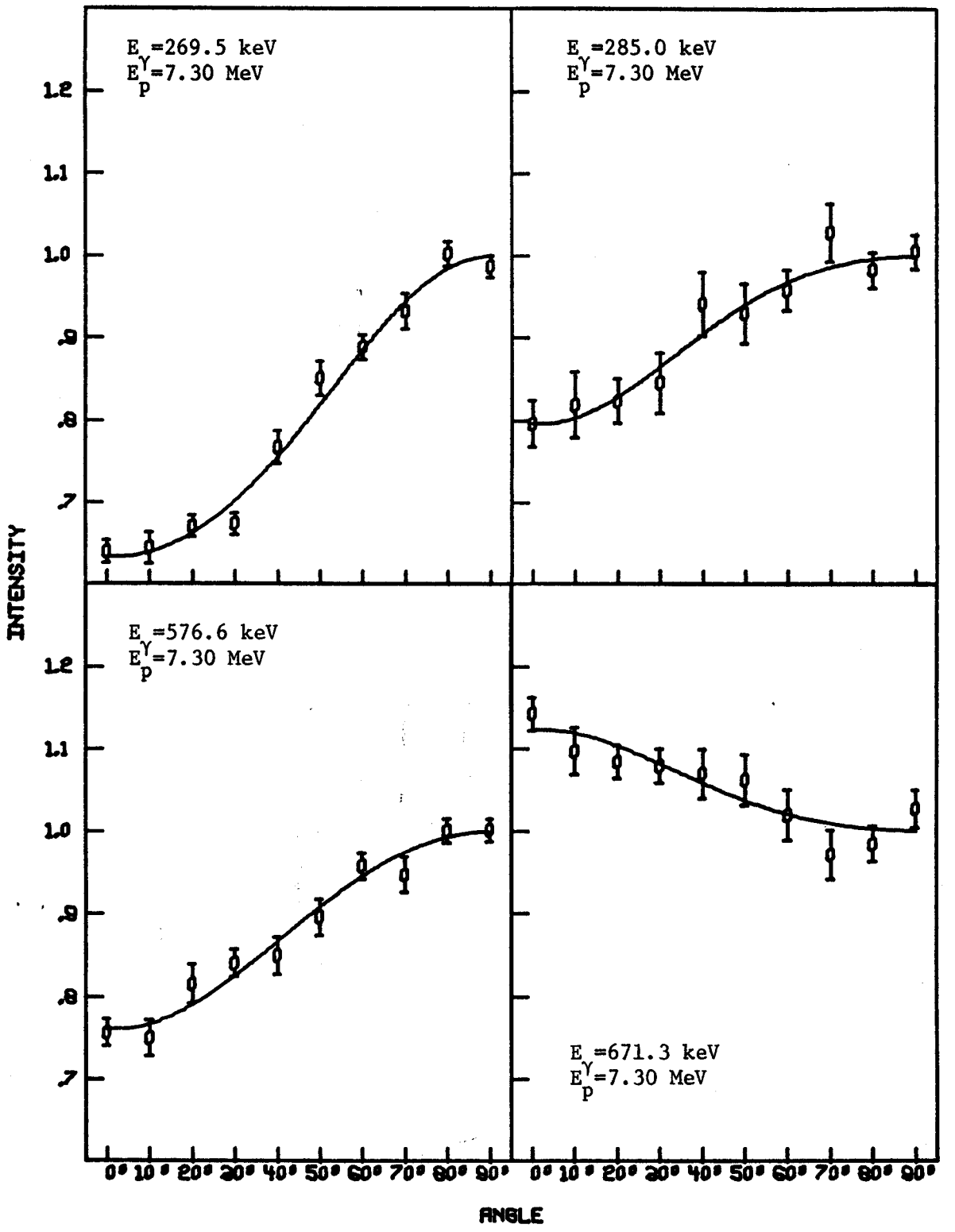

Figure 16 - continued.

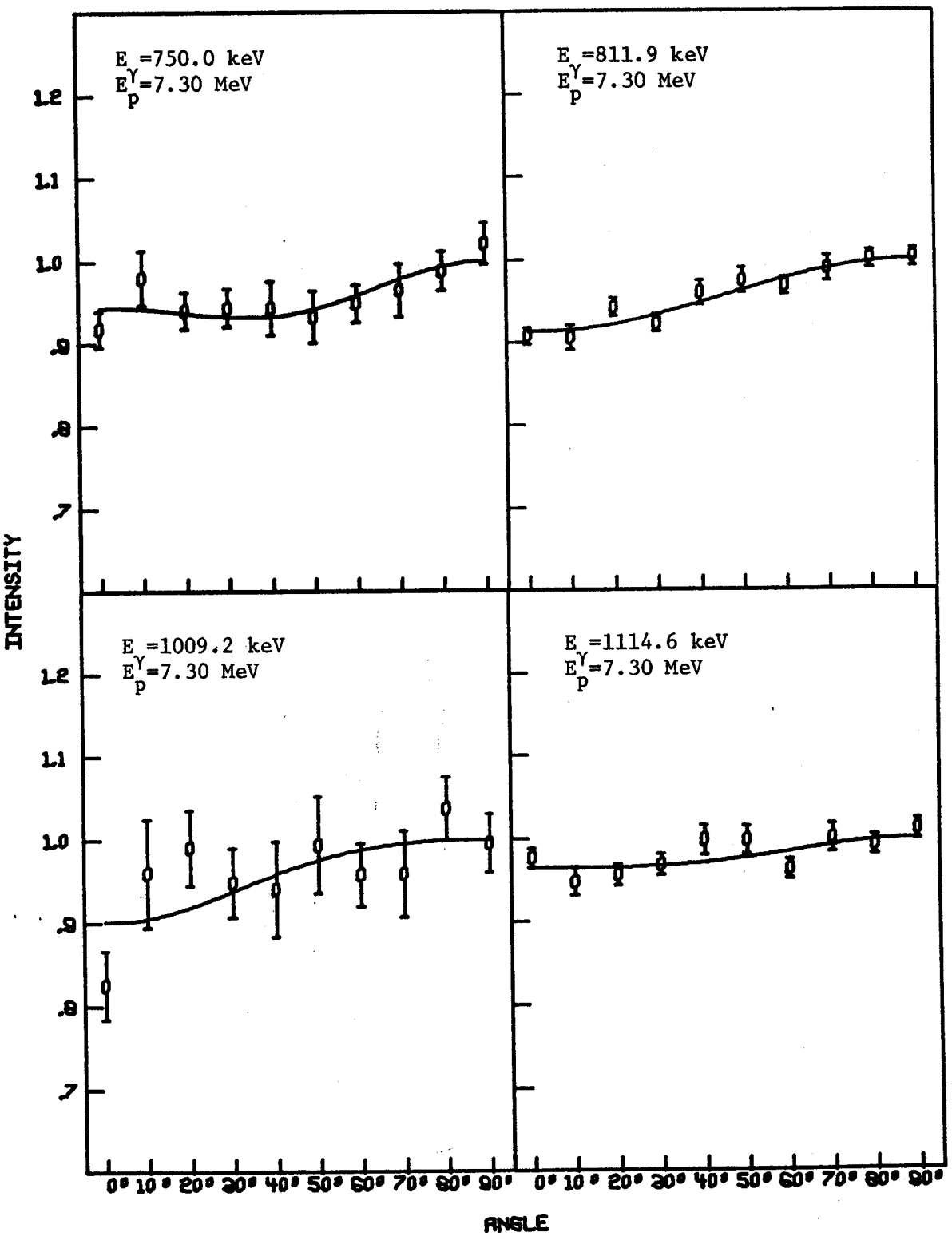

Figure 16 - continued.

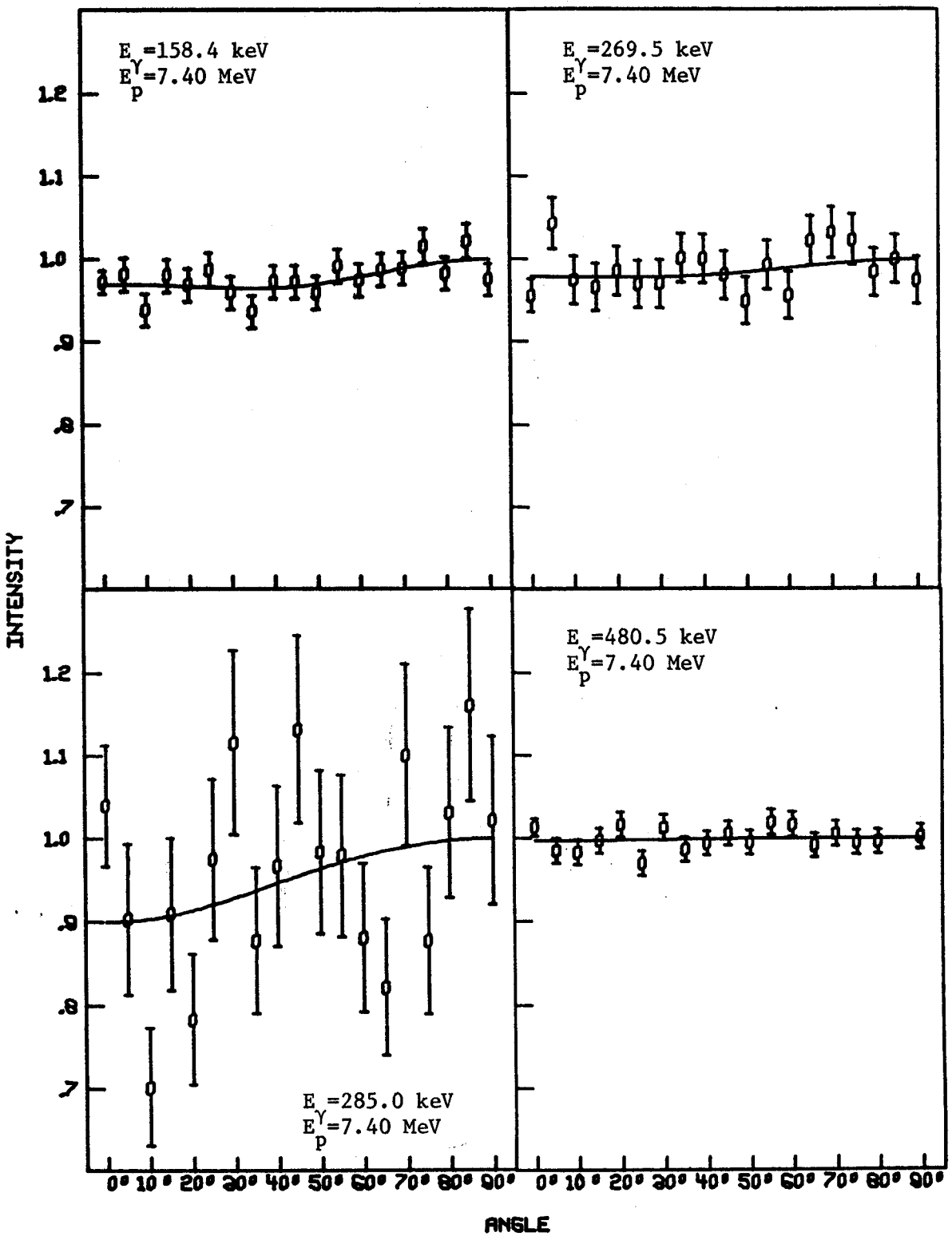

Figure 16 - continued.

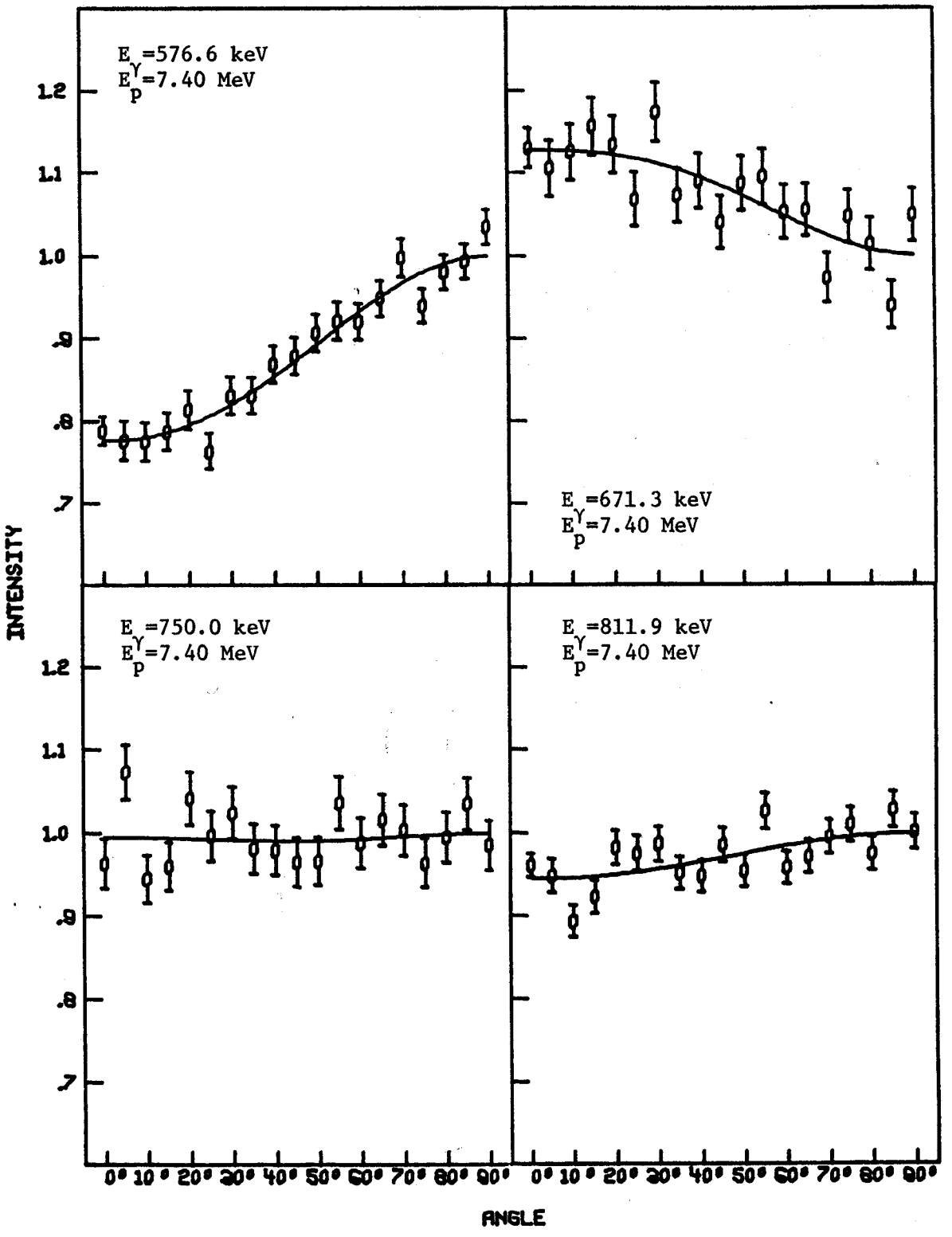

Figure 16 - continued.

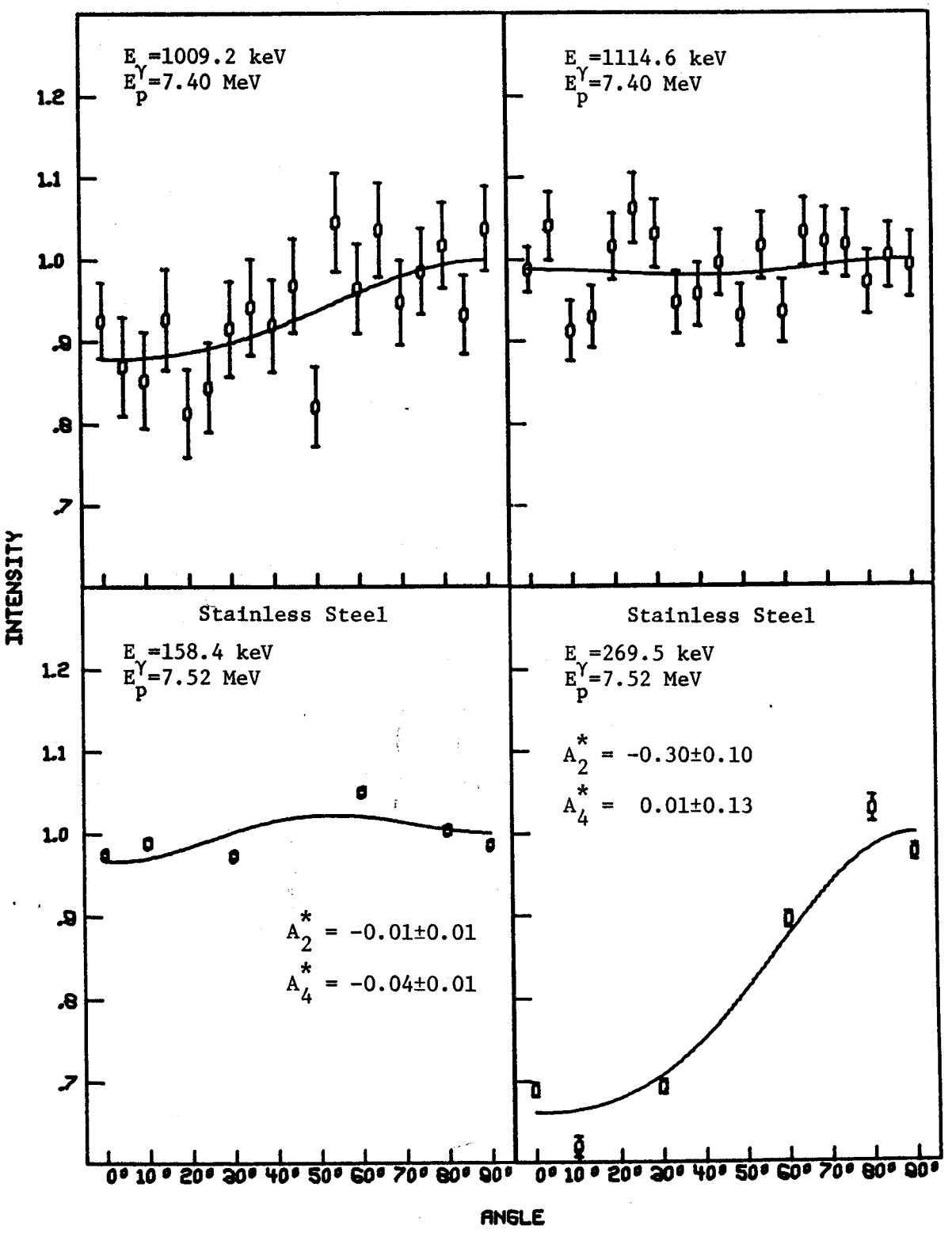

Figure 16 - continued.

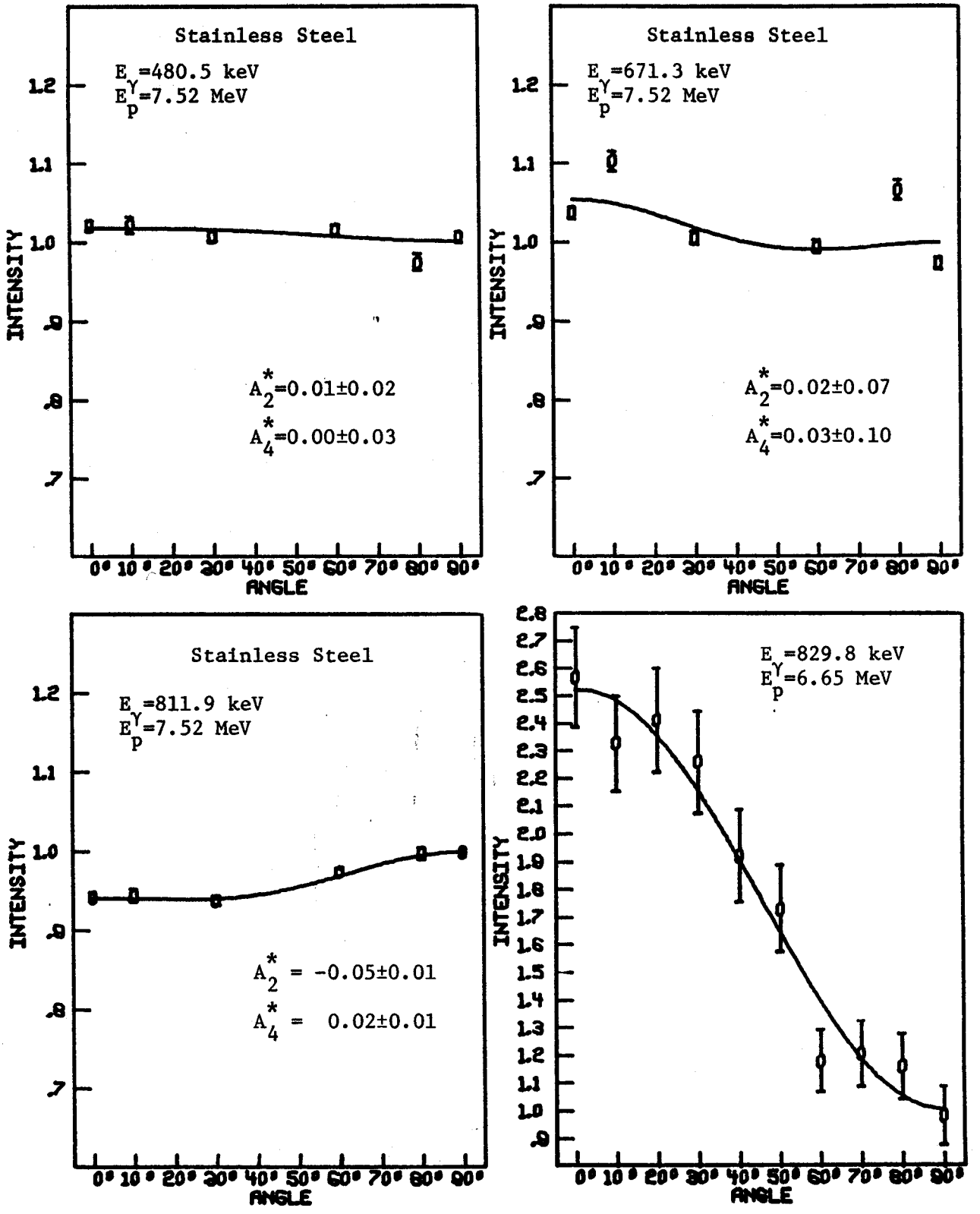

Figure 16 - continued.

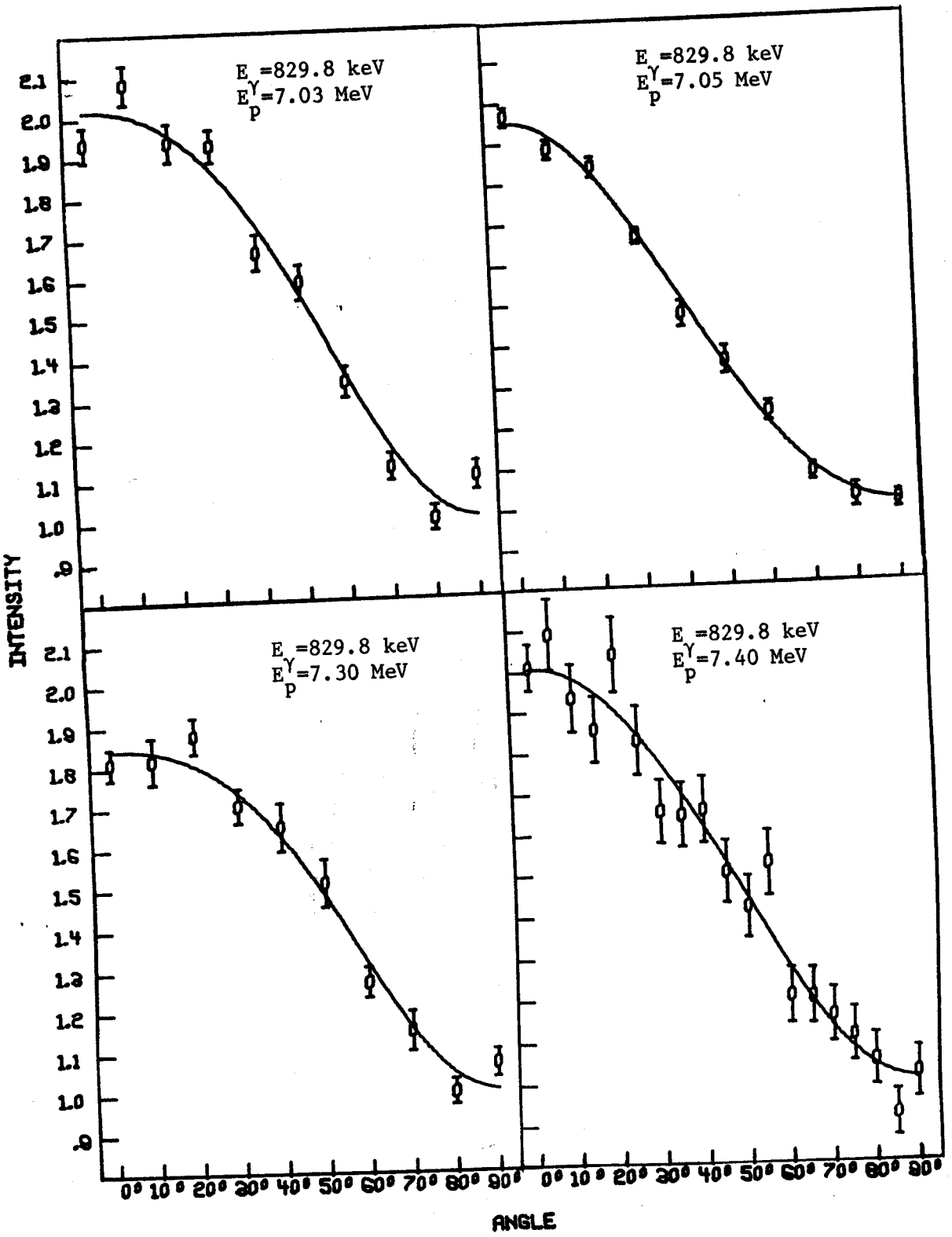

Figure 16 - continued.

APPENDIX D

The Experimental and Theoretical Values of the A_2^* and A_4^* ^{56}Co γ-ray Angular Distribution Coefficients as a Function of the γ-ray Mixing Ratio δ.

Figure 17. Plots of the Experimental and Theoretical Values of the A_2^* and A_4^* ^{56}Co γ-ray Angular Distribution Coefficients as a Function of γ-ray Mixing Ratio δ. (Definitions and descriptions for the calculations are presented in the text.) Only those cases are shown where γ-ray feeding from above was judged to be insignificant. In each case the spin used for the final state was that determined from this experiment; the possible initial state spins and parities label their appropriate δ-ellipses. Approximate locations for the values of δ can be found by comparison with Fig. 12. In each case the 1^+ "ellipse" is a short straight vertical line passing through the point $A_2^* = 0.0$, $A_4^* = 0.0$. The experimental A_2^* and A_4^* coefficients including uncertainties are shown on each plot as a rectangle.

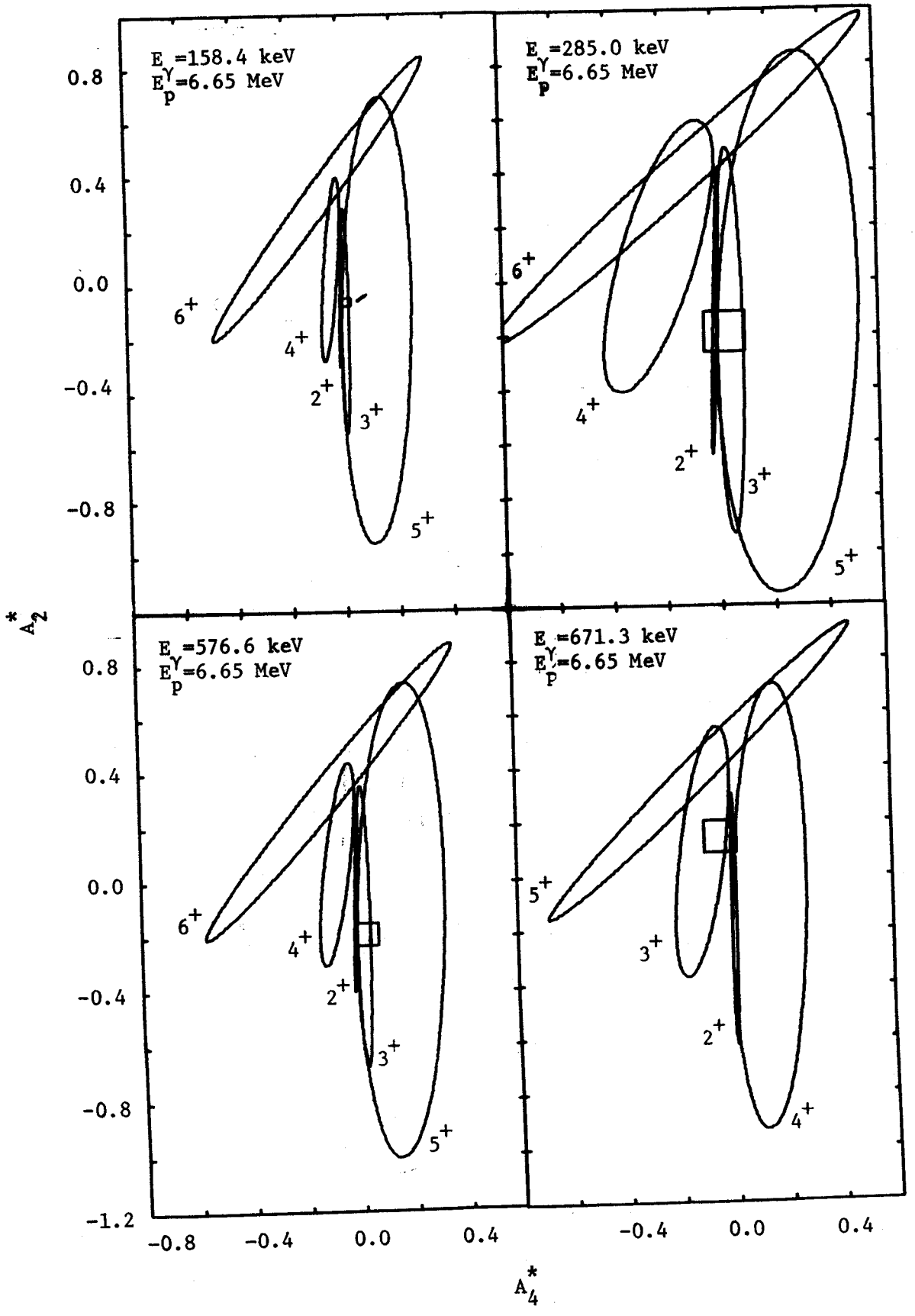
E_γ=158.4 keV
E_p^γ=6.65 MeV
E_γ=285.0 keV
E_p^γ=6.65 MeV
E_γ=576.6 keV
E_p^γ=6.65 MeV
E_γ=671.3 keV
E_p^γ=6.65 MeV
6+
4+
2+
3+
5+
0.8
0.4
0.0
-0.4
-0.8
-1.2
-0.8
-0.4
0.0
0.4
A*2
A*4

Figure 17.

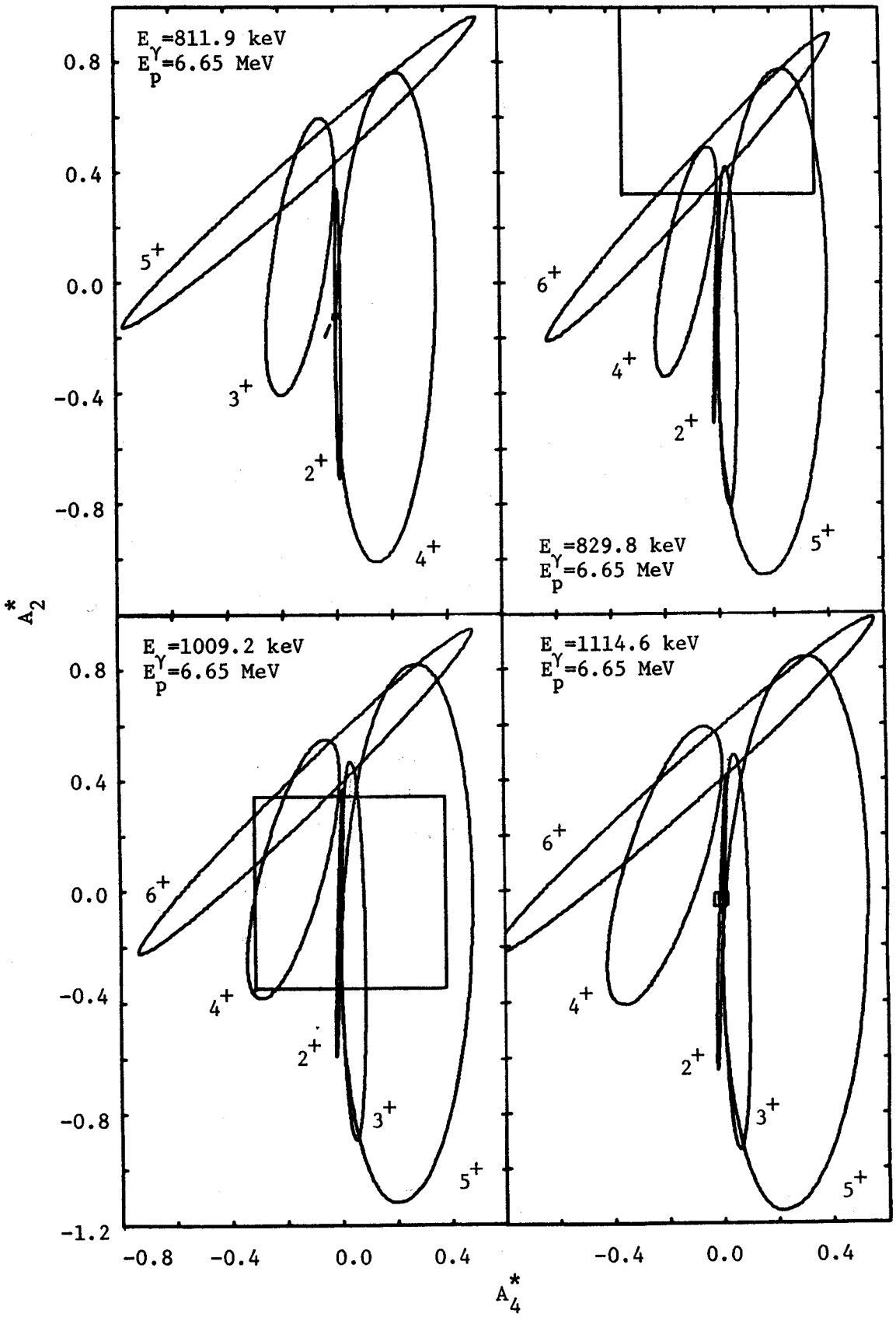

Figure 17 - continued.

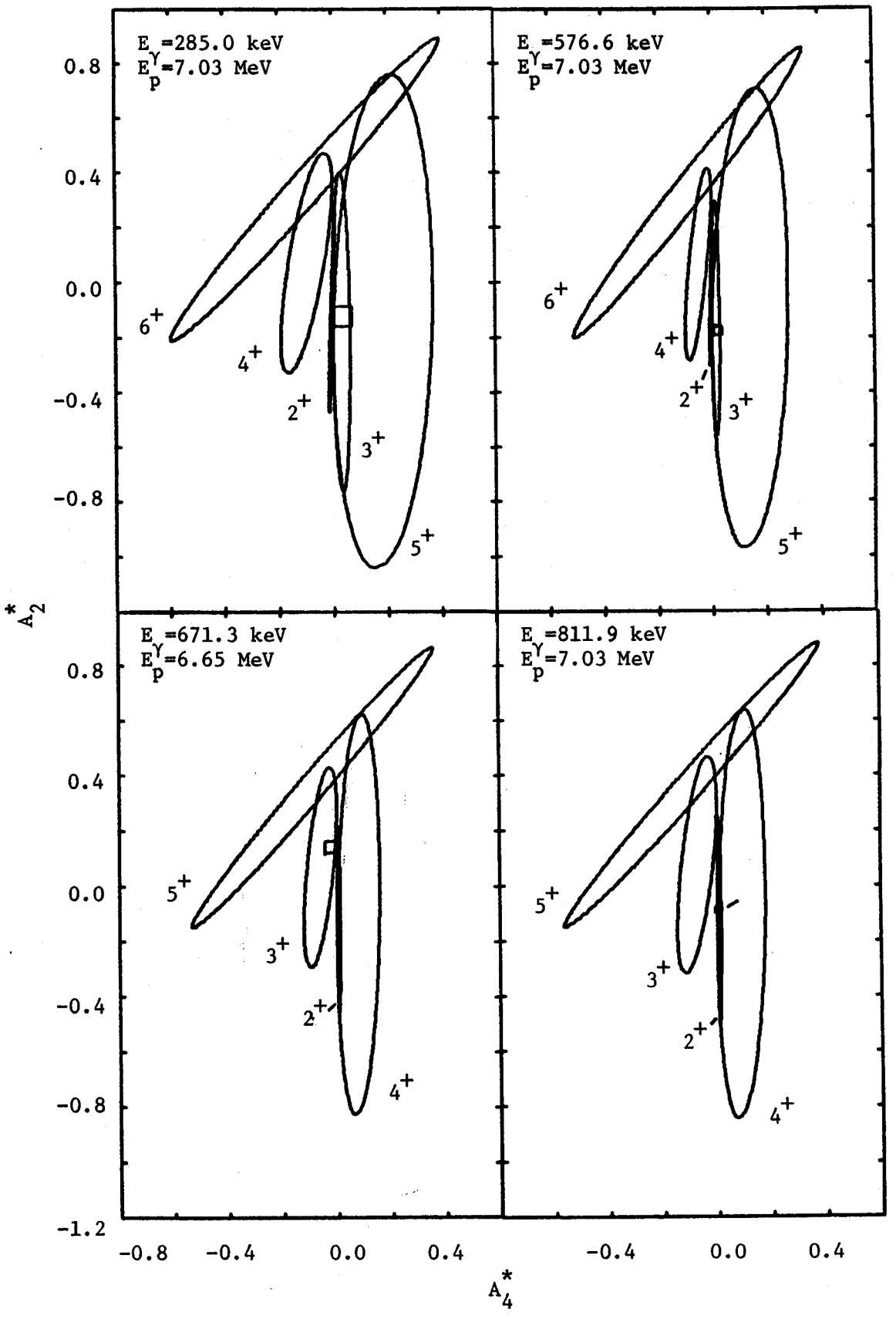

Figure 17 - continued.

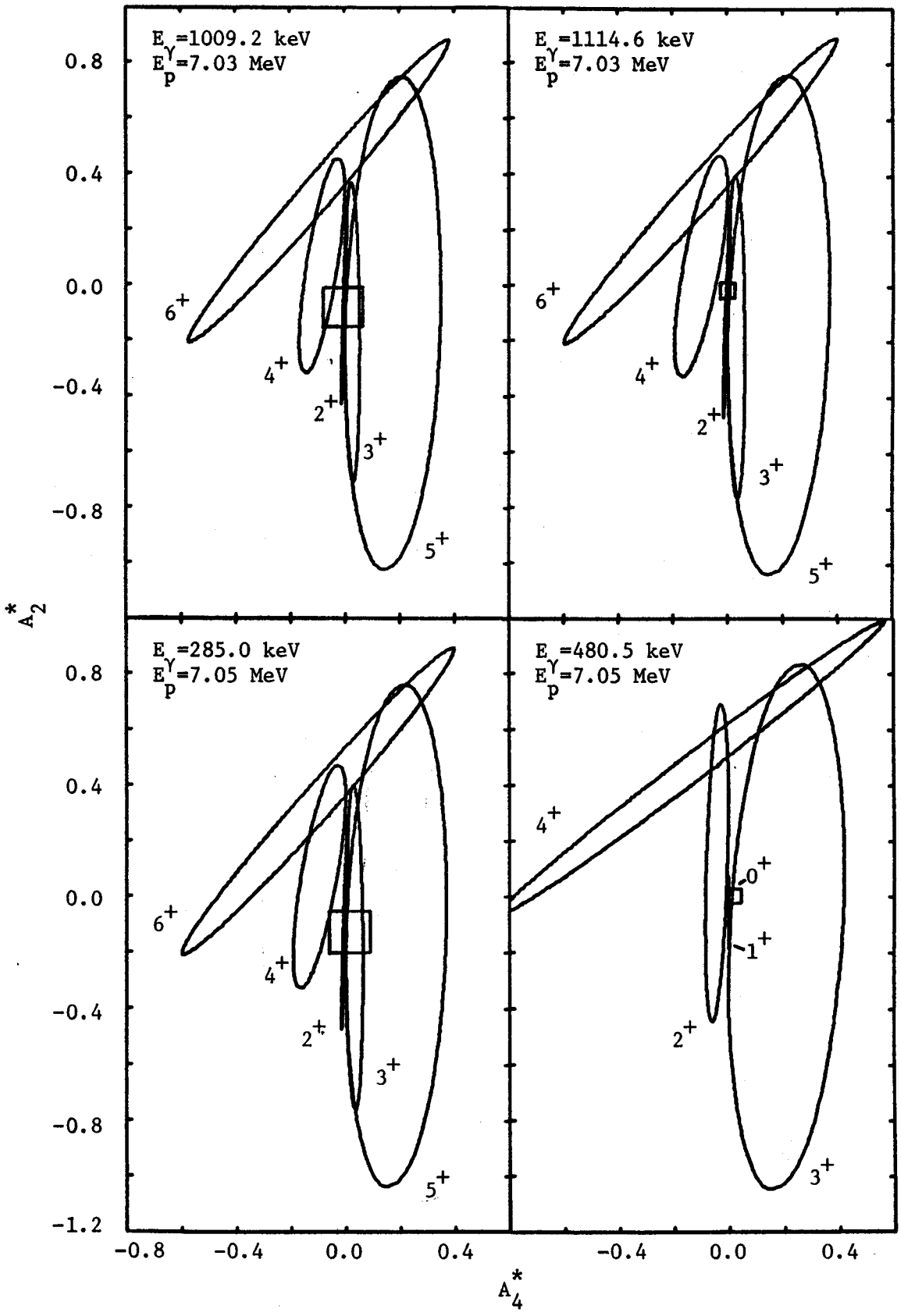

Figure 17 - continued.

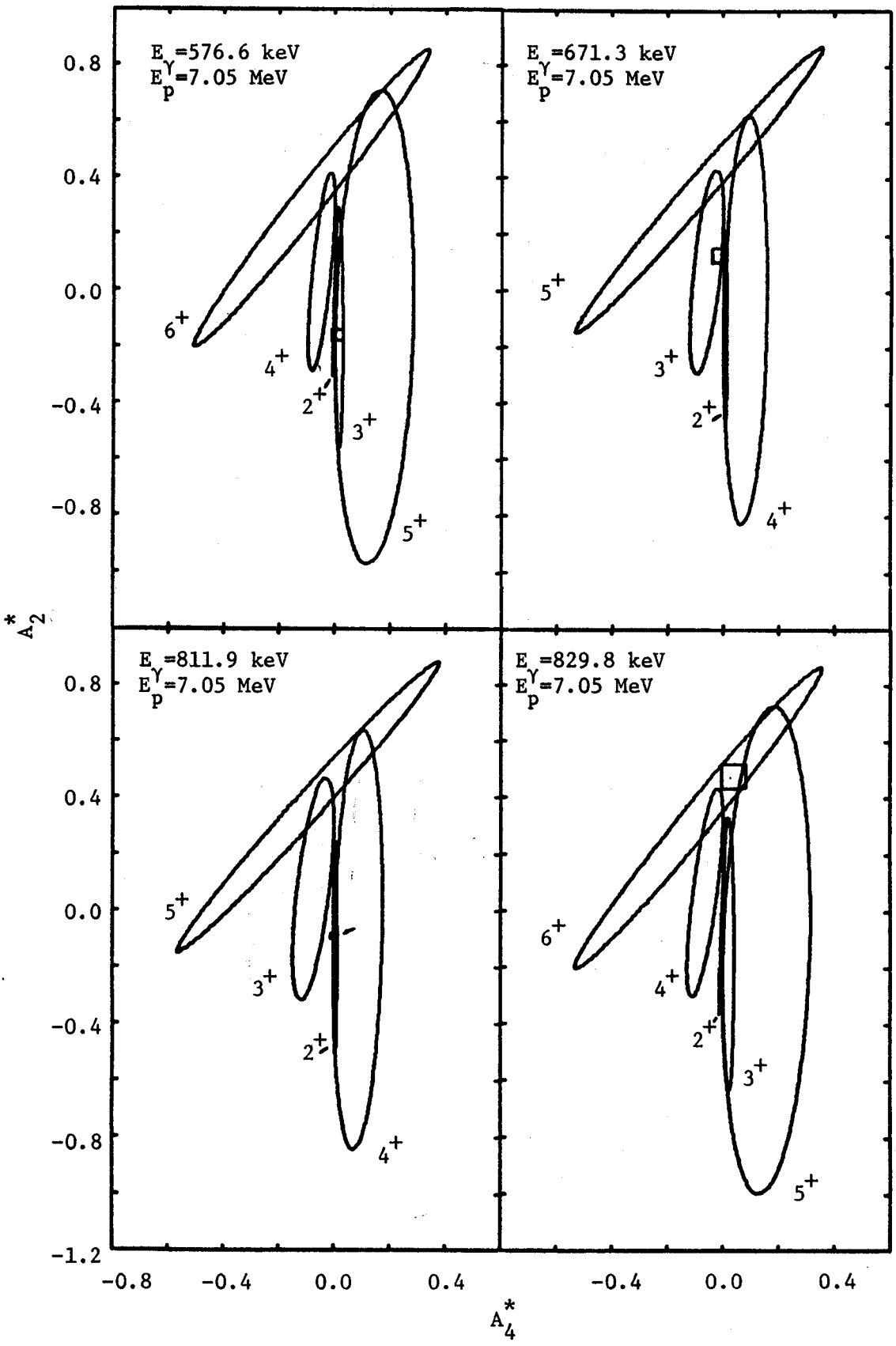

Figure 17 - continued.

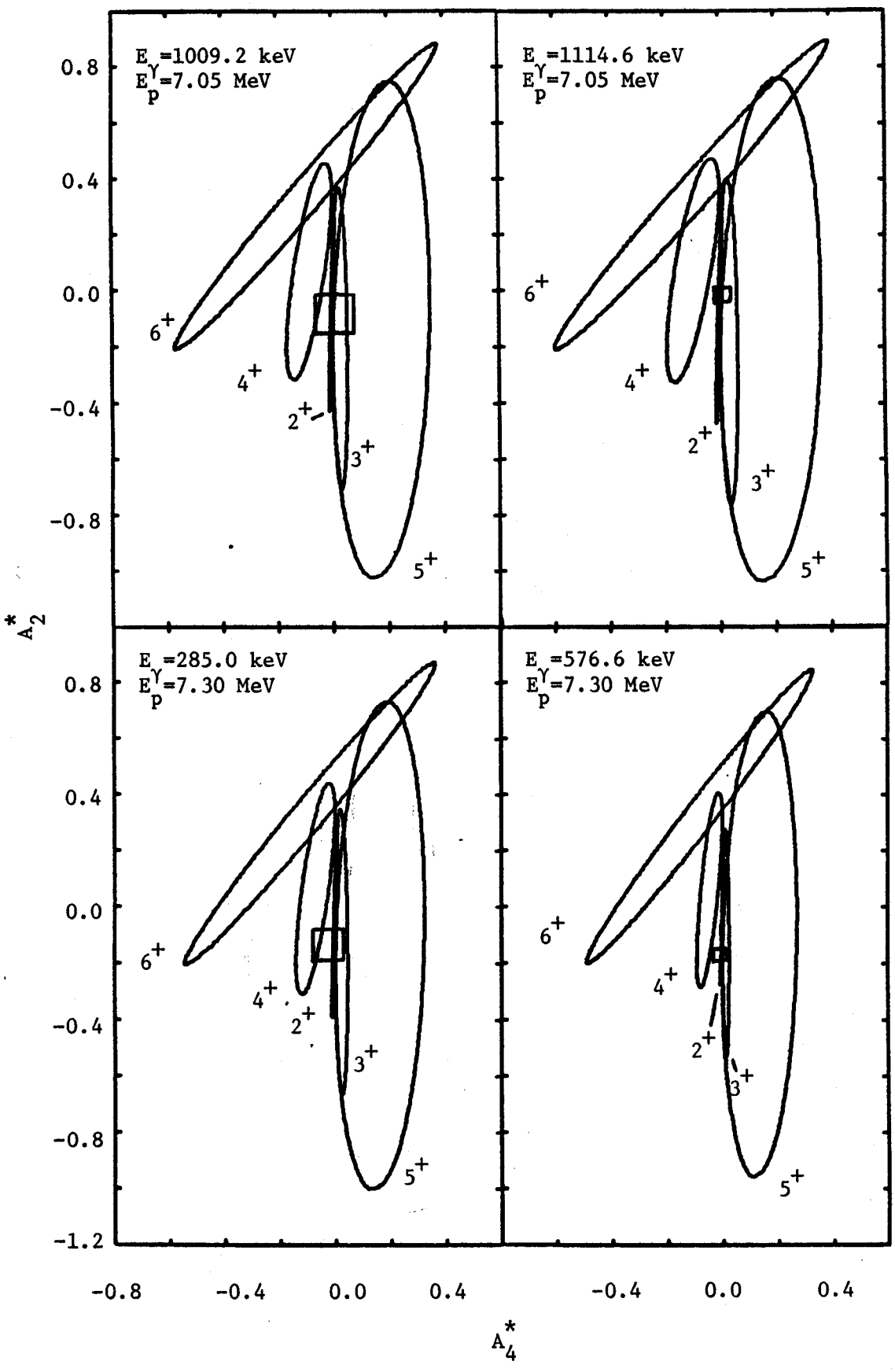

Figure 17 - continued.

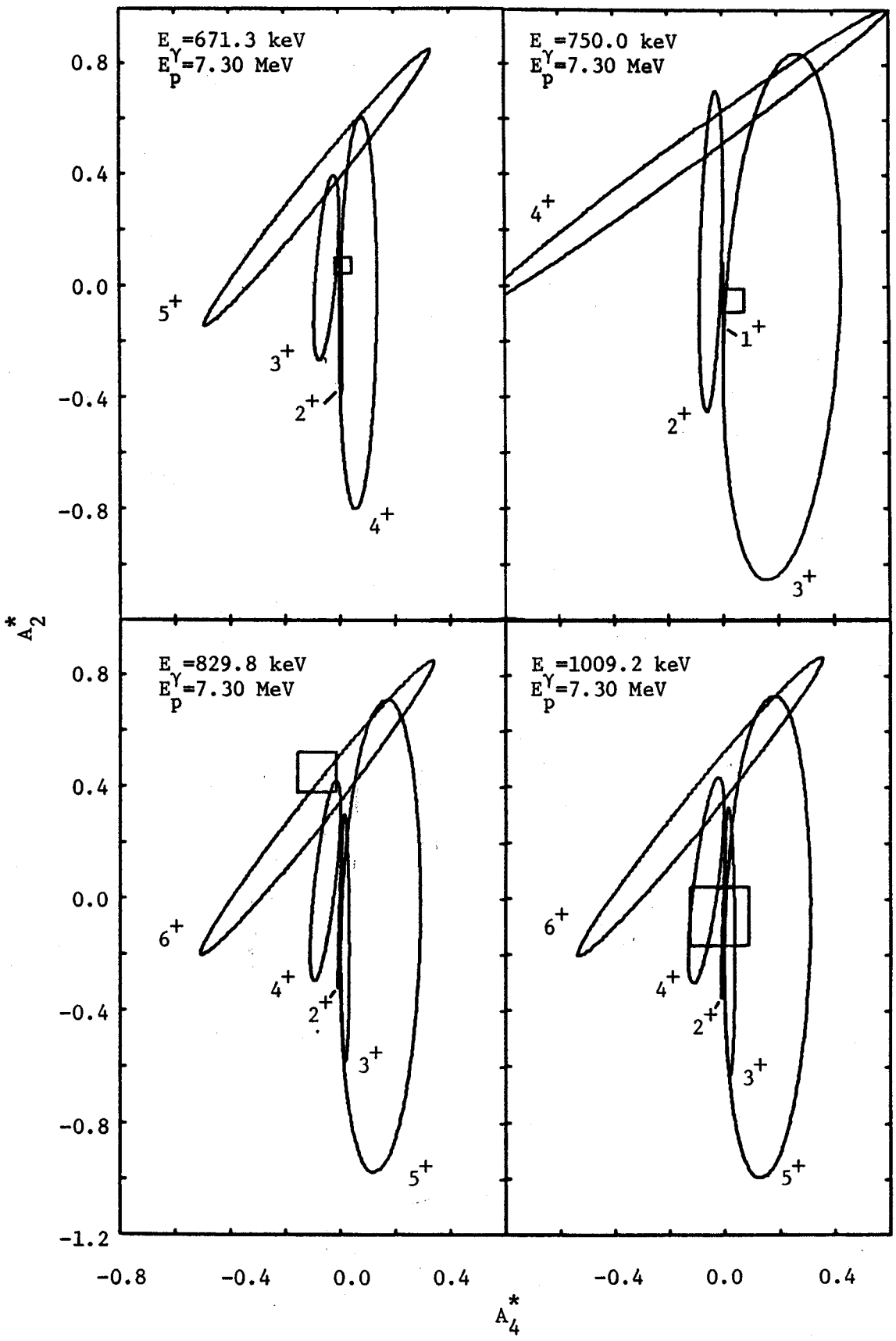

Figure 17 - continued.

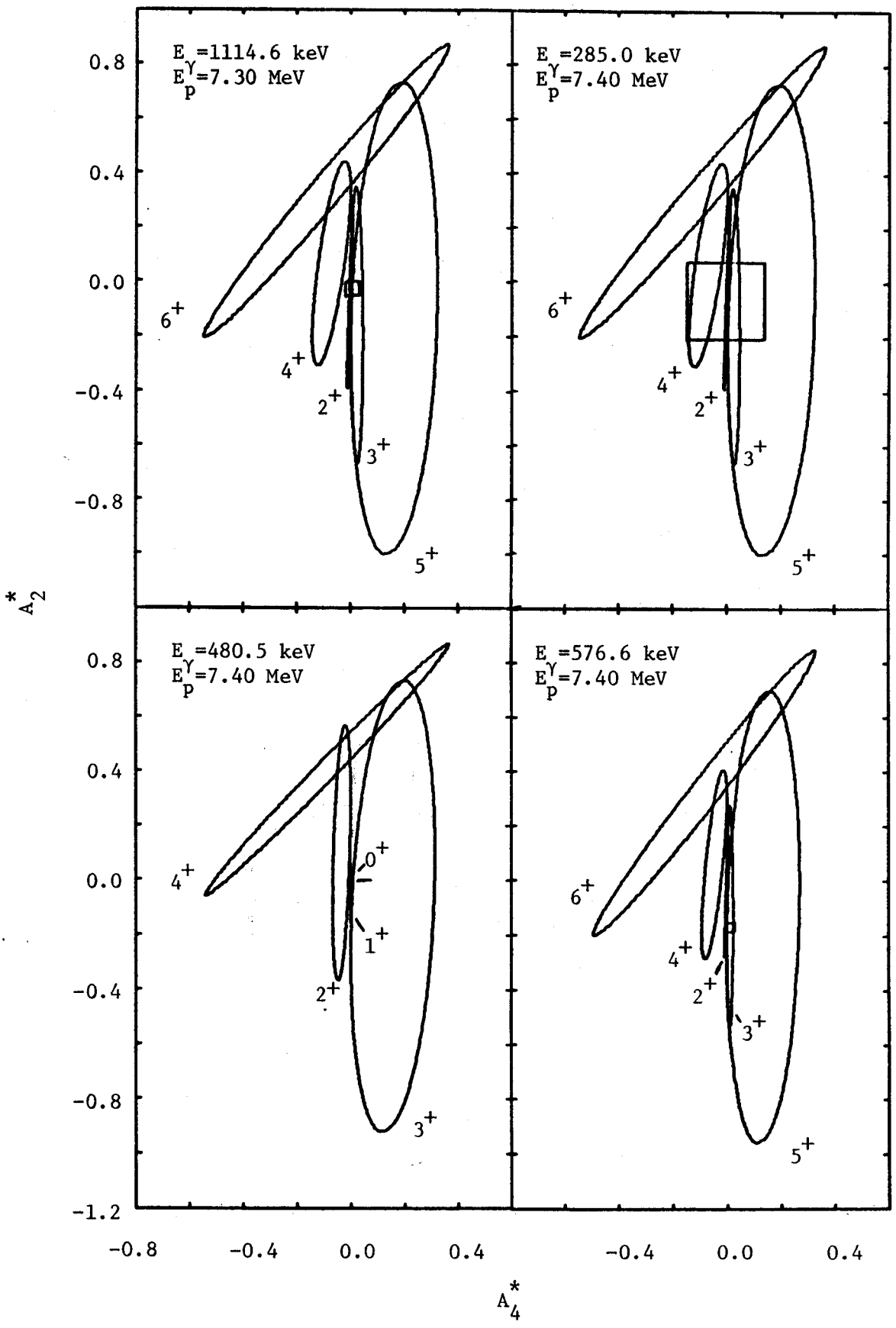

Figure 17 - continued.

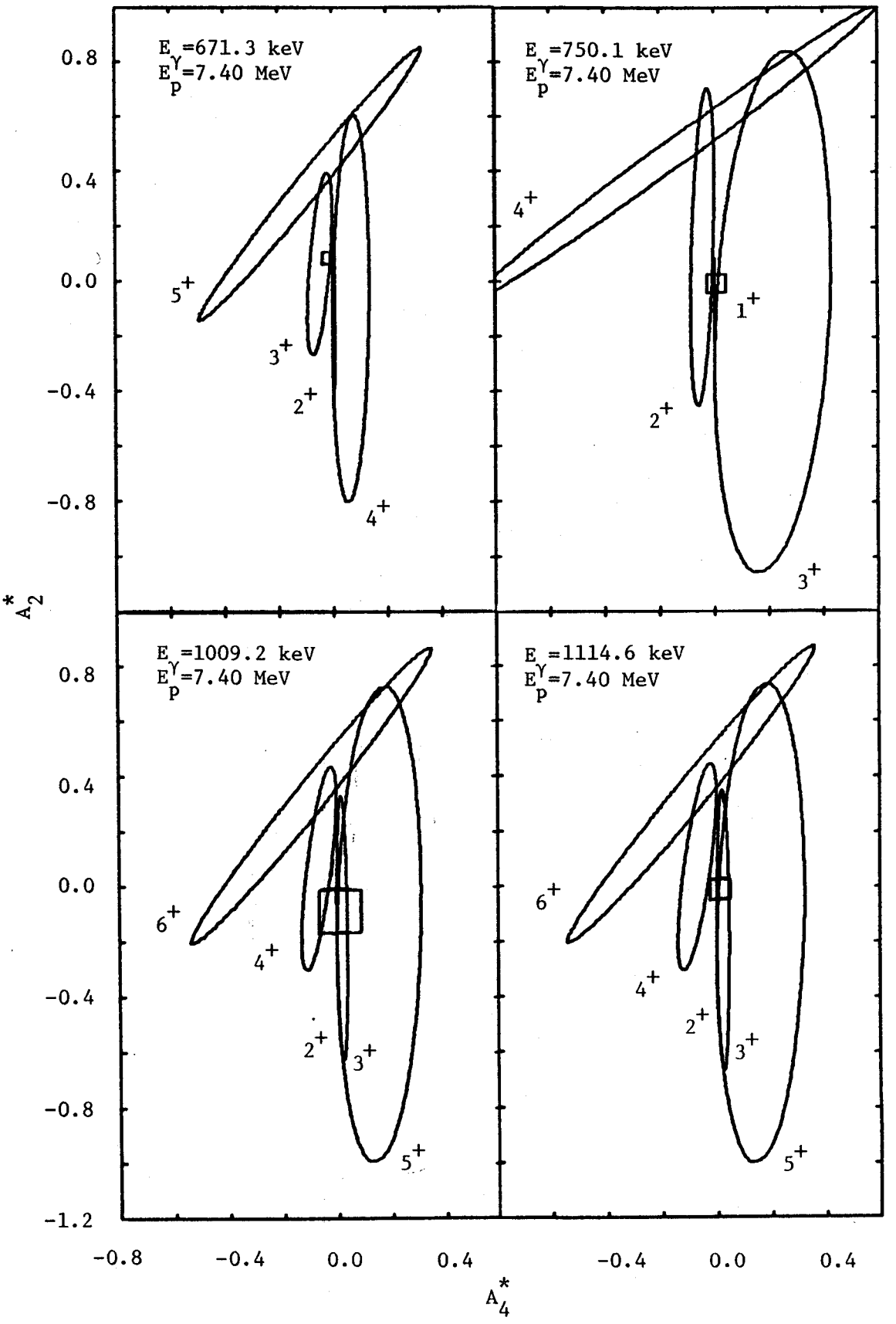

Figure 17 - continued.

APPENDIX E

Relative χ^2 as a Function of Arctan δ for the ^{56}Co γ-ray Angular Distributions

Figure 18. Plots of Relative χ^2 Versus Arctan δ for ^{56}Co γ-ray Angular Distributions. Only those cases are shown where γ-ray feeding from above was judged to be insignificant. Assignment of errors necessary for the determination of χ^2 is outlined in the text. In each case the spin used for the final state was that determined from this experiment; the possible initial state spins and parities label their appropriate curves. It is instructive to compare these plots with the corresponding plot of Fig. 17.

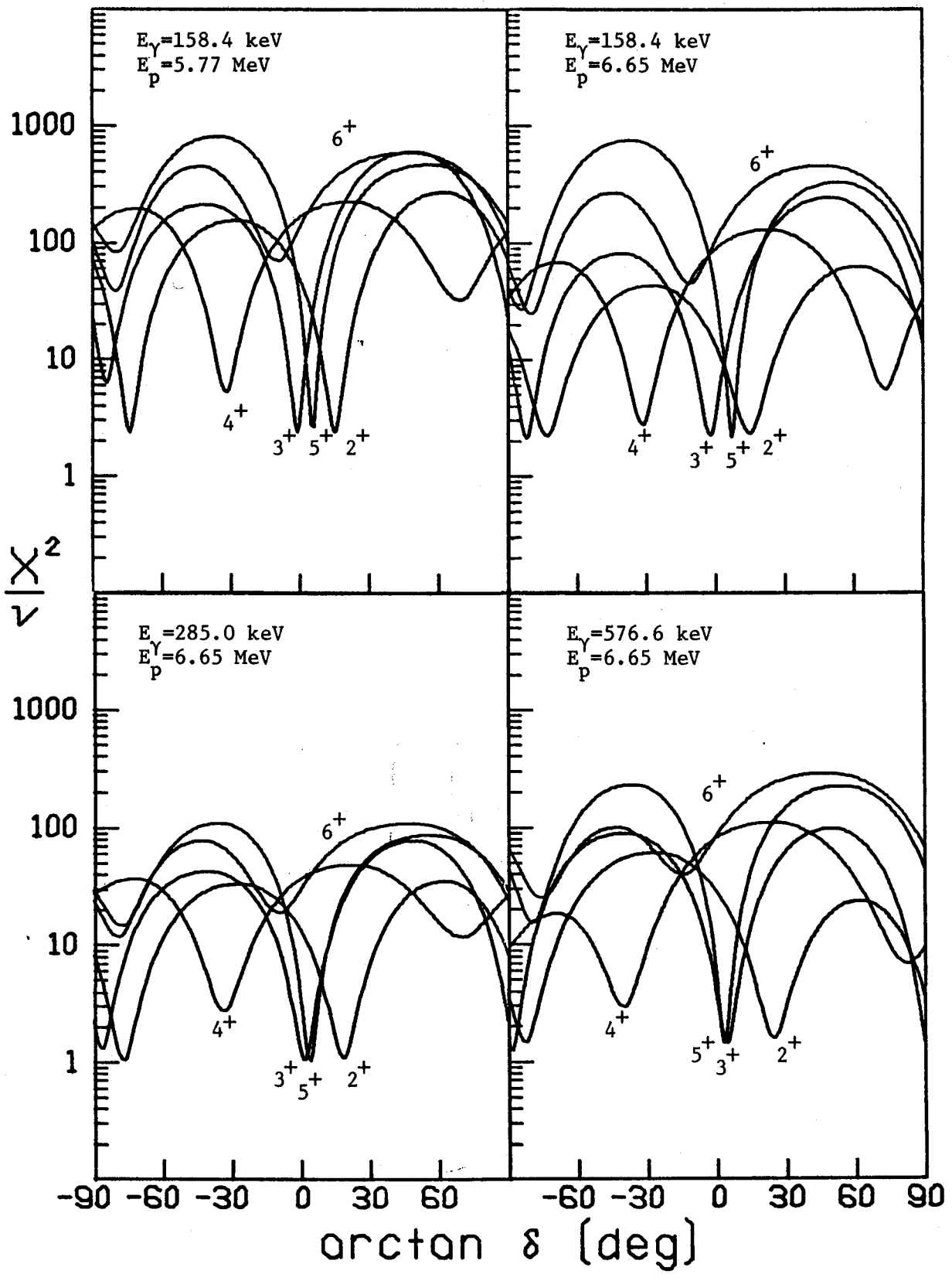
Eγ=158.4 keV
Ep=5.77 MeV
Eγ=158.4 keV
Ep=6.65 MeV
Eγ=285.0 keV
Ep=6.65 MeV
Eγ=576.6 keV
Ep=6.65 MeV
6+
4+
3+
5+
2+
1000
100
10
1
χ²/ν
-90 -60 -30 0 30 60
-60 -30 0 30 60 90
arctan δ [deg]

Figure 18.

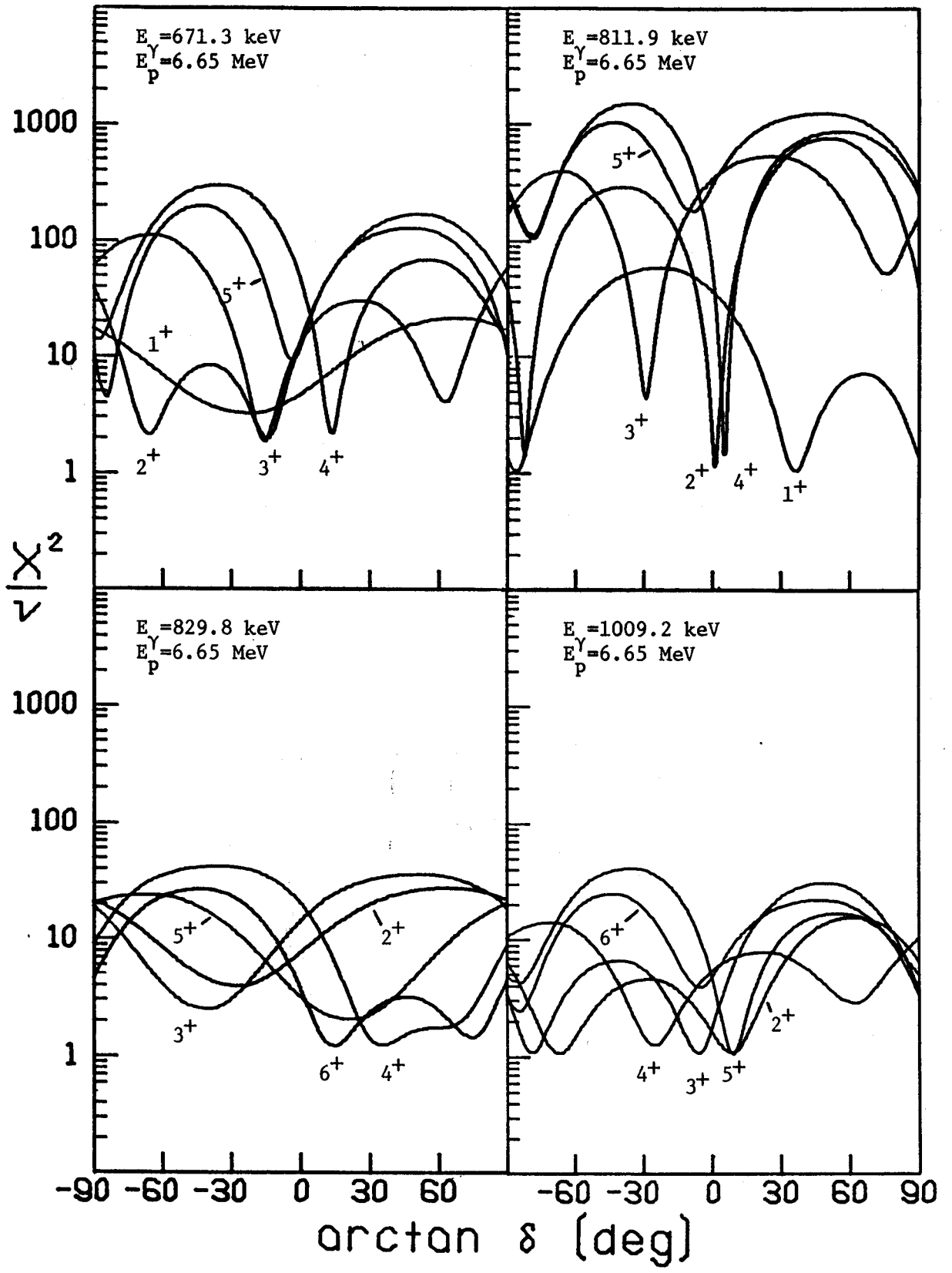

Figure 18 - continued.

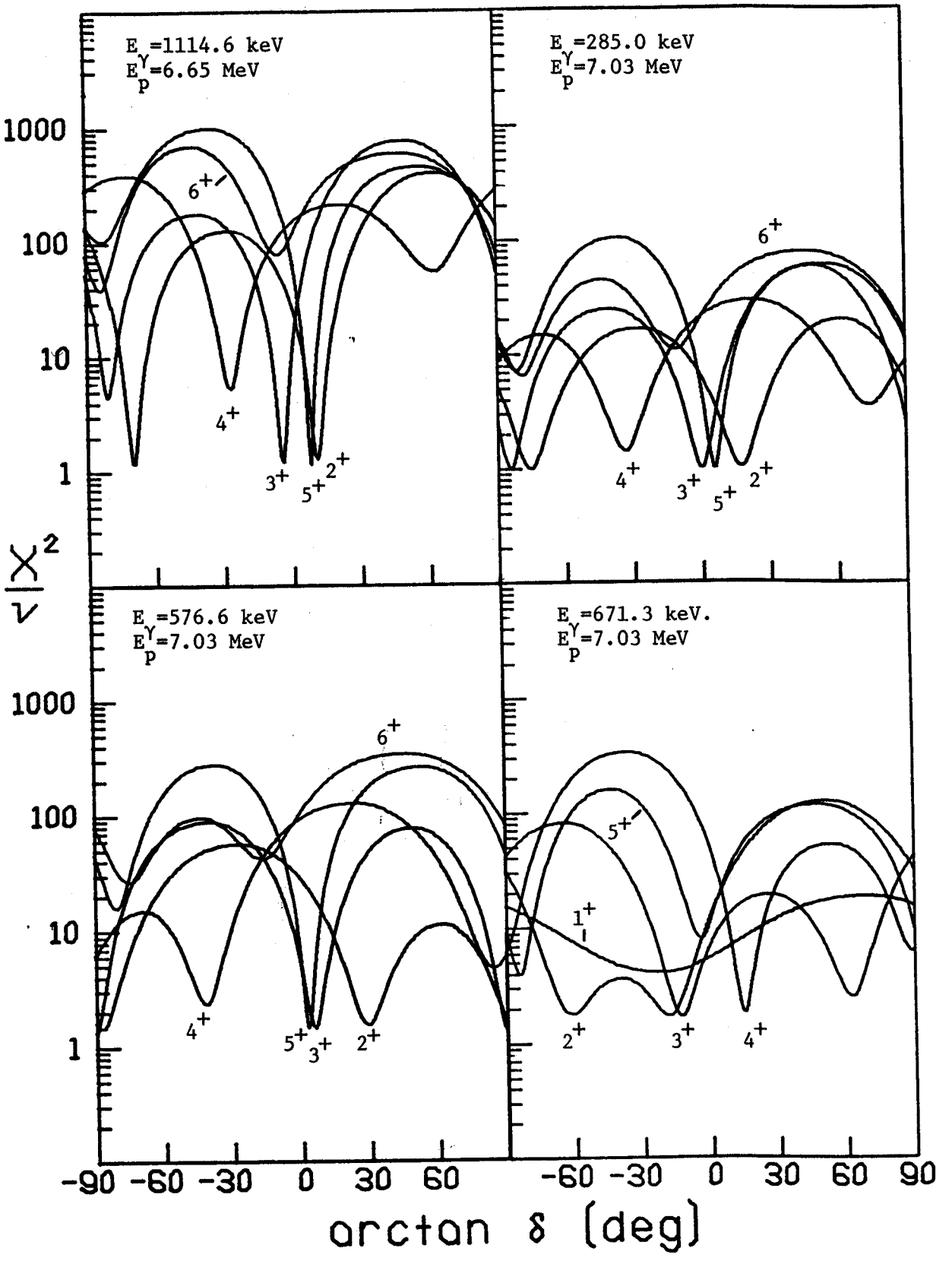

Figure 18 - continued.

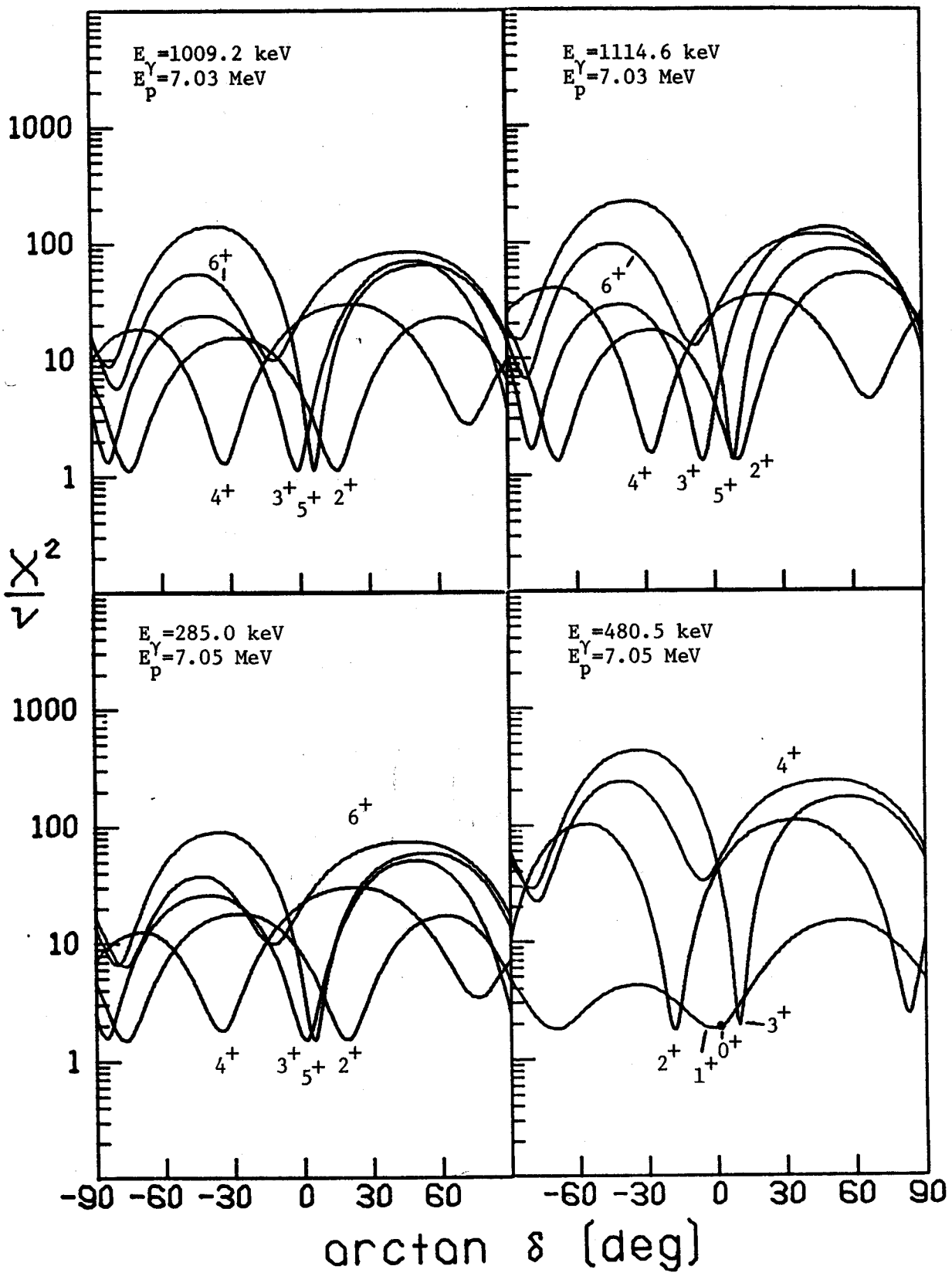

Figure 18 - continued.

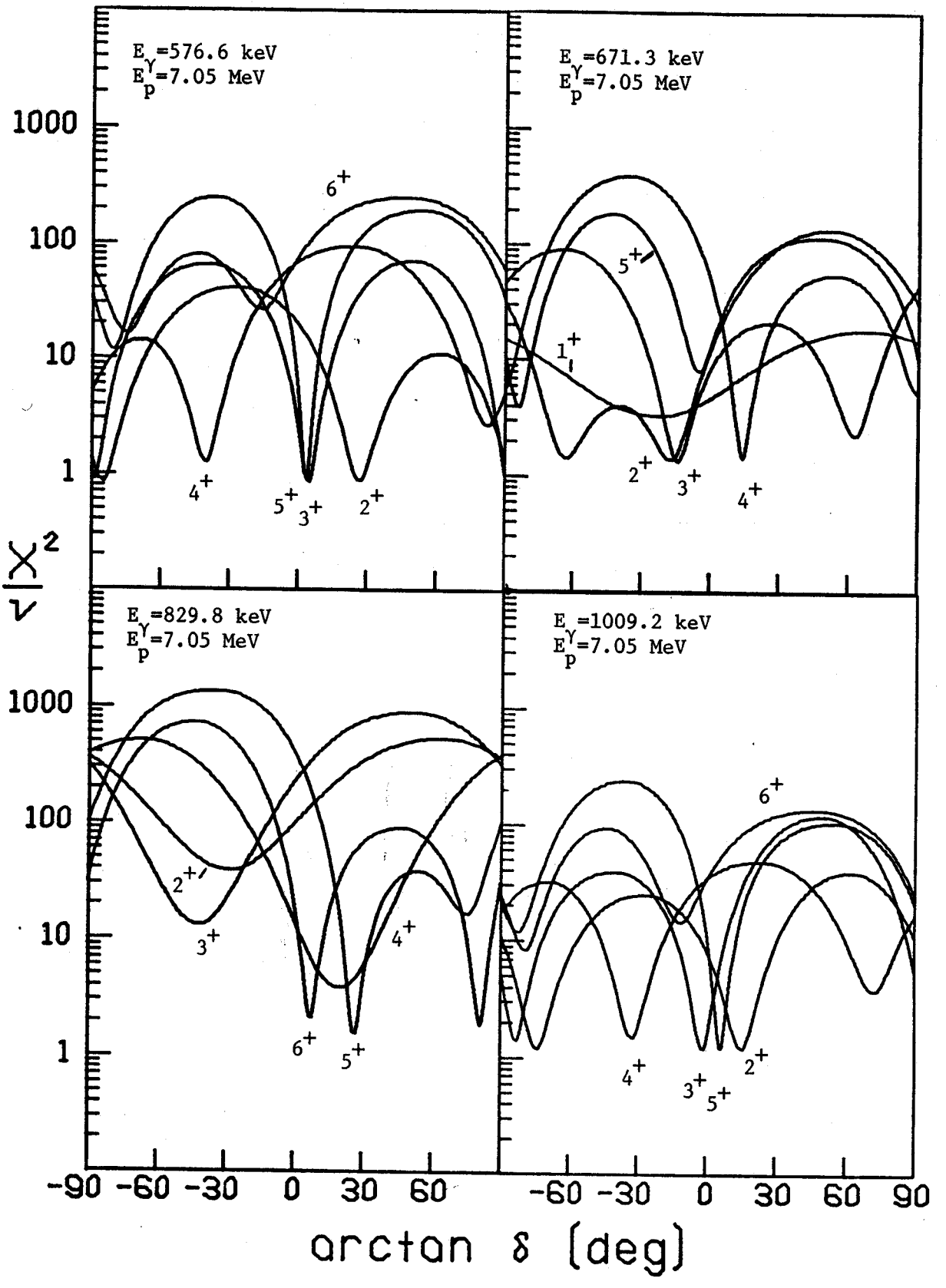

Figure 18 - continued.

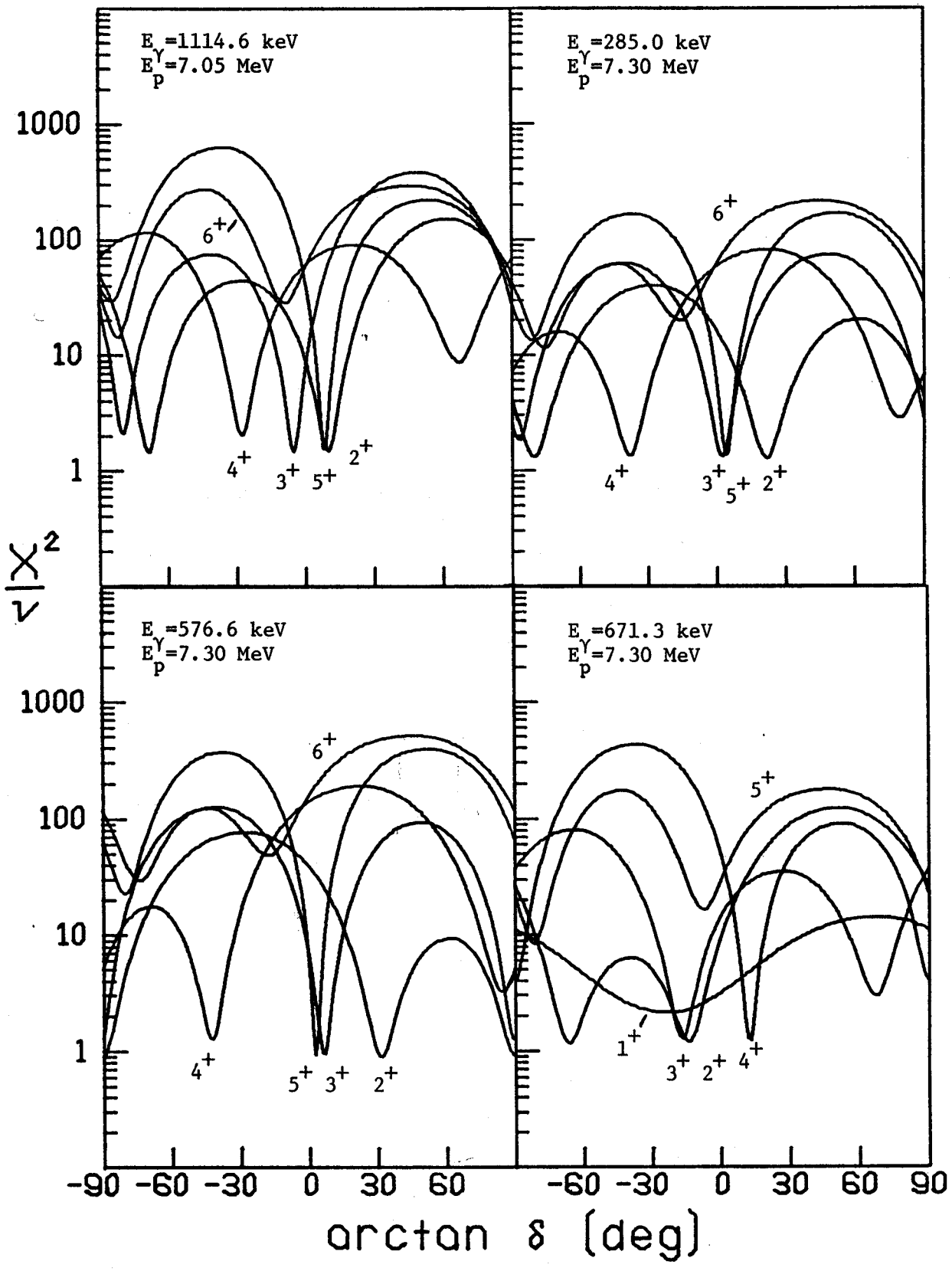

Figure 18 - continued.

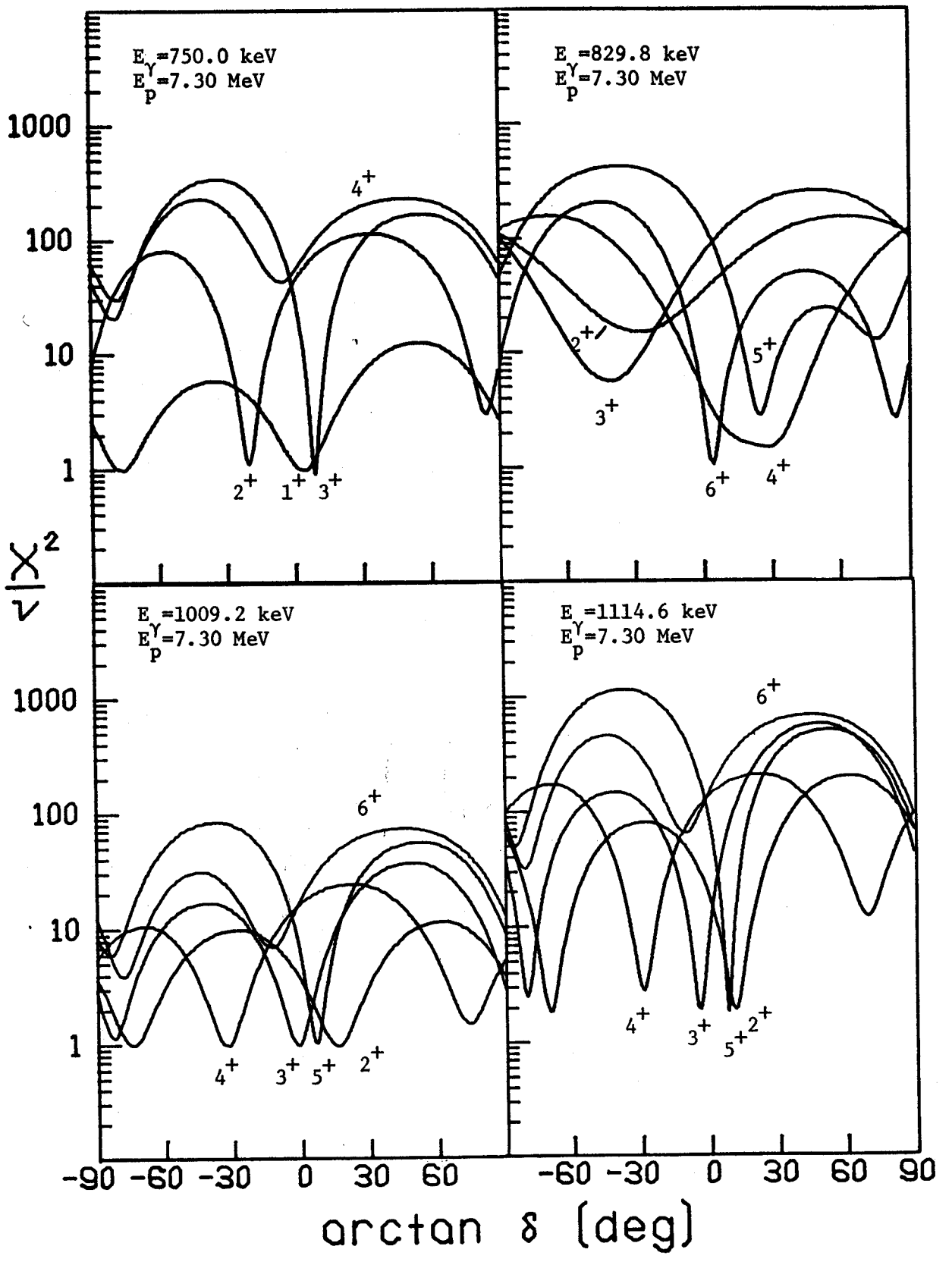

Figure 18 - continued.

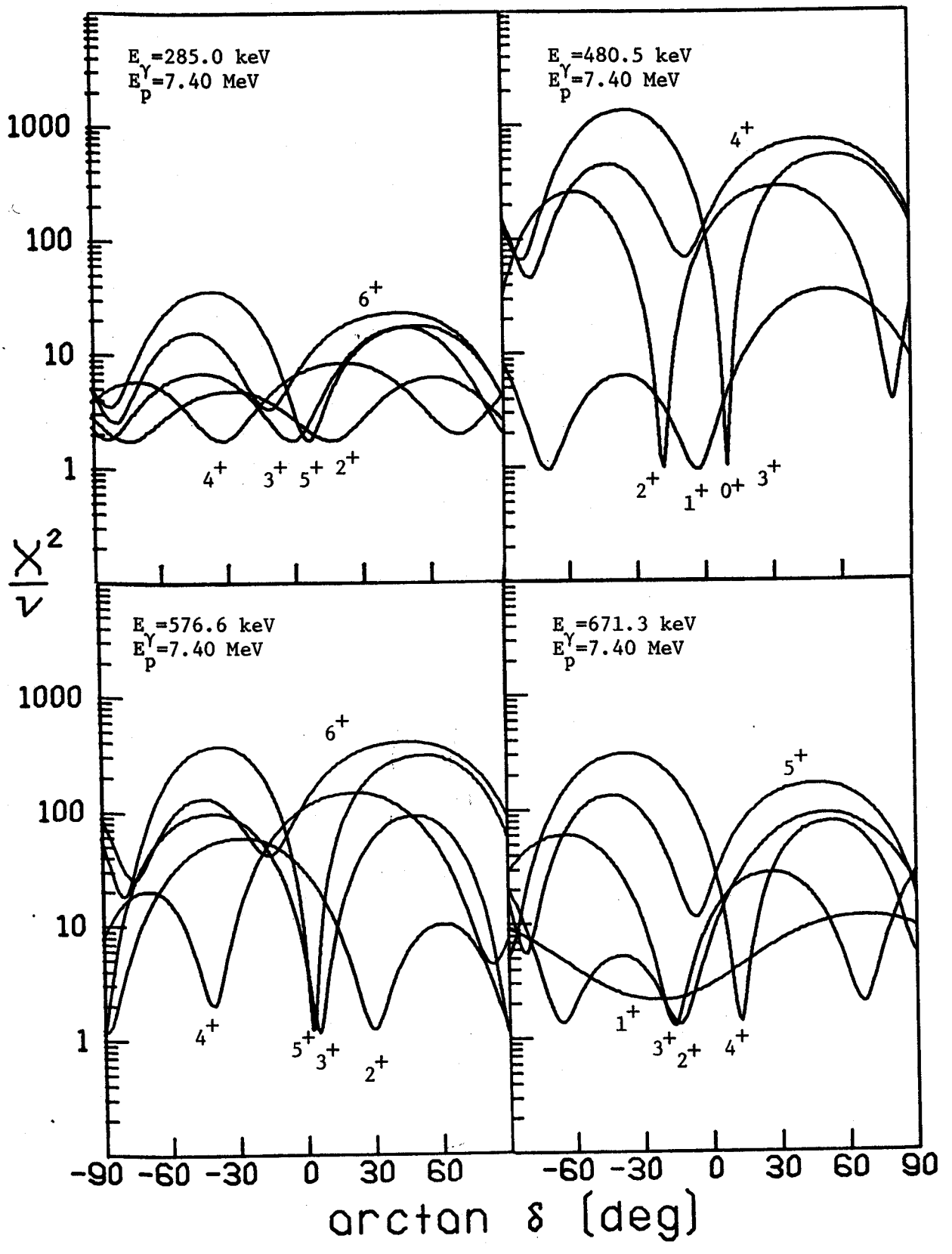

Figure 18 - continued.

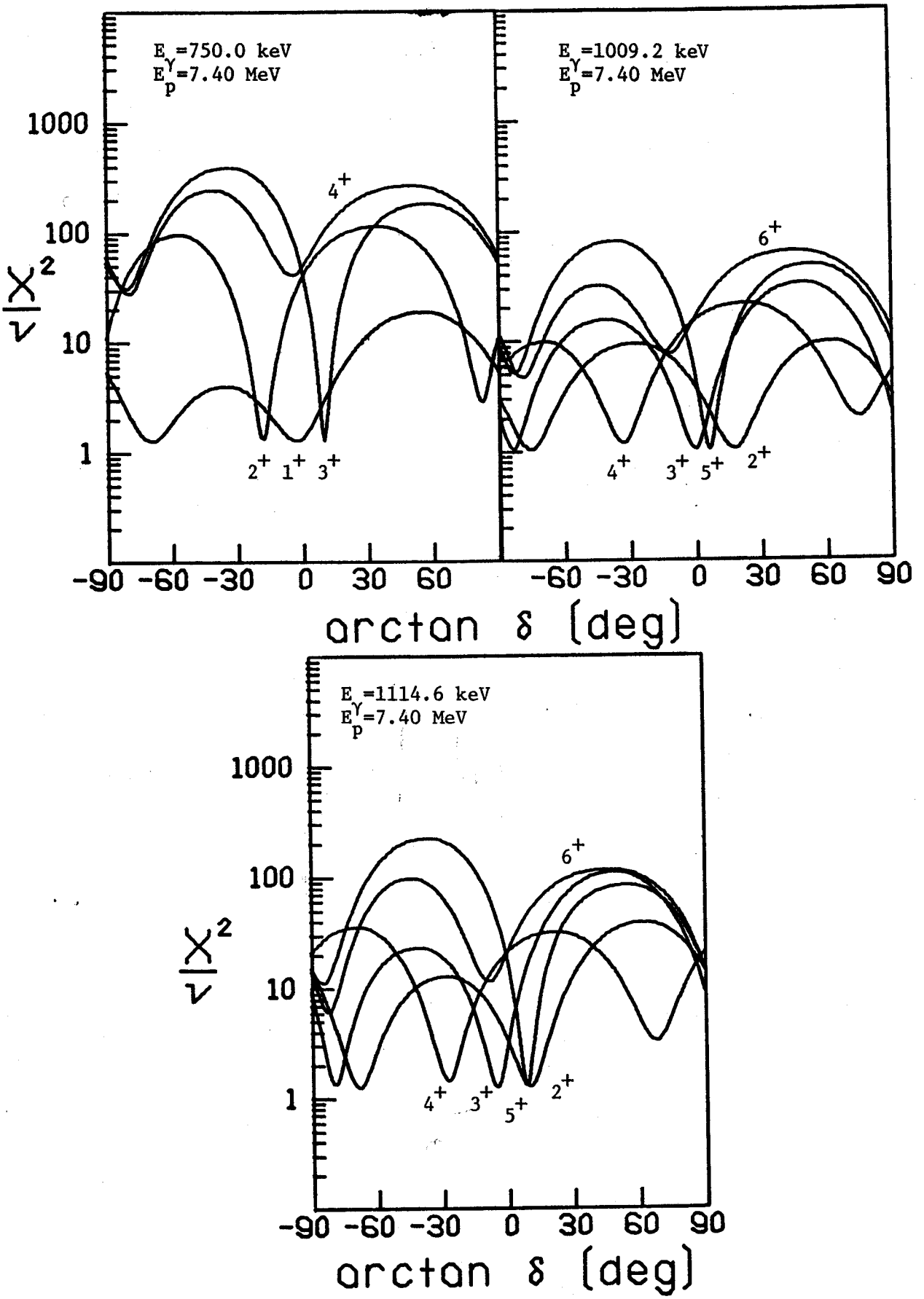

Figure 18 - continued.